Spring 2015

Microstructure and geotechnical properties of St. Peter sandstone in Clayton, Iowa

Amir Hossein Bagherieh

Department: Mining and Nuclear Engineering

MICROSTRUCTURE AND GEOTECHNICAL PROPERTIES OF ST. PETER SANDSTONE IN CLAYTON, IOWA

by

AMIR HOSSEIN BAGHERIEH

A DISSERTATION

Presented to the Faculty of the Graduate School of the

MISSOURI UNIVERSITY OF SCIENCE AND TECHNOLOGY

In Partial Fulfillment of the Requirements for the Degree

DOCTOR OF PHILOSOPHY

in

MINING ENGINEERING

2015

Approved by

Maochen Ge, Advisor
Samuel Frimpong
Kwame Awuah-Offei
Greg Galecki
Wan Yang

ABSTRACT

The St. Peter Sandstone is significantly different from the minerals and rocks which have been studied extensively in mining. It is brittle and characterized by an unusually high friction angle. On the other hand it is friable, and it is nearly cohesionless. The scarcity of the ground control techniques for this particular mining environment has created many difficulties for mine operators. This research aims to establish a fundamental understanding of the basic mechanical and strength properties of the St. Peter Sandstone for engineering design and scientific research. The specific objectives are 1) characterizing the strength of the St. Peter Sandstone, and 2) elucidating the strength mechanics by scientific evidences. The study is essential for developing safe and reliable ground control techniques for mining under this sandstone condition. In this study, extensive conventional rock mechanics testing, as well as a detailed particle structure including optical and scanning electron microscopies studies was carried out on St. Peter Sandstone. An appropriate sample preparation technique for St. Peter Sandstone is proposed. The optimum specimen size for characterizing St. Peter Sandstone was determined. The mechanical behavior of St. Peter Sandstone was investigated under triaxial compressive condition. The results indicated that confining pressure will significantly increase the strength and change the mechanical behavior of St. Peter Sandstone from brittle to ductile. The particle structure of St. Peter Sandstone was studied in terms of porosity, particle size distribution, and density. It was demonstrated that the mechanical and strength properties of the St. Peter Sandstone are fundamentally governed by its particle structure. The systematic presence of Hertzian fractures on the St. Peter Sandstone particle structures were obtained, identified and demonstrated. The finding provides direct evidence to resolve outstanding issues regarding the depositional environment of the St. Peter Sandstone. It was indicated that Hertzian fractures were not the product of eolian action. The contact surface of St. Peter‘s sand grains was investigated. It was found that the majority of contact surfaces are smooth. Hence, the high friction angle of St. Peter Sandstone cannot be attributed to “penetrative surfaces” as hypothesized by locked sand theory.

ACKNOWLEDGMENTS

Foremost, I would like to thank my advisor, Dr. Maochen Ge for his support of my PhD study and research for his patience, guidance, and his knowledge. His guidance in the course of my PhD research and writing of this dissertation is highly appreciated.

I would like to express my everlasting love to my parents, and brothers for their support.

Special thanks to my committee members, Drs. Wan Yang, Samuel Frimpong, Kwame Awuah-Offei, and Greg Galecki for their valuable comments.

Thanks should go to my fellow graduate students in the Mining and Nuclear Engineering department of Missouri S&T, specially Francis Arthur, Ziwei Ding, Saied R. Dindarloo, and Mohammed Azeem Raza.

Last but not least, I would like to thank our sponsor Pattison Sand Company for funding this project.

TABLE OF CONTENTS

LIST OF ILLUSTRATIONS

LIST OF TABLES

NOMENCLATURE

Symbol	Description
σ	normal stress
c	cohesion
φ	the angle of internal friction
τ	shear stress
UCS	Uniaxial Compressive strenght
n	porosity
V_v	volume of voids
V	total volume of the sample
V_s	Volume of solids
RAS	the rate of increase of the axial stress at failure
σ_a	the axial stress at the failure
σ_o	Uniaxial Compressive Strength
σ_c	confining pressure
D_n	particular screen size that n% material can pass
C_u	Uniformity coefficient
W_{sat}	the Weight of saturated sample
W_{dry}	the Weight of dry sample
γ_{fluid}	the density of fluid
γw	the density of water

1. INTRODUCTION

1.1. BACKGROUND

Hydraulic fracturing, also known as fracking, is a technique that uses pressurized fluid to fracture rocks. Vast reserves of shale and tight gas across the United States have become commercially viable because of the advancement of this technique as well as horizontal drilling in recent years. This trend is dramatically changing the US energy landscape (Figure 1.1). Net imports of natural gas will decrease 44% by 2035 if this energy source is properly developed (US Energy Information Administration (EIA), 2010).

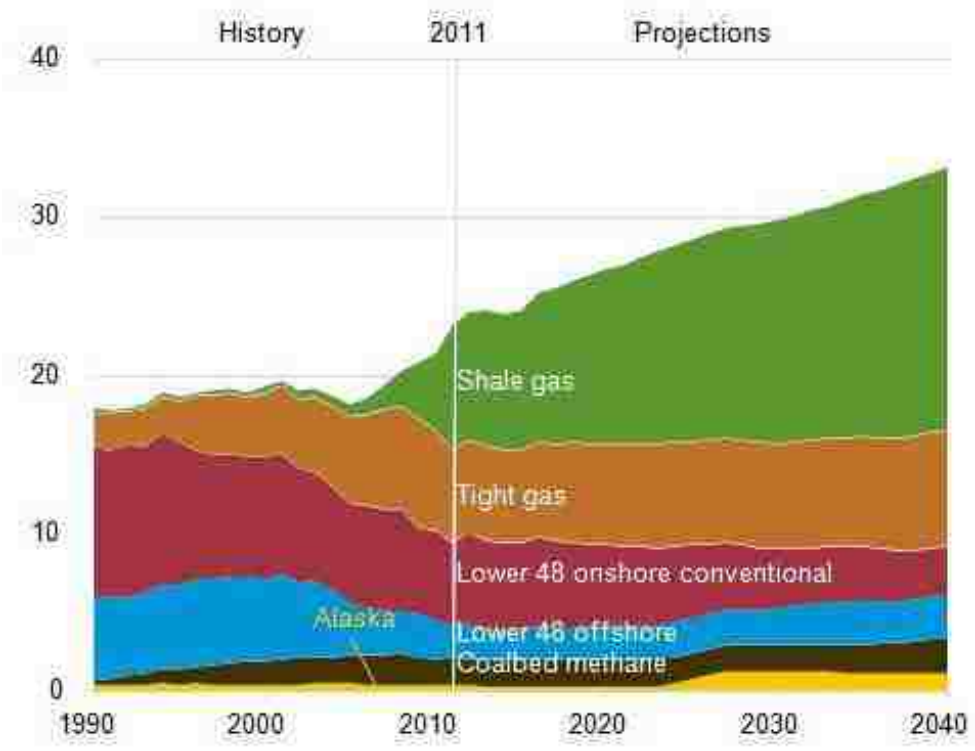

Figure 1.1. Natural gas production (trillion cubic feet) (EIA, 2013)

The fluid used for hydraulic fracturing is a mixture of water, proppants, and chemicals. A proppant is a solid material, which can be naturally occurring sand grains. They

can also be created with man-made ceramic materials. Natural sands are utilized in most cases because they are more economical. Viable proppants, must be durable, round, and high-purity in quartz. Thus, sands that can be used for fracking are limited. In the United States, St. Peter sand exhibits the best characteristics for this purpose making it a major resource of frac sand.

The demand for frac sand has increased rapidly in recent years (Figure 1.2), increasing the demand for sand at a phenomenal rate. The Pattison Sand Company, located in Clayton, Iowa is a product of this sand rush. This company produces frac sand from both surface and underground operations. The underground mine is shallow, with an overburden between 45 and 90 m. The room-and-pillar mining method is utilized in this mine. The extraction ratio is approximately 64%. The average pillar size is 17 x 17 m^2.

1.2. GROUND CONTROL PROBLEMS ENCOUNTERED AT THE PATTISON MINE

The mechanical properties of the St. Peter Sandstone are unique. It is very different from that of the conventional geological materials in mining industry, such as coal, potash, limestone, and granite. It is very brittle, characterized by an unusually high friction angle, and steeply curved failure envelopes. In contrast, it is also friable, possessing extremely low and, in most cases, zero cohesion. As a result, these sandstones are capable of supporting a considerable amount of load when undisturbed. However, they are very weak when disturbed.

Although significant research has been done on the ground control and pillar design for coal and hard rock mines, as demonstrated in the literature (Obert et al., 1946; Krauland and Soder 1987; Sjoberg ,1992), the ground control for St. Peter Sandstone conditions has not received the same attention. The scarcity of ground control techniques for this particular

mining environment has created many difficulties for the mine operators. It has also created serious challenges for the government regulatory agencies. The Pattison mine has three outstanding ground control problems:

- pinch-out failures
- rock reinforcement techniques for the St. Peter sandstone condition, and
- pillar design methods for the St. Peter sandstone condition.

The term "pinch-out failure" is used at the Pattison Mine to describe a failure occurring at the intersections of roofs and pillars (Figure 1.3). The Mine Safety and Health Administration (MSHA) attributed this problem to overly stressed pillars and suggested that the pillar's size be increased by 150–250%. Increasing the pillar's size within this scale would jeopardize the mine's profitability, and eventually make mining economically unfeasible.

Another important problem facing the Pattison mine involves reinforcing the St. Peter Sandstone. Rock bolting has been widely adopted in the mining industry for the rock reinforcement purposes. The effect of this method on the St. Peter Sandstone is, however, limited. Rock bolts and steel strips used to stabilize a pillar are illustrated in Figure 1.4. Unfortunately, this expensive method which would likely work for other types of pillars does not work for St. Peter Sandstone.

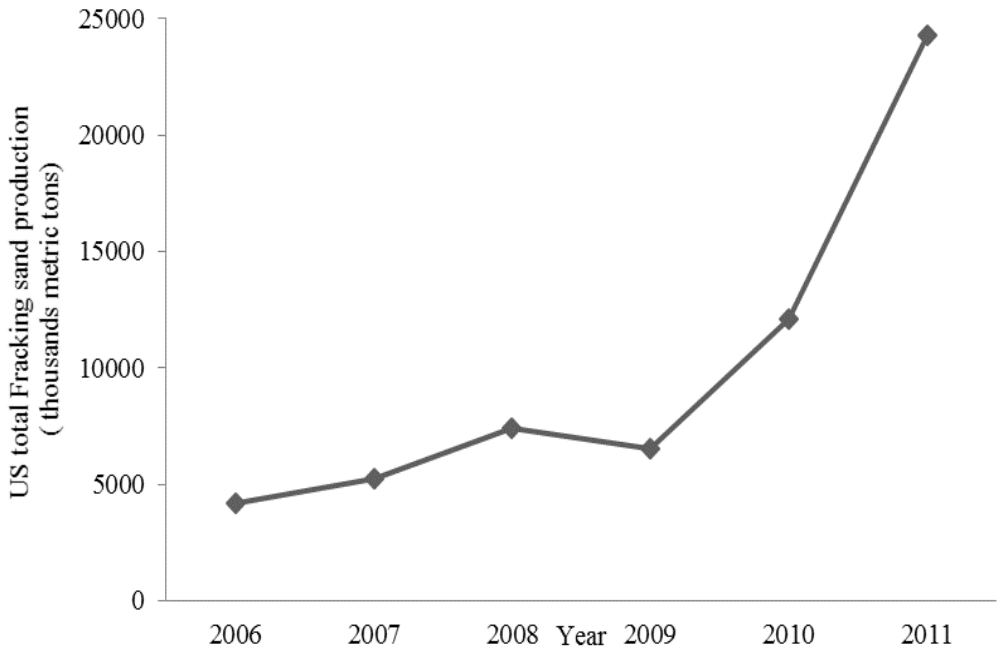

Figure 1.2. Total fracking sand production in the U.S. between 2006 and 2011(USGS Minerals Yearbook for silica (2006-2011).

Figure 1.3. A pinch- out failure in the Pattison Mine

The pillar design methods presently available to the mining industry were developed for coal, salt, and hard rock mine conditions. None of these methods are adequate for the condition that is uniquely associated with St. Peter Sandstone. An urgent issue for the sandstone industry is, therefore, developing an efficient and reliable pillar design method.

Figure 1.4. Reinforcing a sandstone pillar with rockbolts and steel strips.

A wide range of issues need to be addressed before these problems can be resolved. The major obstacle, however, is the lack of basic mechanical properties related to St. Peter Sandstone. For example, characterizing the strength of the St. Peter Sandstone, and identifying the major factors that control the basic mechanical behavior of the St. Peter Sandstone are of importance.

1.3. RESEARCH OBJECTIVE

This research was conducted in an attempt to establish a fundamental understanding of the basic mechanical and strength properties of the St. Peter Sandstone for both engineering design and scientific research. Two specific goals were set:

- Characterize the basic strength properties of St. Peter Sandstone
- Elucidate the strength mechanics of the St. Peter Sandstone by experimental evidences.

1.3.1. Characterizing the Basic Strength Properties for the St. Peter Sandstone. Four important tasks needed to be completed before the basic strength properties of St. Peter sandstone could be characterized:

- develop a sample preparation method for St. Peter Sandstone
- determine the optimum sample size needed to characterize the strength of St. Peter Sandstone
- identify the critical factors that affect St. Peter sandstone's strength
- develop a comprehensive strength assessment method

As discussed earlier, St. Peter Sandstone is cohesionless, which makes it extremely friable. Conventional sample preparation procedures, such as those recommended by the International Society of Rock Mechanics (ISRM) (ISRM, 1981), American Society for Testing and Materials (ASTM) (ASTM, D7012-14) are difficult to apply. The major problem for those conventional methods is the disturbances, such as vibration and water, accompanied with these methods, which are excessive for the St. Peter Sandstone; even if they are negligible for conventional geological materials. An example is sample coring, which is practically impossible for the St. Peter Sandstone. Therefore, a suitable sample preparation procedure for the St. Peter Sandstone needs to be established. Developing a sample

preparation method for St. Peter Sandstone makes it possible to compare the strength of it on a reliable basis.

The strength of a geological material is not an abstract concept. It is closely associated with the sample preparation procedure and method. One of the critical factors is the change of strength with the sample size. In the other words, the strength of a geological material usually refers the strength associated with a particular size, which is chosen based on a number of criteria, including, reliability, repeatability, and practicality. Sample's size becomes a particularly important issue for the St. Peter Sandstone, because of the friable nature of the St. Peter Sandstone and the difficulty to prepare the samples. An important task in assessing the strength of the St. Peter Sandstone is therefore to determine the optimum sample size.

The strength of a rock material can be defined by different parameters. The most common approach is the uniaxial compressive strength. Although the uniaxial compressive strength is also an important index for the St. Peter Sandstone, it could be misleading if this index is used alone. As the strength of the St. Peter Sandstone is largely controlled by its particle structure, basic knowledge of the particle structure, as well as the engineering behavior under the triaxial test is essential in order to study the strength of the St. Peter Sandstone. The final objective on the strength study is to develop a new approach to characterize the strength of the St. Peter Sandstone, which is comprehensive and easy to use.

1.3.2. Elucidating the strength mechanics of the St. Peter Sandstone by Experimental Evidences. The theoretical problem that is discussed most extensively for the St. Peter Sandstone is the mechanics of the extremely high friction angle associated with the St. Peter Sandstone. A dominant view is that this extremely high friction angle is caused by the penetrative surface of the St. Peter sand particles (Dusseault and Morgenstern, 1979).

The essence of the underlying problem is the origin of the strength of the St. Peter Sandstone, which is not only critical for the strength study, but also related to a number of classical geological problems, including deposition environment for the St. Peter Sandstone and the origin of Hertzian fractures observed on the St. Peter Sandstone.

The research on the strength mechanics of the St. Peter Sandstone involves both in-depth theoretical studies and extensive laboratory work. The main objectives of this research for this particular aim is to provide the solid experimental evidences in the following areas: 1) particle structures of the St. Peter sandstone, 2) characteristics of particle contact surfaces and their effect on sandstone strength, 3) the stress condition associated with the particle structure, and 4) cause of high friction angle.

1.4. DISSERTATION OUTLINE

This dissertation includes seven chapters. Chapter 2 is a literature review on the related studies. The main objective of this chapter is to provide readers the background information of this research, the major findings and lessons learned from the past research, and the outstanding issues resulted from the previous researches.

Chapter 3 discusses the uniaxial compressive strength of St. Peter Sandstone based on an extensive laboratory tests carried out in this study as well as the available data from the previous researches. The chapter is an introduction of the basic strength characteristics of the St. Peter Sandstone. The specific issues addressed in this chapter include methods of the sample preparation, large variations of the test result, sample size effect, and initial assessment of the impact of sand particles.

The focus of Chapter 4 is the triaxial test carried out by this research and its implications on our understanding of the basic mechanical properties of the St. Peter Sandstone. The result of the triaxial test performed by this research is very consistent, which

convincingly confirms the extremely high frication angle associated with the St. Peter Sandstone. It shows that the strength of the St. Peter Sandstone is much higher and much more consistency under the triaxial test condition. Most importantly, it reveals the critical role of the particle size distribution on the triaxial strength.

Chapters 5 and 6 are devoted to exploring the particle structure and how this structure affects the basic mechanical behavior of the St. Peter Sandstone. Chapter 5 covers the conventional methods, including density, porosity, and particle size distribution. There are two main objectives for the studies carried out in this chapter. The first one is to collect the basic information which allows us to characterize the particle structure quantitatively. The second one is to determine whether a close correlation exists between density, porosity and particle size distribution, which can then be used for the strength assessment.

Chapter 6 covers the advanced microstructural study of the St. Peter Sandstone, which makes use of two special techniques: thin section and scanning electron microscope. The aim of this study is to elucidate the strength characteristics of the St. Peter Sandstone by microstructural evidence. This study also resolves two classical problems faced by the researchers regarding the origin and deposition environment of the St. Peter Sandstone. These two problems are the nature of the contact surface and the cause of Hertzian fractures (Johnson et al, 1989).

Chapter 7 is the last chapter, which concludes this research. There are three parts to this chapter. The first one is a summary of the methodology regarding how to assess the basic mechanical properties of the St. Peter Sandstone, a comprehensive analysis of the research results presented in Chapter 3 through Chapter 6. The second part is a brief discussion on how to use the knowledge gained from this research for resolving three ground control

problems faced by the sandstone industry outlined in section 1.2. The last part is the future research problems.

2. LITERATURE REVIEW

Arenaceous is a term derived from the “arena”, a Latin word for sand. This term was adopted by geologists to describe a sand deposit irrespective of its composition (Pettijohn et al, 1978, De Freitas, 1993). St. Peter Sandstone is a unique type of areneceous material that is at the borderline between sand and sandstone. Though many have questioned how to classify it (e.g. either sand or sandstone), geologists refer to St. Peter Sandstone as sandstone. Geotechnical engineers may classify it as sand, because it is almost cohesionless. This group of geological material is more dense than normal sands. It also possesses a higher internal friction than other soils and rocks (e.g. loose and dense sands). Standard sampling and sample preparation methods conventionally used for rock and soils are not usually applicable to them because of this material’s peculiar properties. Thus, the materials in the transitional zone between sand and Sandstone have received less attention than material within arenceous spectrum (Barton, 1993; Creswell, 1999).

The geology and strength properties of St. Peter Sandstone are discussed in Sections 2.1 & 2.2 respectively. It’s followed by Section 2.3 that covers high friction angle of St. Peter sandstone and the related theory for it.

2.1. THE GEOLOGY OF ST. PETER SANDSTONE

Sardeson (1891) reported the first observations about St. Peter Sandstone and the reason for calling it St. Peter sandstone. St Peter Sandstone was first described by Captain Carver in 1766-1768. Carver wrote about a cave in a soft material that could be cut with knife. Long (1817) described St. Peter Sandstone as whitish-yellowish material that could be called sand (Sardeson, 1891). Owen (1847) first described geologically the St. Peter Sandstone, calling it St. Peter sandstone because of its exposure below Fort Snelling at the St.

Peter's River. Although the name of St. Peter river changed to the Minnesota River the name of St. Peter sandstone remained unchanged.

Research on the geology of St. Peter Sandstone was undertaken in 1920s, and 1930s (Dake , 1921; Lamar, 1928; Gilies, 1930; Thiel, 1935).

St. Peter Sandstone is an arenaceous, ortho-quartzitic, sublittoral cratonic sheet sand of Middle Ordovician age. It covers a large area (Figure 2.1), 576,000 km^2, in North America that includes Minnesota, Wisconsin, Iowa, Missouri, and Arkansas.

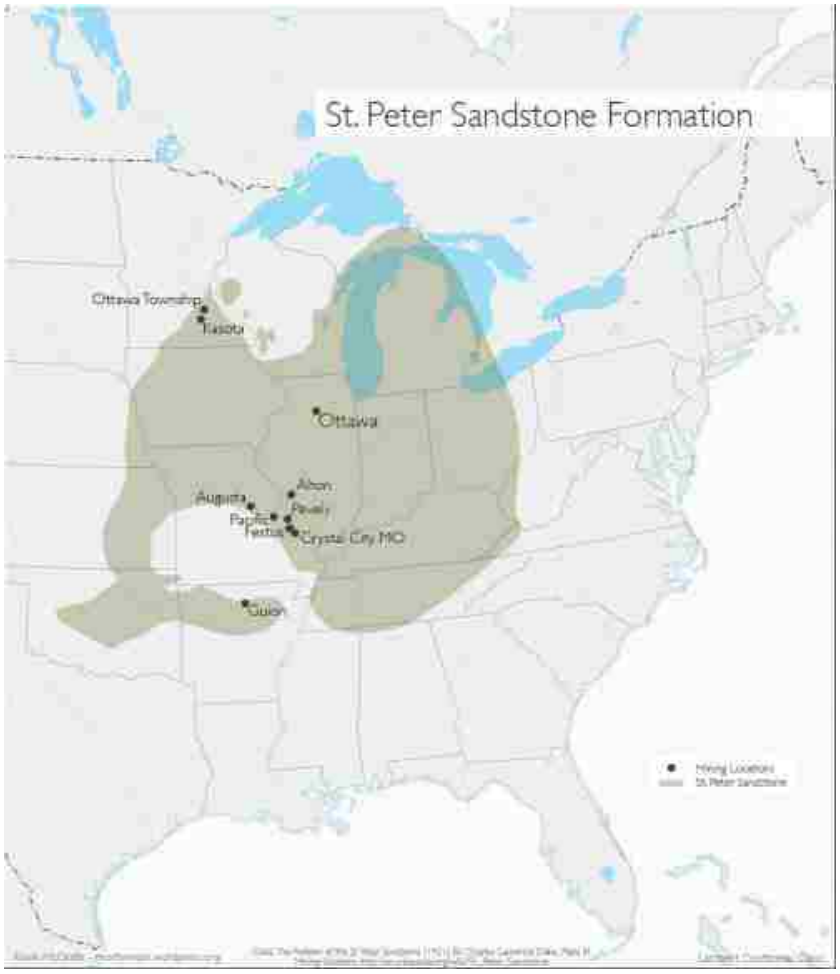

Figure 2.1. The brown area shows the extent of St. Peter sandstone in US(http://mostlymaps.wordpress.com/)

The thickness of this formation is variable from a very thin layer in eastern Wisconsin to 500 ft at Joliet, Illinois. St Peter Sandstone is only exposed in the upper Mississippi River valley (Thiel, 1935).

Thiel (1935) conducted a comprehensive study on the sedimentology of St. Peter Sandstone. His results indicated that St. Peter sandstone is extremely well sorted and its particle size distributed in a narrow range. In many samples of St. Peter Sandstone, nearly ninety percent of particle size fall between the range of 125 and 250 micron.

Kamb (1932) ran porosity tests on St. Peter sandstone collected from Twin- cities, Minnesota. His results indicated that the porosity of St. Peter sandstone is in the range of 24.6% to 31.1%, with the average of 28.3%. Dusseault and Morgenstern (1979) conducted porosity measurement test on St. Peter sandstone samples of Minnesota. Their results indicated that St.Peter Sandstone possess 27.0% porosity as an average.

Thiel (1935) conducted chemical analyses on St. Peter sandstone samples taken from different states. His results indicated that St. Peter formation is a pure silica sand.

Quartz constitutes approximately ninety nine percent of St. Peter sandstone. In other words, for all practical purposes the formation can be considered monomineralic (Payne, 1967).

The grains of St. Peter sandstone show different degrees of rounding. In general, the larger grains are more rounded than smaller grains. Very few of rounded grains are spherical. However, many grains are oval, egg-shaped, kidney-shaped, spindle-shaped and conical (Thiel, 1935).

St. Peter Sandstone is uncemented in most parts. In this dissertation, the name St. Peter Sandsone is used for uncemnted part, and cemented St. Peter Sandstone is used for Cemented part.

Due to the homogeneous character of St. Peter sandstone, bedding is conspicuous. However, upon close examination, the bedding planes may be observed (Payne, 1967).

2.1.1. Depositional Environment of St. Peter Sandstone. An environment in which sediments are deposited is called depositional environment or sedimentary environment. Depositional environments are classified as follows (Boggs, 2006)

- Continental (Terrestial) environments (e.g. fluvial, eolian (windblown sediments), lacustrine, glacial)
- Marginal- Marine Environments (e.g. deltaic, beach**)**
- Marine Environments (e.g. shallow marine clastic, deep marine)

Probably one of the most controversial subjects regarding St. Peter sandstone is its depositional environment. There are two views about the depositional environment of St. Peter sandstone. Eolian and/or marine environment are considered as possible depositional environment by geologists.

Winfree (1983) reported that Berkey (1906) is one who believed that St. Peter sandstone deposited under eolian environment. Twenhofel and Thwaites (1919) favored a non-marine depositional environment for St. Peter sandstone. Round grains, sorting and frosting of grains were used as evidence for eolian depositional environment (Winfree, 1983). Dake (1921), however, rejected eolian depositional environment for St. Peter sandstone. He noted that the texture was probably inherited from the origin. He also noted that St. Peter sandstone lacks large scale cross bedding that is typical for eolian sands. He favored a marine depositional environment for St. Peter sandstone based upon fossils and burrows. Dapple (1955) suggested shallow marine depositional environment for St. Peter sandstone based on regional stratigraphy of Wisconsin. Mazzullo and Ehrlich (1983) employed a

combination of Fourier grain-shape analysis and scanning electron microscopy to analyze St. Peter Sandstone in southeastern Minnesota. Their results indicated that there are two grain-roundness types exist in various proportions in all the samples studied: one of them extremely smooth and well-rounded grains, whereas the second is a population of irregular, angular grains. Using Scanning electron microscope examination of quartz surface textures, they stated that the smooth and well rounded type was created during a stage of eolian transport and abrasion, they also stated that the second grain-roundness type is relatively unabraded and was probably transported in less abrasive fluvial environments. Amral and Pryor (1977) studied the environment of deposition for St. Peter Sandstone in southwestern Wisconsin. They concluded that grain-size parameters of the St. Peter Sandstone bear closer resemblance to modern shallow marine shelf sands than to either eolian or beach sediments. Winfree (1983) studied the depositional environment of the St. Peter sandstone of upper Midwest. He used dish-shaped concavities on St. Peter grains and broken cleavage plates as evidences for supporting eolian depositional environment. However, quartz has no cleavage plane. Those "cleavage plates" could be formed during sample preparation. Johnson et al (1989) used partial Hertzian cracks observed on St. Peter sandstone grains as evidence for eolian depostional environment. However, their observation on Hertizan fractures on St. Peter sandstone grains are limited. Moreover, they did not observe the stress trajectory associated with St. Peter Sandstone grains.

2.2. PREVIOUS STRENGTH STUDIES OF ST. PETER SANDSTONE

Although extensive studies have been conducted on both ground control and geotechnical properties of coal, hard rock (e.g. Obert et al., 1946; Krauland and Soder 1987; Sjoberg, 1992), no research was conducted on St. Peter Sandstone from ground control point of view, to the knowledge of researcher.

For over a century, St. Peter sandstone in Twin City, Minnesota have been used in different civil engineering projects. The majority of bridges crossing the Mississippi River in Twin City area are in part supported by St. Peter Sandstone (Payne, 1967). Three dams are located on St. Peter sandstone. St. Peter Sandstone has been used as a foundation in different parts of Twin City. A number of sewer tunnels were excavated in St. Peter Sandstone. A few strength tests were performed in the course of the investigation for these projects. In the 1970's, researchers from University of Minnesota conducted research on St. Peter Sandstone because of their interest of construction of underground parking facilities at the University of Minnesota. The results of these studies are discussed in Sections 2.2.1 and 2.2.2.

2.2.1. Uniaxial Compressive Strength Tests. Payne (1967) compiled engineering studies conducted on St. Peter Sandstone prior to 1967.

He noted that Schwartz (1939) was the first researcher to perform uniaxial compressive strength (UCS) tests on the St. Peter Sandstone. He performed two UCS tests on wet samples, and one UCS test on a dry sample. Twin city Sanitary conducted one test during site investigation on Pigs Eye Lake site (Payne, 1967). Studies on mechanical properties of St. Peter Sandstone continued in the 1970s because of an interest in the design of an underground space in St. Peter Sandstone (Sterling, 1977; Petersen; 1978). Petersen (1978) reports that two sets of UCS tests were performed at the university of Minnesota. In the first set, a UCS test was performed on ten cubic samples, which were prepared using blocks taken from the Mississippi River channel outcrops near the university campus. The second set of tests, however, were performed in-situ during excavation of the underground test room (Table 3.4). Petersen (1978) conducted UCS tests on samples with dimentsion the range of 13 to 305 mm in lenght. He did not investigate the effect of specimens size on

uniaxial compressive strength of St. Peter sandstone. Dittes and Labuz (2002) conducted UCS tests on dry specimens with diameter 50-100 mm. They also performed in-situ pressuremeter tests; the result of which indicated slightly lower value for Young's modulus.

Previous research on mechanical properties of St. Peter sandstone were limited and they were not able to explain the variability in mechanical properties of St. Peter sandstone. In addition, the modes of failure of specimens after the tests were not studied. Furthermore, an appropriate sample preparation for St. Peter Sandstone was not developed. Moreover, previous studies did not investigate the optimum sample size for characterizing the strength of St. Peter Sandstone.

2.2.2. Triaxial Compressive Strength Tests. Triaxial compression tests were performed on St. Peter Sandstone. The aim of these tests was to determine the bearing capacity of St. Peter Sandstone for foundations. Watson (1938) conducted triaxial compression test on St. Peter Sandstone of Twin Cities, Minnesota for Corps of Engineer. His results indicated high friction angle and the lack of cohesion. Payne (1967) reported that Victor Gruen Associates (1961) also ran several triaxial compressive tests on intact St. Peter Sandstone. However, there is no information on the method which was used for their tests. Payne (1967) reported triaxial compression tests on three sets of test samples for site examination of the new Dayton's department store in St. Paul. The results of their test revealed high angles of friction ranging from 48^{O} to 60^{O}. However, Payne (1967) did not report with regard to degree of cementation for specimens tested. The specimens were more likely collected from cemented part of the St. Peter Sandstone. The triaxial tests on St. Peter Sandstone was also conducted by Labuz et al. (1998). Their results indicated high friction angle and lack of cohesion. Dittes and Labuz (2002) performed in-situ pressuremeter tests on wet St. Peter Sandstone. The friction angle obtained from in situ tests were within the range

measured in the laboratory. These research did not investigate the cause of unique shear strength characteristics of St. Peter sandstone (e.g., high friction angle, being coheisonless).

Although the results of previous studies provide useful information regarding the shear strength properties of St. Peter sandstone, they did not investigate the effect of confining stress on axial stress-axial strain behavior of this type of geological material.

2.3. HIGH FRICTION ANGLE OF ST. PETER SANDSTONE AND FRICTION ANGLE

As it was mentioned in Section 2.2, previous triaxial tests indicated that the St. Peter Sandstone is cohesionless and possess very high friction angle. Mohr- Coulomb failure criterion is discussed in Section 2.3.1. Furthermore, the existing theories for high friction angle of St. Peter Sandstone is discussed in Section 2.3.2.

2.3.1. Mohr- Coulomb Failure Criterion. Mohr (1900) presented a theory in which the failure of material is considered as combination of normal stress and shear stress. The relation between normal stress and shear strength can be expressed as

$$\tau = f(\sigma) \tag{2.1}$$

Where τ is shear strength

σ is noral stress

The failure envelope defined by equation (2.1) is not necessarily linear. However, in most cases, the shear stress on failure plane is considered as a linear function of normal stress (Coulomb,1776). This function is written as follows

$$\tau = c + \sigma tan\varphi \tag{2.2}$$

Where c is cohesion

φ is the angle of internal friction

σ is normal stress

τ is shear strength

Eq 2.2 is knowns as Mohr- Coulomb failure criterion.

Figure 2.2 reveals the shear stress versus normal stress based on Mohr- Coulomb failure criterion. The shear strength of geological material when no normal stress is applied is cohesion. The slope of Mohr- Coulomb failure envelope is the angle of internal friction.

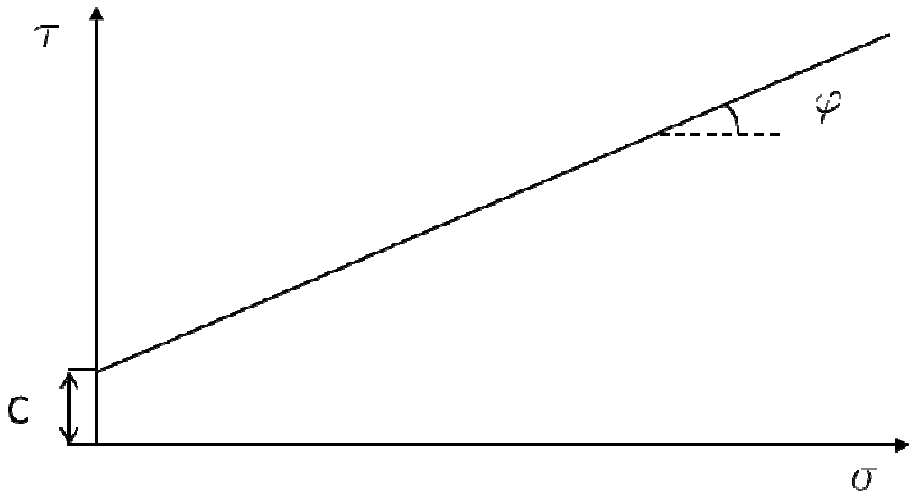

Figure 2.2. Mohr-Coulomb failure envelope

Typical values of the angle of internal friction is given in appendix B. As mentioned in section 1.2, the friction angle for the St. Peter sandstone typically ranges from 57˚ to 63˚. which is 15˚ to 20˚ higher than the highest friction angle we know for geotechnical materials. This raises a fundamental question regarding the cause of this unique behavior in St. Peter Sandstone.

2.3.2. Existing Theories For High Friction Angle of St. Peter Sandstone. In the 1970s, the research was carried out on geotechnical properties of the oil rich sandstone

comprising Athabasca tar sands because of the growing interest in this giant energy resource (Miligan; 1976; Dusseault, 1977; Dusseault and Morgenstern, 1979). Dusseault and Morgenstern (1979) introduced the term “locked sands” for a group of geological material. Locked sands are cohesionless with high friction angle.

Dusseault and Morgenstern (1979) suggested that “penetrative contact texture” of these material observed in optical microscopy is responsible for high friction angle of this group of geological material. Cresswell (1999) proposed a conceptualized model for locked sand. He hypothesized that grains of locked sands are locked together by interlocking asperities. This model is not applicable to St. Peter Sandstone because the grains of St. Peter Sandstone are mostly rounded and those “asperites” are not significant enough to cause such a high friction angle. Furthermore, Dusseault and Morgenstern (1979) also mentioned that the interlocked texture of St. Peter Sandstone is subtle. Hence, “penetrative contact surface” is not significant for St. Peter Sandstone. Therefore, high friction angle of the St. Peter Sandstone is less likely caused by “penetrative contact surface”. This study reveals that the cause of the extremely high friction angle is primarily due to the particle structure of the St. Peter Sandstone.

3. UNIAXIAL COMPRESSIVE STRENGTH OF ST. PETER SANDSTONE

3.1. INTRODUCTION

The uniaxial compressive strength is a basic parameter for characterizing the strength of geological materials and used extensively for a variety of engineering design purposes in mining, civil, and geotechnical engineering. St. Peter Sandstone is a unique geological material that lies in a transition zone between soils and rocks. It resembles typical soils for its particle structure. Its behavior, however, is similar to rocks for its elastic property.

The two most distinctive properties of the St. Peter Sandstone are the extremely high friction angle (within a range of 57˚ - 70˚), and the cohesionless particle structure. As a result of these unique properties, the strength characteristics of the St. Peter Sandstone differ significantly from other kinds of rocks extensively studied in mining, civil and geotechnical engineering.

This chapter looks into key issues, which are particularly relevant to the St. Peter Sandstone. The first one is the sampling technique. A unique problem faced by studies examining the St. Peter Sandstone is the severe impact of the disturbance caused by the standard sampling techniques. Therefore, minimizing the disturbance caused by sampling techniques and procedures is of particular importance for determining the strength of the St. Peter Sandstone. It is followed by analyzing the strength characteristics of the uniaxial compressive strength for St. Peter Sandstone. First, the failure mechanics will be discussed in terms of the laboratory test result, the field observations, and theoretical considerations. It is shown that the failure mechanics are fundamentally governed by the basic mechanical properties of the St. Peter Sandstone.

A factor that has a profound impact on the test result of the uniaxial strength of the St. Peter Sandstone is the size of specimens. The uniaxial compressive strength is not an

abstract concept. It is defined with the associated test condition. Specimen size is one of them. In the course of this study, the size effect was studied extensively based on both our test results and the results from previous research. As a result of this study, the optimum specimen size was identified. Following the discussion of the size effect, the shape effect of test specimen will be briefly discussed. One of the most important achievements of this project is the demonstration that the strength of the St. Peter Sandstone is fundamentally governed by its particle structure. This study was begun with the uniaxial compressive test. However, since a comprehensive and in-depth discussion on this issue requires the knowledge of the triaxial test, the full discussion will be presented in the Chapter 4.

The elastic properties, namely, Young's modulus and Poisson's ratio, will also be discussed in this chapter as these two important parameters are conventionally obtained from the uniaxial compressive tests. The discussion will be based on the results from this investigation, as well as those of the previous research. The last topic to be discussed in this chapter is the strength of the St. Peter Sandstone with cementation.

3.2. SAMPLE PREPARATION

A particular problem encountered in St. Peter Sandstone research is the difficulty to prepare cylindrical specimens. Cylindrical specimens are conventionally prepared by coring, using this technique. However, it is almost impossible for the St. Peter Sandstone. The only successful attempt was an on-site investigation where a NX diamond core barrel was used in conjunction with a moderately dense drilling mud (Payne, 1967). Early researchers also tried unconventional methods for cylindrical samples, such as split tube and Shelby tube samplers, and none of them were successful (Payne, 1967).

The results of this study also show that coring uncemented St. Peter Sandstone is virtually impossible. At the Pattison mine site, Clayton, Iowa, where this research was

conducted, the cumulative drilling length in the St. Peter formation for the geological prospection is over 400 meters and no single core piece utilizable for the uniaxial test was obtained.

Coring cylindrical samples from St. Peter sandstone blocks was also tried at the rock mechanics laboratory, Missouri University of Science and Technology, and it failed miserably. Figure 3.1 shows an example of the failed attempts.

Figure 3.1. An unsuccessful coring operation for St. Peter sandstone

In the picture the core barrel was just lifted from the cored sample. As it can be seen, the sample was badly damaged and by no means could be used for any testing purposes. The fragile nature of coring St. Peter sandstone is also evident from the reason that stopped this coring process: the sample block was broken into two pieces during the operation. One piece

of this broken block can be seen on the left side of the picture. The best sample from our coring operation is a disk with the thickness less than 25 mm (Figure 3.2).

Figure 3.2. The best sample obtained from the coring operation
(a disk with the thickness less than 25mm.)

The difficulty encountered in obtaining cylindrical specimens is not just operational; it is much more fundamental. The underlying problem revealed by this difficulty is the incompatibility of the material property of the St. Peter Sandstone and the standard sample preparing practice that is recommended by ASTM (ASTM, D7012-14) and ISRM (1981), and closely followed by the engineering community.

A practice adopted by St. Peter Sandstone researchers from early days (Schwartz, 1939) is to use cubic or rectangular type of specimens. This practice is undoubtedly an important and necessary step for the St. Peter Sandstone research. It is, however, important to note that this step alone is not enough. In order to minimize the disturbance caused by the

conventional sampling techniques, a close attention must also be paid to cutting and grinding operations.

Various handheld and small table saws were utilized for cutting operations in this investigation. Handheld saws, including both powered and non-powered, were used primarily for cutting sand blocks (Figure 3.3). There are two advantages to use handheld saws. First, the disturbance is significantly less than those caused by large blade saws that are conventionally used for this purpose. Secondly, handheld saws are flexible and easy to handle, which is particularly important when the sample block is irregular and the required cutting pattern is complex.

Small table saws were also utilized in this investigation. Table saws can be either a blade saw or a chain saw. Table saws were mainly used for shaping the loading ends of specimens. For the uniaxial compressive test, the loading ends should be parallel and smooth, which are conventionally achieved by grinding operations. For the St. Peter Sandstone specimens, grinding is a much more challenging operation, which may not produce a consistent result. Because of this the cutting operation by table saws is critical, and the quality of the specimen ends prepared by this operation must be of a high quality. Figure 3.4 shows a table saw operation.

In addition to handheld and small table saws, water jet was also tested for trimming specimens from a sandstone block (Figure 3.5). A distinct advantage of the hydraulic cutter is that it causes almost no vibration, and as a result, the damage to the sample caused by cutting is minimum. The problems are the complicated operating procedure and the need for trained and skilled operators.

Figure 3.3. Processing a sandstone block by a hacksaw

Grinding is a difficult operation for the St. Peter Sandstone. There are two particular problems. The first one is the stress concentration caused by the grabbing device that is conventionally used to hold specimens during the grinding operation. Our solution to this problem is to use several steel blocks to hold the specimen in place as shown in Figure 3.6. In the figure, the specimen was first confined by two L shaped steel blocks (white), and this arrangement was further reinforced in the longitudinal direction by two large steel blocks. The other problem is the surface chipping by grinding wheels, that is, the surface under grinding can be easily chipped by the grinding wheel even with a minimum feeding. Because of these problems, the function of grinding for the St. Peter Sandstone is severely limited.

Figure 3.4. Shaping specimen ends by a table saw.

Serious disturbance to specimens may also occur prior to the laboratory work at the stage when sample blocks were formed and collected. For instance, sample blocks may contain fractures caused by blast vibrations during a blasting operation. Therefore, care has to be taken during the process of collecting sample blocks because of very friable condition of St. Peter Sandstone. Sample blocks taken from the field should be carefully inspected to ensure that they are free of major flaws and visible fractures.

The other important factor that has to be considered during the sample collection and preparation stages is the size of specimens. An important finding made in this investigation is the optimum specimen size for the uniaxial compressive test for the St. Peter Sandstone, which is 51 mm. Hence, an important consideration during the sample block collection stage is whether the block under the inspection is suitable for producing 51 mm specimens.

Figure 3.5. Trimming sand blocks by hydraulic cutter.

Particle structure is the other important factor in t of St. Peter Sandstone's strength. St. Peter Sandstone 's strength is fundamentally governed by its particle structure. The particle structure of St. Peter sandstone can be characterized by either particle size distributions or porosity. For instance, the porosity for the St. Peter Sandstone varies from 24% to 31%. The results of this study show that the specimens with these porosities will show very different strength characteristics. For this reason, it is important to group specimens and to document the origin of each group so that the strength data can be lined directly to the sandstone structure. This is important not only for a general understanding of the strength variation of the St. Peter Sandstone, but also for how to apply the strength data for specific engineering problems.

Figure 3.6. Grinding a St. Peter sandstone specimen

In conclusion, the sampling process for the St. Peter Sandstone is governed by the special properties of the St. Peter Sandstone, which is significantly different from the standard methods recommended by (ASTM, D7012-14) and ISRM (1981). There are three outstanding issues for preparing and processing the St. Peter Sandstone specimens, which are minimizing the disturbance by the sampling technique, using the optimum specimen size, and data management for linking strength and particle structure data.

First, it is extremely important to note that the St. Peter Sandstone is extremely sensitive to the vibrations generated by the mechanical processing techniques because of the cohesionless property of the St. Peter Sandstone. The first principle for preparing the St. Peter Sandstone specimen is therefore to minimize the disturbance caused by the processing techniques. Hence, coring should be excluded. Furthermore, cutting and grinding operations should be carried out with a great caution as discussed earlier. Severe disturbances may also occur at the stage when the sample blocks are formed and collected. Therefore, the sample blocks should be carefully inspected to avoid major flaws and visible fractures before they

are brought back to the laboratory.

The second one is the specimen size. The optimum size that will yield most stable and representative values for the St. Peter sandstone is 51 mm. Hence, 51 mm or similar size of specimens should be used if possible. ASTM specifies the optimum core diameter as 54 mm. The results of this study show that the strength of the St. Peter Sandstone will be seriously underestimated if a size significantly smaller than 51mm is used.

As discussed earlier, the strength of the St. Peter Sandstone is fundamentally governed by its particle structure. It is therefore important to link the strength data to the data on particle structures. This requires a special data management effort: specimens from the same location or even the same block should be grouped and documented so that the strength data for these specimens can be analyzed in terms of the associated particle structure. This information is critical for both theoretical studies and practical applications.

3.3. TEST RESULT AND FAILURE MODE

A total of 95 uniaxial compressive tests were carried out during this investigation. All samples were originally collected from the Pattison mine site, Clayton, Iowa, and prepared in the rock mechanics laboratory at Missouri S&T according to the method discussed in the previous section. Part of these specimens is shown in Figure 3.7. Detailed information of these test specimens is given in Appendix A.

The tests for all 95 specimens were successful and the results are summarized in Table 3.1. There are six sample size groups, which are 12, 25, 38, 51, 76, and 102 mm. The adoption of these size groups is to facilitate the study of the sample size effect.

Figure 3.7. Specimens ready for uniaxial compressive test

Table 3.1. Laboratory Testing results for Uniaxial Compressive Strength

Nominal Size(mm)	Individual Results (MPa)	Mean (MPa)	Standard Deviation(MPa)
12	0.10 0.17 0.23 0.24 0.31 0.43 0.50 0.81 0.81 0.87 0.95 1.03 1.12 1.22 1.29 1.30 1.43 1.45 2.03 2.06 2.12 5.38	1.18	1.12
25	0.24 0.55 0.71 0.72 0.82 1.22 1.31 1.33 1.78 1.83 1.95 2.23 2.31 2.90 3.79 4.22 4.98 5.04 6.06 6.36 7.27 11.78	3.16	2.83
38	0.82 0.82 0.93 2.02 2.43 2.48 2.76 2.81 2.91 3.33 3.74 4.37 4.60 4.61 4.95 5.38 6.59 7.22 8.13 8.93 9.18 15.02	4.73	3.39
51	1.80 2.13 2.20 3.00 3.25 3.43 3.50 3.60 3.66 3.81 3.81 4.14 4.21 4.37 5.32 7.00 8.69 8.95 10.63 12.85 21.99 24.55	6.68	6.10
76	1.53 1.84 2.83 5.25 17.67	5.82	6.78
102	0.95 4.36	2.65	2.41

There are two distinctive features that can be immediately observed from the test results. The first one is the large variation of the strength data. The uniaxial compressive strength varies from 0.1 to 24.55 MPa and the standard deviation for each size group is at the same order of the associated mean. The large variation is not a surprising feature for the St.

Peter Sandstone as it also characterizes the results from the previous studies (Payne, 1967; Petersen, 1978).

The large variation is due to many reasons, and the major ones are the friable nature of the rock because of the cohesiveless property, sample size, sample shape, and sand particle structure. An important goal of this investigation is to establish a better understanding of the mechanics of these factors so that the uniaxial compressive strength can be determined more reliably.

The other distinctive feature of the test result is the failure mode. The failure mode for the St. Peter Sandstone is very different from those exhibited by conventional geological materials. Six tested specimens are presented in Figure 3.8 for illustrating the main features of the failure mode that is commonly observed for the St. Peter Sandstone.

There are two prominent failure formations for the St. Peter sandstone: vertical splitting and steeply dipped shearing. Figure 3.8a is a typical example of vertical splitting. Vertical splitting can also be observed in Figures 3.8c and 3.8d. In Figure 3.8c, vertical splitting was developed with steeply dipped shearing, showing a compound formation. In Figure 3.8c, vertical splitting is shown by the fact that the remaining pieces are all broken vertically. Vertical splitting is largely due to the cohesionless property of the St. Peter sandstone, which makes specimens extremely vulnerable when they have to expand horizontally due to the compression in the vertical direction. Although vertical splitting is also observed for other geological materials, it is not a dominant failure formation and is mostly caused by local anomalies.

Steeply dipping shearing is the dominant failure formation for the St. Peter Sandstone observed from test results. Figures 3.8b, 3.8c, 3.8d, and 3.8e are the examples of this failure formation. As it can be seen from these examples, the shearing planes are very steep, ranging

from 70˚ to 80˚. These very steep failure planes are the confirmation of the unusually high friction angle, in the range of 57˚-63˚, reported for the St. Peter sandstone (Watson 1938; Corps of Engineers, 1958; Labuz et al., 1998; Dittes and Labuz, 2002). According to the Mohr-Column failure criterion, the angle of failure planes (measured from the horizontal plane) under the condition of the uniaxial compressive test is $45 + \varphi/2$, where φ is a friction angle (Obert and Duvell, 1967). If we take an average friction angle of 60˚, the angle of these failure planes predicted by the Mohr-Column failure criterion is 75˚, which is exactly what was observed. It is very interesting to note that joints in the St. Peter Sandstone formation are also steeply oriented.

The other important feature of the St. Peter Sandstone is its irregular pattern of failure locations. For most geological materials, there usually exists a pattern. As an example, some Indiana limestone specimens tested by students at the Missouri University of Science and Technology for their laboratory studies are shown in Figure 3.9. It is obvious from the figure that there is a clearly defined pattern: fractures start from the edge of one end and extend to the other end following the angle defined by the Mohr-Column criterion.

For the St. Peter Sandstone, it appears that fractures can start at any location. In Figure 3.8a, vertical splitting occurred at a corner. In Figures 3.8b and 3.8c, a sharp wedge, formed by two steep shearing surfaces, developed in the middle of the specimen. Figures 3.8d and 3.8e indicate failure planes developed across the specimens. Figure 3.8d reveals a complex combination of vertical splitting and steeply dipped shearing. Figure 3.8e shows steeply dipped shearing is a dominant failure formation. It was hypothesized that irregular pattern reflects the friable nature of the St. Peter Sandstone caused by its cohesionless property.

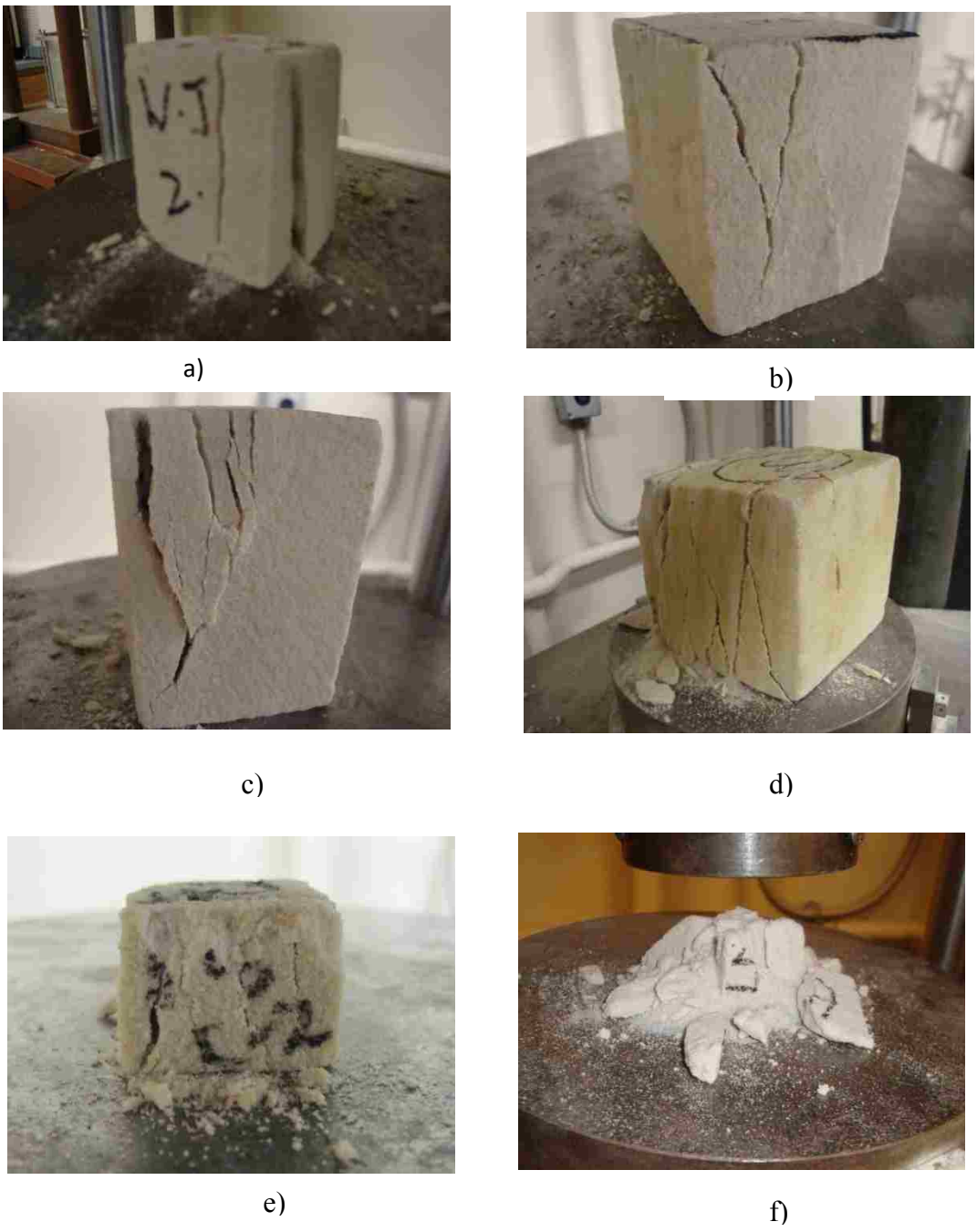

Figure 3.8. Failure modes observed from the uniaxial compressive tests of St. Peter Sandstone specimens

Figure 3.9. Failure mode associated with Indiana limestone

Failures for the St. Peter Sandstone specimens are much more sensitive to local conditions. Therefore, failures are most likely to start at the locations with local anomalies or preexisted fractures. This is also an important reason responsible for the large variation of the uniaxial compressive strength.

In summary, the characteristics of the failure mode are fundamentally governed by the basic properties of the St. Peter Sandstone. Vertical splitting is a result of the cohesionless property. However, steeply dipping shearing is caused by the high friction angle associated with the St. Peter Sandstone. Irregular failure pattern is a reflection of the high sensitivity to local weaknesses for the test condition.

Failure characteristics provide direct evidence on the engineering behavior of the St. Peter Sandstone. Vertical splitting and irregular failure pattern explain in part the large strength variation associated with the St. Peter Sandstone; and steeply dipper shearing

confirms the high friction angle of the St. Peter Sandstone determined by other laboratory methods.

3.4. SAMPLE SIZE EFFECT

Size effect refers to the impact of the specimen size on the strength obtained from the test. This section discusses the size effect exhibited for the St. Peter Sandstone and the optimum specimen size for the uniaxial compressive test for the St. Peter Sandstone.

3.4.1. Typical Specimen Size Effect for Geological Materials. A general trend for most rock materials is that the strength decreases with the increase of the specimen size. Figure 3.10 shows this effect for iron, diorite, and coal (Bieniawski, 1984). The underlying mechanics for this trend is that the potential for a larger rock block to contain defects or fractures, which may significantly reduce the strength, is much higher than a smaller block. In rock mechanics, this phenomenon is also known as the scaling effect.

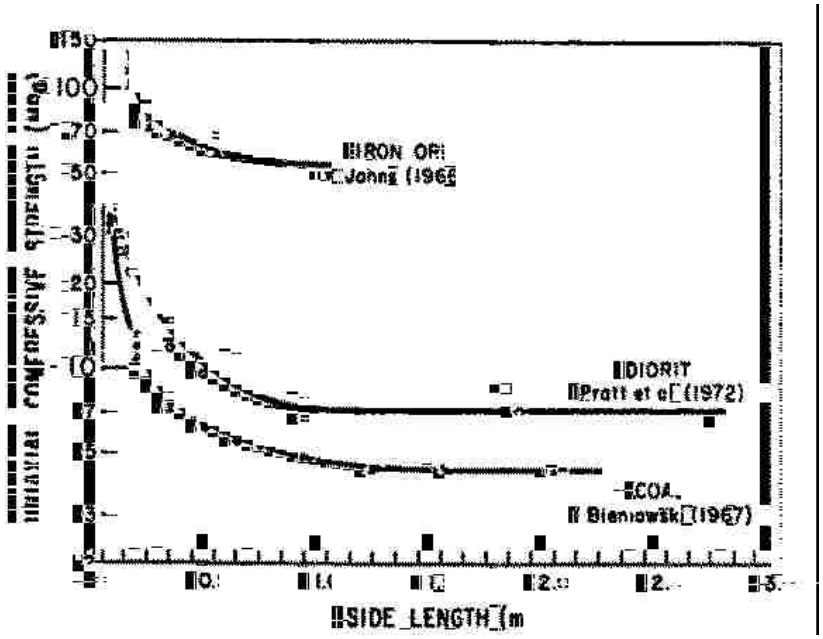

Figure 3.10. Variation of rock strength with specimen size (Bieniawski, 1984)

3.4.2. Size effect for St. Peter sandstone determined from this investigation. The uniaxial compressive strength of the St. Peter sandstone is also seriously affected by the specimen size despite the large variation (Table 3.1). Figure 3.11 further illustrates this effect. It is clear from the figure that the mean strength increases gradually with the sample size until it reaches its peak at the sample size of 51 mm. The strength then begin to decrease gradually.

The size effect depicted in Figure 3.11 for the St. Peter Sandstone differs significantly from the size effect shown in Figure 3.10. The scaling effect that is responsible for the size effect shown in Figure 3.10 is undoubtedly an important factor that also affects the strength of the St. Peter Sandstone. The fact that the strength decreases for the large samples as observed in this study is most likely due to this reason. For the St. Peter Sandstone, however, this is not the only mechanics which causes the size effect. The other one, which is much more critical with regard to the St. Peter Sandstone, is the disturbance caused by the sample preparation process.

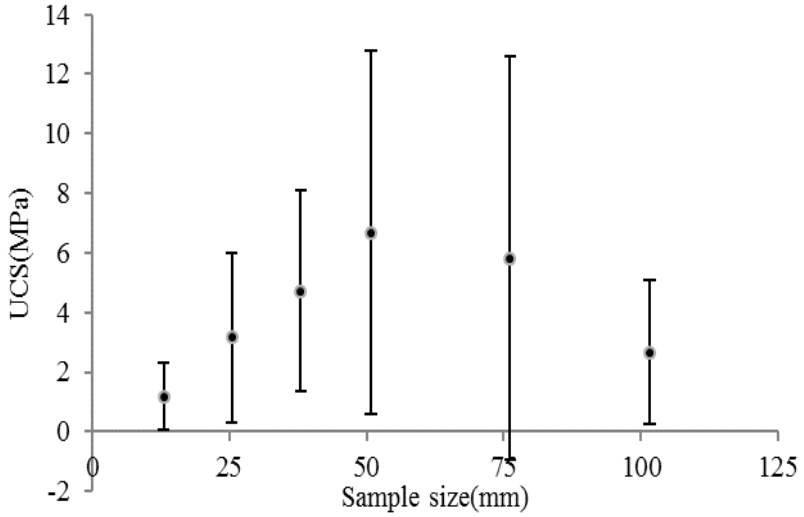

Figure 3.11. Effect of specimen size on the UCS of St. Peter Sandstone

As discussed in section 3.1, one of the most important factors that can significantly alter the test result is the disturbance caused by the sampling techniques. The vibration caused by cutting and grinding operations is the primary source of the disturbance. As the St. Peter Sandstone is cohesionless, it is extremely vulnerable to any vibrations, especially for small specimens. This is why the strength for very small specimens, such as 13 and 25 mm specimens, is significantly lower.

3.4.3. Size Effect for St. Peter Sandstone Observed from Previous Investigations. The size effect for the St. Peter Sandstone, as determined from this investigation, can also be observed from and confirmed by the previous studies. The studies carried out by Petersen (1978), Sterling (1978), and Yardley (1978) are particularly significant in this regard. Howere, they did not analyze their results in terms of size and shape effects. All these studies were related to the underground development in St. Peter formation in Minneapolis/St. Paul area.

Yardley (1978) studied the uniaxial compressive strength for a set of 10 specimens. The size of these specimens were between 25 and 57 mm.

The results are listed in Table 3.2. It is apparent from the table that the strength increases with the increase of the specimen size. This trend is consistent with the trend observed from our test result.

The study carried out by Petersen (1978) was to determine the strength that could be used for the pillar design purpose. Petersen performed 33 tests with the sample's size varying from 13 to 305 mm. The result is summarized in Table 3.3.

To demonstrate the size effect, Petersen's test results are also plotted in Figure 12. It is evident from the figure that Petersen's data shows a similar trend as observed in our tests with the strength peaked at the specimen size of 51m.

Table 3.2. Uniaxial compressive strength (Yardley, 1978)

Size (mm.)		Equivalent* Width(mm)	UCS(MPa)
Width	Length		
25	25	25	2.14
32	32	32	1.93
51	38	44	2.34
51	44	48	2.83 3.03
64	38	48	3.31
60	51	49	3.93
64	51	55	3.86
57	51	57	3.72
64	51	54	3.52

* Equivalent width is the square root of the product of specimen width and length.

Table 3.3. Uniaxial Compressive Strength of St. Peter sandstone (Petersen, 1978)

Nominal Size(mm)	Specimen's shape	UCS (MPa)	Mean (MPa)	Standard Deviation (MPa)
13	Cube	1.03 1.28 1.38 1.59 2.00 2.07 2.28	1.66	0.46
25	Cube	1.45 1.59 1.59 1.79 2.38	1.76	0.37
38	Cube	2.34 2.48 2.55 2.55 2.96 3.03	2.65	0.28
51	Cube	3.38 4.21 4.76 4.96	4.33	0.71
51	Cylinder	2.86 3.14 3.48 3.69 3.96 4.07 4.31 5.69 6.69	4.21	0.52
305	Cylinder	3.59 3.79	3.69	0.15

In addition to the general trend, the study by Petersen (1978) was also unique for two specific features. The first one is that the 51 mm size for specimens includes both cubical and cylindrical shapes. It is very interesting to note that the mean strengths for these two group specimens are very close, which are 4.33 MPa for cubical specimens and 4.21 MPa for cylindrical specimens. The second feature is that two very large cylindrical specimens were

tested. The diameter for these two specimens is 305 mm, the largest specimen size that has been reported so far for the St. Peter sandstone. It is also interesting to note that the mean strength for these two specimens is 3.69 MPa, a value that is less than the strength for 51 mm specimens

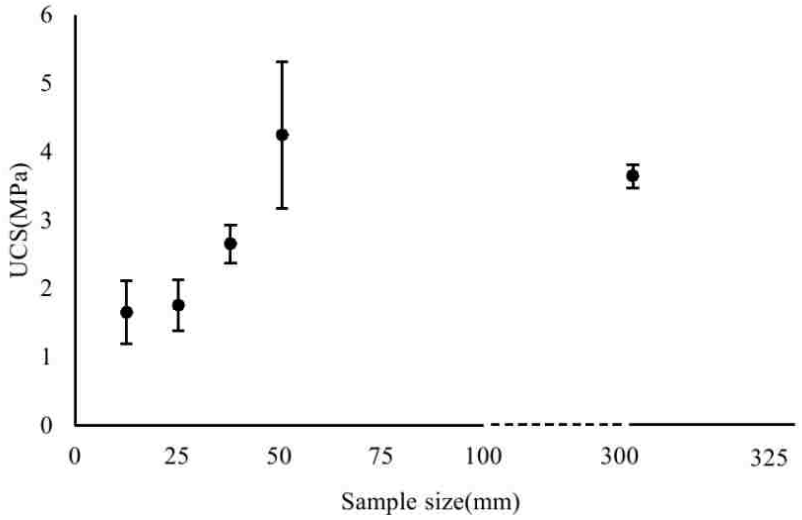

Figure 3.12. Effect of specimen size on UCS of the St. Peter sandstone (Petersen, 1978)

The tests carried out by Sterling (1978) also have several very interesting features. The first one is the test condition. The tests were carried out in the field during the excavation of the underground test room (Sterling, 1978). The specimens were rectangular in shape and formed in-place with a chain saw. The axial load was provided by a hydraulic jack braced against the roof. The sample size was large, ranging from 190 to 211 mm, because of in-situ test condtion. The uniaxial compressive strength obtained from this field test ranges from 1.43 to 6.83 MPa with an average of 3.80 MPa (Table 3.4).

Table 3.4. Uniaxial compressive strength by Sterling (1978)

Test No	Size (mm)			Equivalent width(mm)	Height/Width ratio	UCS (MPa)
	Width	Depth	Height			
1	292	152	279	211	1.32	4.56
2	305	152	178	216	0.82	6.83
3	216	203	229	209	1.09	2.31
4	203	203	254	203	1.25	1.43
5	203	229	203	216	0.94	3.19
6	229	229	241	229	1.06	5.82
7	203	203	165	203	0.81	3.10
8	178	203	254	190	1.34	1.60
9	191	203	178	197	0.90	3.22
10	203	203	102	203	0.50	5.92

In comparison with the result from Petersen (1978) (Table 3.3), the average strength determined from this field test is very close to the strength of the largest specimens used by Petersen (1978). It is interesting to note that the strength of 3.80 MPa, determined by the field test, is still somewhat lower than the strength for 51 mm specimens determined by Petersen (1978).

The second very important feature that can be observed from Sterling's data is the shape effect, which will be discussed in section 3.5.

3.4.4. Optimum Specimen Size for the Uniaxial Compressive Test for St. Peter Sandstone. The studies carried out by Petersen (1978), Sterling (1978), and Yardley (1978), as reviewed in the previous section, are the confirmation of the specimen size effect determined by this investigation. A particular significance of this work is that it lays a foundation for determining the optimum specimen size for the St. Peter Sandstone.

It is understood from the discussion of the specimen size effect that the uniaxial compressive strength is not an abstract concept; but rather it is intimately related to the specimen size. Thus, the strength obtained from the uniaxial compressive test must refer to

the size of the specimen.

There are two commonly adopted standards: one by American Society for Testing and Materials (ASTM) and one by International Society for Rock Mechanics (ISRM). The specimens suggested by both institutions are right circular cylinders with very similar dimensions. For ASTM cylindrical specimens shall have a height to diameter ratio of 2.5-3.0 and a diameter not less than 54 mm (ASTM D7012-14). For ISRM the suggested height to diameter ratio is 2.0 to 2.5 with a diameter that is not less than 47 mm (ISRM, 1981). These suggested specimen dimensions are based on both theoretical and practical considerations. For instance, both standards specify the lower limits of the specimen size, which are 47 and 54 mm, respectively. An important consideration for this limit is the scaling effect as the strength for a small size specimen could be significantly higher, as illustrated in Figure 3.10.

The optimum specimen size for the St. Peter Sandstone should be the one that would minimize the negative impact that is directly related to the specimen size while it is economically attainable. It is understood from the earlier discussion that the size effect exhibited by St. Peter Sandstone specimens is governed by two factors: the disturbance caused by sampling techniques and the scaling effect. Specimens of the St. Peter Sandstone are particularly vulnerable to the disturbance caused by sampling techniques, and this is especially true for smaller specimens. Thus, the strengths for smaller specimens are significantly lower for larger specimens. For specimens with any size larger than 50 mm, the strengths are significantly lower. This is caused by both scaling effect and the disturbance caused by sampling techniques. In addition to the theoretical advantages of 50 mm specimens, the results of this study has shown that specimens with this size are much easier to process.

3.5. SAMPLE SHAPE EFFECT

The shape here is defined as the ratio of specimen height to specimen diameter (width), or height/width ratio. The shape of specimens can affect the test result significantly. If a specimen is too thin, it may lose its stability due to bending. If it is too short, the tested strength can be much higher due to the constraints exerted by the test system at the specimen ends. To minimize the bias caused by the shape of specimens, ASTM suggested a ratio range of 2.5-3.0 (ASTM D7012-14) and ISRM suggested a ratio range of 2.0-2.5 (ISRM, 1981).

A unique feature that can be observed from the study carried out by Sterling (1978) is the shape effect of the St. Peter Sandstone (Figure 3.13).

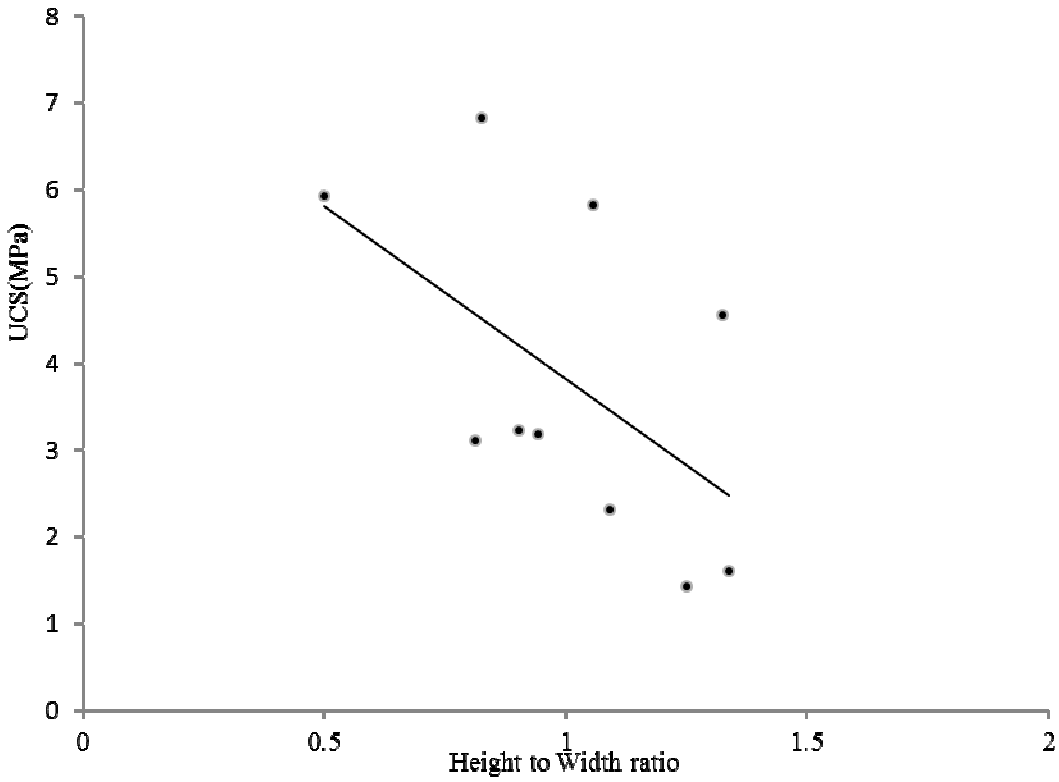

Figure 3.13. Shape effect for the UCS of St. Peter Sandstone (Sterling, 1978)

Although the data is somewhat scattered, the trend is apparent: the strength decreases

with the increase of the height/width ratio. This result shows that the tested strength will be higher for the specimens with a low height/ width ratio. It is difficult to prepare specimens with a height/width ratio greater than 2, because St. Peter Sandstone is friable. Practically, cubic specimens are widely used. However, according to the shape effect demonstrated in Figure 3.13, specimens with the ratio less than 1 should be avoided if possible.

3.6. ELASTIC PROPERTIES OF ST. PETER SANDSTONE

3.6.1. Analysis of the Young's Modulus and Poisson's Ratio. The Young's modulus and Poisson's ratio were evaluated for the St. Peter Sandstone during this investigation. Six specimens were measured for the Young's modulus and four of them were also measured for the Poisson's ratio. The basic data of these specimens and the test results are summarized in Table 3.5. It is noticed that these six specimens originated from two sandstone blocks, 1S and 6AR. The main differences between these two sandstone blocks are that 1) 1S is lack of fine particles associated with 6AR, and 2) 1S is somewhat coarser than 6AR. The details on the particle structure difference between these two sandstone blocks will be given in Chapters 5 and 6.

Table 3.5. Elastic properties of the St. Peter Sandstone

Sample ID	Dimension (mm)	UCS(MPa)	Young's modulus(GPa)	Poisson's ratio
1S-2	52×49×81	3.50	2.76	0.02
1S-4	52×49×92	3.81	2.29	0.03
1S-3	51×51×79	3.43	2.50	0.07
1S-6	50×49×85	2.20	1.79	0.05
6AR-3	50×48×52	4.21	1.33	---
6AR-6	54×53×61	2.13	1.43	---

The stress-strain curves for the tests are presented in Figures 3.14 and 3.15. There are three observations regarding the Young's modulus. First, all stress-axial strain curves are

linear or near linear till they approach the failure stage, which is a typical stress-strain characteristic for brittle-elastic materials. Furthermore, the test results are quite consistent. The standard deviations for 6AR specimens and 1S specimens are only 0.07 and 0.41 GPa, respectively. Finally, it is noticed that the Young's modulus for 1S specimens is significantly higher than that for 6AR specimens. The mean values of the Young's modulus for these two groups are 2.33 and 1.38, respectively.

The Poisson's ratio is a function of both axial and lateral strains. In order to have a perspective view on this parameter, understanding the behavior of stress-lateral strain curves is essential. For the stress-lateral strain curves presented in Figure 3.15, the lateral strain appears to have a three-stage development process. At the initial stage, which may cover the first 40 – 40% loading range, the lateral strain is very small and the stress-lateral strain curve is almost a perfect straight line. For instance, if stress considered 1.50KPa in Figure 3.15b as the end point of this range. The lateral strain for the second stage is larger than that for the first stage, but still small. The stress-lateral strain curve for this stage may still be considered linear eventhough it begins to show the nonlinear behavior. This stage ends at a point with a sudden change of the stress-lateral strain curve, which signals the beginning of the third stage. For the stress-lateral strain curve Figure 3.15b, the stress level of 2.46 KPa can be considered this point. The rapid increase of the lateral strain during the third stage indicates that the specimen is heavily fractured, or in a failure stage. This conclusion can also be confirmed by the stress-axial strain curve at the corresponding stage, which is either ended interruptedly as shown in Part a or becomes highly nonlinear shown in Figure 3.15d.

The elastic parameters were also measured by Petersen (1978), Sterling (1978), and Dittes and Labuz (2002). Their results are given in Table 3.6. For comparison purpose, the results from this investigation are also included in the table. The Young's moduli determined

by all these investigators are in similar ranges.

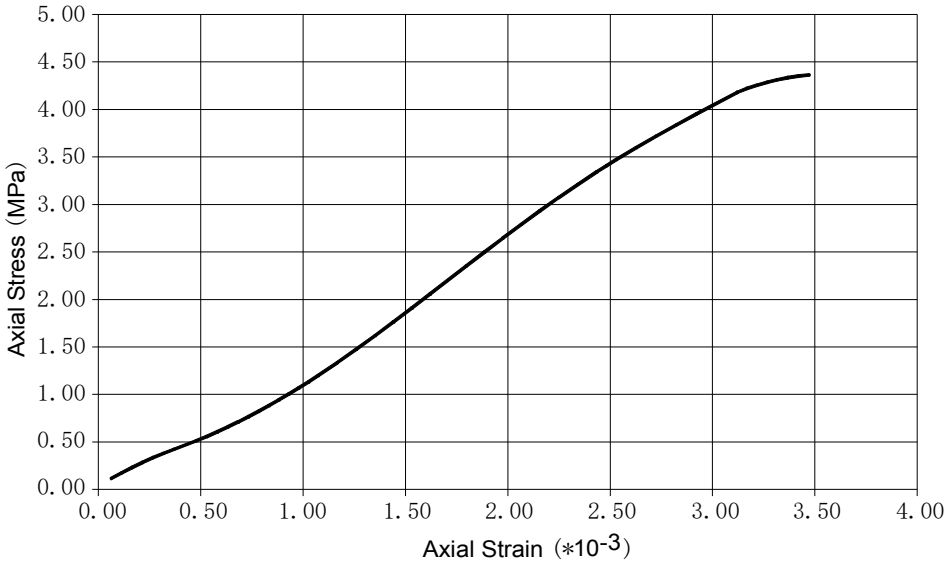

a) Stress-strain curve for St Peter sandstone specimen ID: 6AR-3

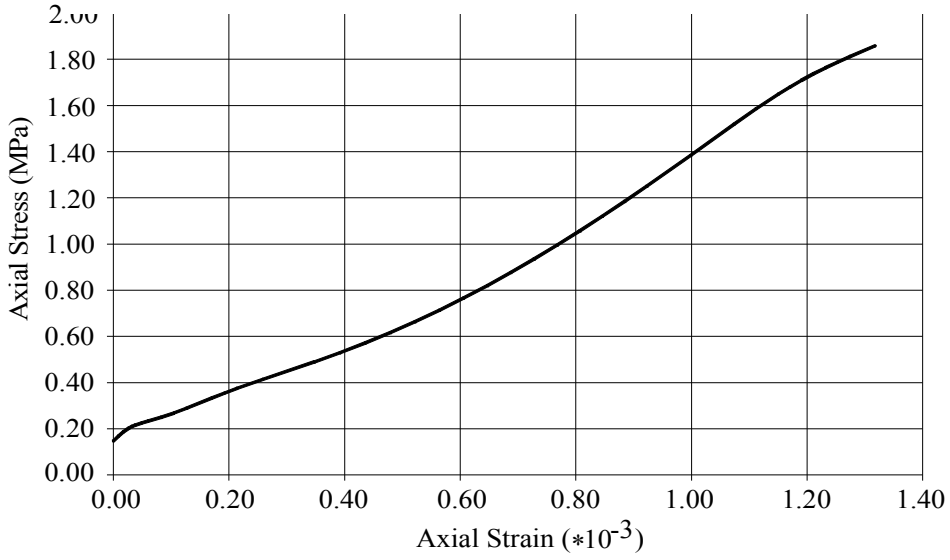

b) Stress-strain curve of St Peter sandstone specimen ID: 6AR-6

Figure 3.14. Stress-strain curves for 6AR specimens

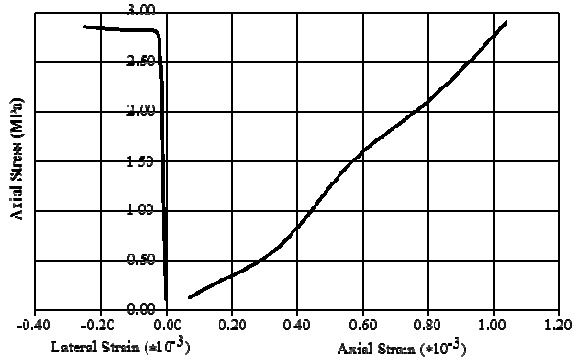

a) Stress strain curve Specimen Id:1S2

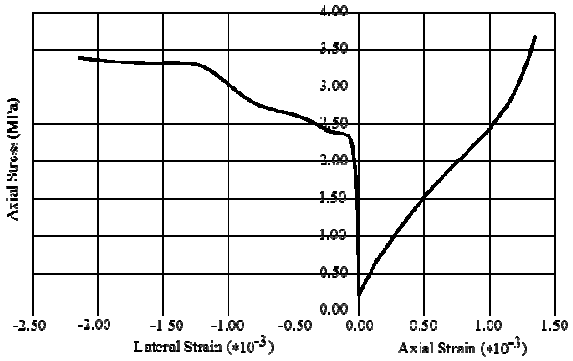

b) Stress strain curve Specimen Id:1S3

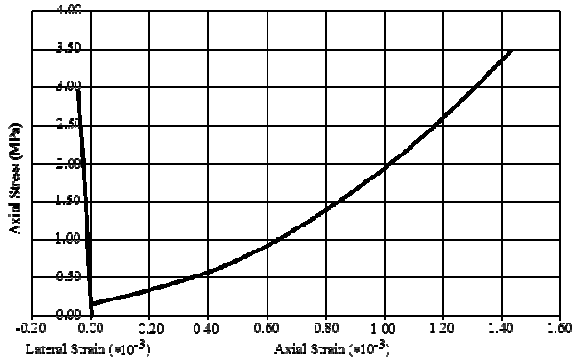

b) Stress strain curve Specimen Id:1S4

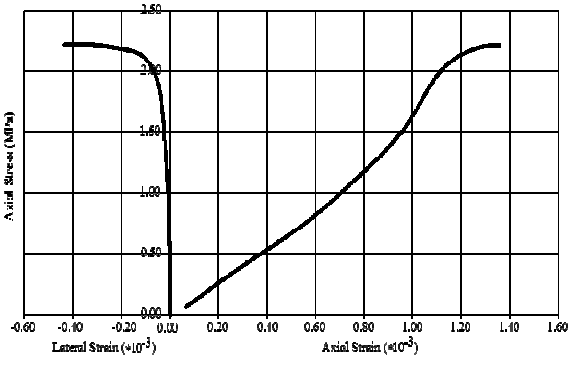

c) Stress strain curve Specimen Id:1S6

Figure 3.15. Stress-strain curves for 1S specimens

Table 3.6. A comparison of the Elastic properties of the St. Peter Sandstone

Source	UCS (MPa)	Young's Modulus Range (GPa)	Young 's modulus Mean (GPa)	Poisson's ratio
Dittes and Labuz (2002)	0.60-2.00	0.40-2.00	1.10	0.20-0.33
Petersen (1978)	2.34-6.69	0.90-1.54	1.16	---
Sterling (1978)	1.43-6.83	0.86-4.27	2.23	---
Missouri University of Science and Technology	1.80-24.55	1.30-2.70	2.00	0.02-0.07

The Poisson's ratio, as determined by Dittes and Labuz (2002), is much higher than that observed from this investigation. Only by considering the linear portion, it seems that Poisson ratio should be much lower according to our data. It is noticed that their high range

of 0.33 is typically associated with a relatively “soft” material. The St. Peter Sandstone is recognized as a very brittle material.

3.6.2. A General Discussion of the Elastic Properties of the St. Peter Sandstone. The St. Peter sandstone is a unique geotechnical material, which lies in a transition zone between soils and rocks. The elastic property makes it behave like rocks and the cohesionless character is of typical soils.

In addition to the laboratory test, the elastic property of the St. Peter Sandstone can be observed from the field test. Corps of Engineers (1958) perfomed nine in-situ bearing capacity tests on St. Peter Sandstone at the St. Anthony Falls Lower Lock. Their results show that the displacements were recovered completely after removal of the load. It is also another indication of elastic behavior for St. Peter Sandstone

The elastic behavior is the major difference between the St. Peter Sandstone and other cohesionless materials. Understanding the elastic behavior of St. Peter Sandstone is the key for resolving a number of significant problems such as the structure model, and the cause of the high friction for the St. Peter Sandstone.

3.7. THE STRENGTH OF CEMENTED ST. PETER SANDSTONE

The objective of this study is to investigate the basic mechanical and strength properties of the St. Peter Sandstone that is cohesionless, or uncemented. Although it is true that shallowly burried St. Peter Sandstone formation in Minnesota, Wisconsin and Iowa can be categorically considered cohesionless. However, some parts of St. Peter Sandstone formation are cemented. For instance, the upper contact zone of the St. Peter Sandstone formation with Glenwood Shale is cemented with varying degrees. The structure of a cemented St. Peter Sandstone is very different from uncemented one. Figure 3.16 is a comparison of the microstructures of the cemented and uncemented St. Peter sandstone

samples. Because of this structural difference, the strengths for cemented and uncommented St. Peter sandstones are very different.

In order to study the basic mechanical properties of the cemented St. Peter sandstone, 5 sandstone blocks with varying cementations were collected from the Pattison mine site, Clayton, Iowa. The images of these sandstone blocks are given in Figure 3.17. For the purpose of comparison, the image of an uncemented block is also included. All these sandstone blocks were tested for their uniaxial compressive strength and indirect tensile strength (Brazilian test). Part of the specimens used for the test is shown in Figure 3.18.

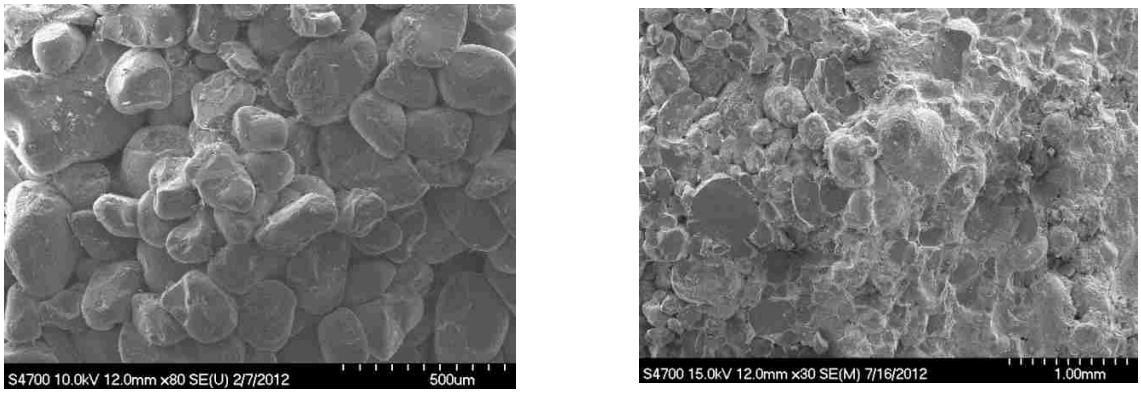

a)Uncemented St. Peter Sandstone

b) Cemented St. Peter Sandstone

Figure 3.16. Scanning electron microscope (SEM) images of the cemented and uncemented St. Peter Sandstone samples.

The test results for the uniaxial compressive strength and the indirect tensile strength are given in Tables 3.7 and 3.8, respectively. The uniaxial compressive strength is very high for the cemented specimens, ranging from 14 to 124 MPa, which are 5 to 8 times higher than that for uncemented specimens with the compatible size.

a)

b)

c)

d)

e)

f)

Figure 3.17. Images of cemented and and uncemented St. Peter Sandstone

Figure 3.18. Specimens of cemented St. Peter Sandstone

Table 3.7. Uniaxial compressive strength for cemented St. Peter Sandstone

Sample block ID	# of specimens	Mean (MPa)	Standard Deviation (MPa)
BK4	4	18.89	3.20
7AI-2	5	28.21	6.20
BK5	4	42.09	6.99
En	6	59.89	13.88
BK1	6	95.23	21.39

Table 3.8. Indirect tensile strength for cemented St. Peter Sandstone

Sample block ID	# of specimens	Mean (MPa)	Standard Deviation(MPa)
7AI-2	6	2.46	1.14
BK5	5	3.61	1.12
En	8	4.78	2.15
Bk1	7	6.94	1.92

From the discussion provided in this section it can be understood that there exist significant differences between cemented and uncemented St. Peter Sandstones. Mixing the information from these two categories can cause major problems.

3.8. CONCLUSIONS

In the course of this investigation a total of 95 uncemented specimens were prepared and tested for the uniaxial compressive strength for the St. Peter sandstone, the greatest research effort dedicated to this special topic. Another major research on the uniaxial compressive test was performed by Petersen (1978) and a total of 33 specimens were tested.

A comprehensive and in-depth study was carried out on St. Peter Sandstone. The objective was to establish a scientific understanding of the uniaxial compressive strength associated with the St. Peter Sandstone for reliably determining and using this data.

A particular problem encountered in the St. Peter Sandstone research is the incompatibility of the material property of the St. Peter Sandstone and the standard sample preparing practice that is recommended by ASTM (1972) and ISRM (1981). The sampling techniques recommended by ASTM (1972) and ISRM (1981) can easily disintegrate the specimen being processed. Therefore, the first principle for preparing St. Peter Sandstone specimens is to minimize the disturbance caused by the sampling techniques. The outcome of this study was a sample preparation method for minimizing the disturbance

The failure mode is a record of the failure process and holds the critical information for understanding the strength property of a rock material. The contribution of this study is threefold. The mechanics of two dominant failure mode (vertical splitting and steeply dipping shearing) were investigated. It was reaveled the failure modes are linked to the basic mechanical properties of the St. Peter Sandstone: Vertical splitting is caused by cohessionless property of the St. Peter sandstone and steeply dipping shearing is the result of high friction angle of the St. Peter sandstone. Secondly, steeply dipping shearing is another independent evidence of the high friction angle and provides the quantitative information for the friction angle calculation. Third, the irregularity of failure locations observed from the sandstone specimens reflects the sensitivity of the failure process to local anomalies, which is also a

result of the cohesionless property of the St. Peter sandstone. The sensitivity to local anomalies as manifested by vertical splitting and irregularity of failure locations is one of the main reasons responsible for the large variance of the uniaxial compressive strength associated with the St. Peter Sandstone.

The size effect of specimens for the St. Peter sandstone is very different from the one that is typically exhibited by most geological materials. The size effect for the St. Peter Sandstone is the result two factors: scaling and disturbance by sampling techniques. The factor of disturbance is unique for the St. Peter Sandstone and its impact can significantly overshadow that of scaling, especially for small specimens. This is why the strength of small St. Peter Sandstone specimens is significantly lower than the strength for other specimen sizes.

The optimum size of 50 mm determined in this investigation is based on several factors. In addition to the theoretical considerations, scaling and disturbance, as illustrated by the laboratory results, the other two factors are the field investigation and practical considerations. A field investigation was conducted to back calculate the uniaxial compressive strength for existing pillars. It appears that the strength of 50 mm specimens matches well with the result from this field investigation. Practical considerations are also an important factors for determining the optimum size. Based on extensive sampling experiences of this study, 50 mm specimens are the size that can be economically attainable

The shape effect for St. Peter Sandstone specimens has not been discussed in any previous research. Although the available data is limited and the discussion provided here is preliminary, it is an issue that cannot be ignored. A practical implication is that the height/width ratio should not be too low, at least not less than 1.

The elastic properties of the St. Peter sandstone, namely Young's modulus and

Poisson's ratio were also studied during this investigation. The unique contribution of this research is a detailed study of the stress-strain curves. The results of this study show that the stress-strain curves can be roughly divided into three stages. The stress-strain curve behaviors almost perfectly linear for most test periods, about 60-70% of the failure stress. The stress-strain curve at the second stage can still be regarded linear even though it begins to show the non-linear behavior. The second stage ends with a sudden change of the stress-strain curve, which signals the beginning of the third stage. For the stress-axial strain curve, it is an abrupt rupture. For the stress-lateral strain curve, it changes direction and extends almost horizontally. The characteristics of the stress-strain curves, as exhibited by the St. Peter Sandstone, are typical for a brittle-elastic material.

Previous studies on strength properties of St. Peter Sandstone were reveiwed. The Young's moduli determined by previous researches are very close to what was determined in this study. The Poisson's ratio determined by Dittes and Labuz (2002), however, shows a large discrepancy, which ranges from 0.20 to 0.33. This range, especially the upper value, appears too high considering the very friable nature of the St. Peter Sandstone. The results of this study show that the lateral deformation before the failure is very small. This observation is consistent with the cohesionless property, which makes the St. Peter Sandstone extremely weak for its tensile strength. Vertical splitting, one of the dominant failure formations for the St. Peter Sandstone is primarily caused by this cohesionless property.

The last problem in this chapter is the uniaxial strength of cemented St. Peter Sandstone. The need for this discussion is twofold. First, the basic mechanical property of the cemented St. Peter Sandstone is important in order to handle various ground control problems associated with the St. Peter Sandstone formation. It was noticed during this investigation that the strength data for cemented and uncemented St. Peter Sandstone were mixed

sometimes. However, the confusion between the strength data for these two groups could be avoided if the significant difference between these two sandstones are clearly understood.

In the course of this investigation, an extensive test was carried out to determine the uniaxial compressive strength. The results show that the uniaxial compressive strength for the cemented sandstone can be 5 to 8 times higher than that for uncemented sandstone depending on the degree of cementation. Furthermore, the microstructures of two types of sandstones were compared, which demonstrate that the large strength difference is fundamentally rooted in the material properties.

A very important issue that is critical for understanding the strength characteristics of the St. Peter Sandstone, but not discussed in this chapter, is the sand particle structure. The reason is that it would require the advanced knowledge from the triaxial test carried out in this investigation. This issue will be discussed in next chapter:

4. STRENGTH OF ST. PETER SANDSTONE UNDER TRIAXIAL TEST CONDITIONS

4.1. INTRODUCTION

This chapter is dealing with the strength of the St. Peter Sandstone under triaxial test conditions. This will allow one to study the strength of St. Peter Sandstone from a very different perspective than the uniaxial compression test conditions studied in Chapter 3. Although the experimental arrangement for a triaxial test is much more complicated, the concept, as illustrated in Figure 4.1, is very simple: the test specimen is subjected to a confining pressure while under compression in the axial direction.

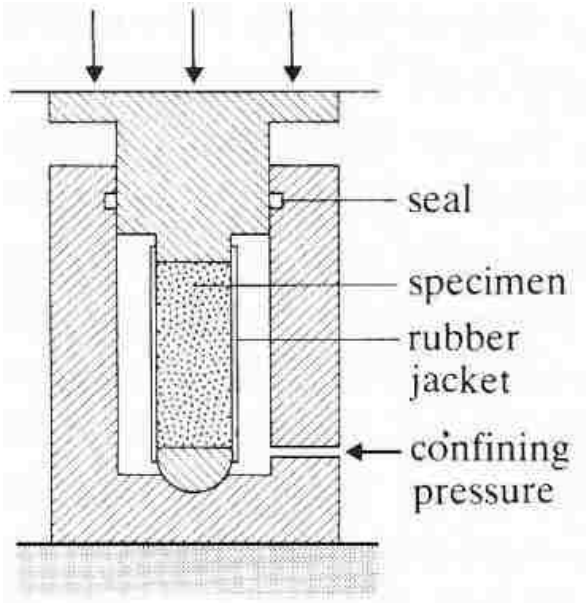

Figure 4.1. Elements of a conventional triaxial testing apparatus (Brady and Brown, 1993)

The study of strength under triaxial test conditions offers a number of important advantages. First it allows us to examine the strength as a function of confining pressures. The strength characters here refer not only to the magnitude of the strength, but also the

mechanical behavior of the material. This concept is illustrated in Figure 4.2.

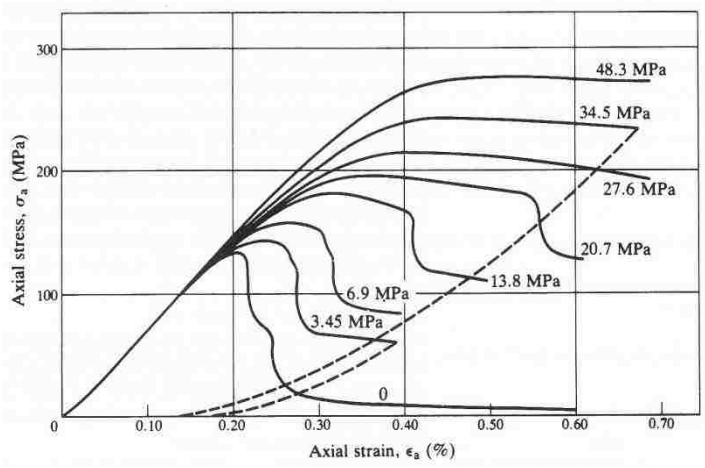

Figure 4.2. Complete axial stress-axial strain curves under triaxial compression tests on Tennessee marble (Wawersik and Fairhurst, 1970).

This figure shows that the strength of the Tennessee Marble increases with an increase in confining pressure and the rate of the strength increase is much faster than the rate of increase for the confining pressure. The ratio is about 3 for Tennessee Marble. In addition to the strength increase, the behavior of the tested material also changed. For the uniaxial compression test, the specimen fails abruptly, showing a typical brittle-elastic behavior. This behavior, however, changes rapidly with the increase of the confining pressure. Most of the curves in the figure are of a typical ductile-elastic behavior.

The other distinctive advantage of the triaxial test is that it allows one to quantitatively evaluate failure conditions in terms of axial stress and confining pressure. A piece of very important information that can be drawn from this work for any rock mechanics study is the friction angle. This concept is explained with the help Figure 4.3.

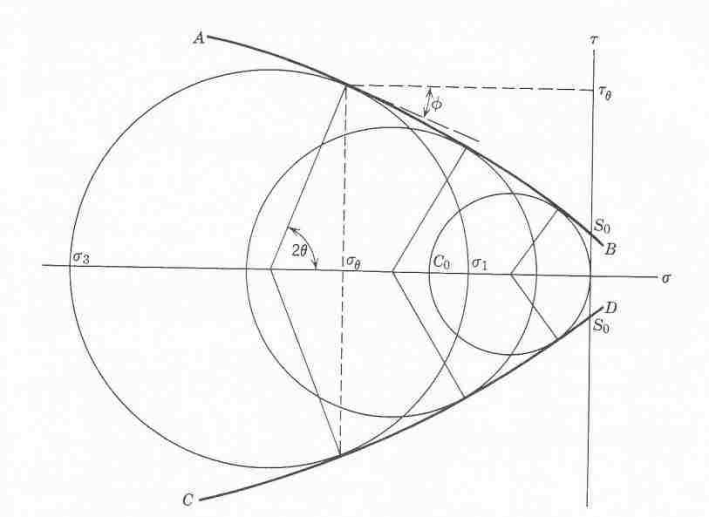

Figure 4.3. Concept of Mohr's failure envelope

Figure 4.3 shows that a failure envelope also known as Mohr failure envelope, will be formed if there are sufficient data (Mohr circles) from the triaxial test. The significance of this failure envelope is two-fold. First, it allows one to predict the chance of failure for a specific stress condition. It will be safe if the resulting Mohr circle is within the envelope. Otherwise, failure may occur. Secondly it provides information about the friction angle, which is illustrated in the figure as φ, the angle that is between the tangent line and the horizontal line.

In this chapter, three important observations from past studies will be reviewed, which are high friction angles for St. Peter Sandstone observed from the triaxial test, comparison studies on the friction angles for St. Peter sands, and large dilations associated with direct shear test.

Next the mechanics of the sand particle structure will be discussed in terms of the information obtained from the triaxial test. This is an important issue because the basic mechanical and strength properties of St. Peter Sandstone are fundamentally governed by the

particle structure of the sandstone. Hence, understanding the particle structure holds the key for St. Peter sandstone research. A particular advantage of utilizing the triaxial test technique for this investigation is that the test result is significantly less affected by local anomalies, which makes it possible to compare the mechanical responses of different structures quantitatively. This is one of the most important aspects of this investigation.

The study discussed in this chapter is not only significant from a theoretical point of view, but also of a great practical importance. The final part of this chapter is a brief discussion on how the theories developed in this study may be used for resolving a number of critical rock mechanics and ground control problems.

4.2. MAJOR FINDINGS AND OBSERVATIONS FROM PREVIOUS STUDIES

The first triaxial study of St. Peter Sandstone was carried out by Watson (1938). The test included eight hand-trimmed cylindrical specimens. These specimens are large (165 mm long with a diameter of 70 mm).

4.2.1. Unusually High Friction Angle Observed from the Triaxial Test Result. The test results are shown in Figure 4.4. The friction angles which are measured individually from each Mohr circle range from 59˚ to 69˚ with an average value of approximately 63˚.

This friction angle is unusually high, approximately 15˚ higher than the high range of friction angles known by the geotechnical community.

The triaxial tests for uncemented St. Peter Sandstone were also conducted by Dusseault and Morgenstern (1979), and Labuz et al. (1998). The result of Labuz et al. (1998) is shown in Figure 4.5, which is very similar to the result by Watson (1938).

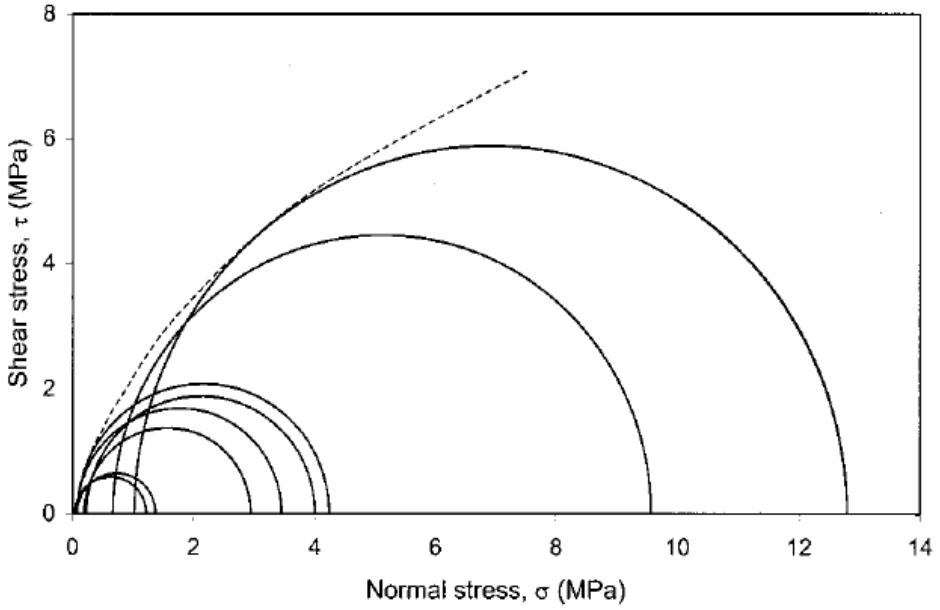

Figure 4.4. Mohr envelope of St. Peter Sandstone (Watson, 1938)

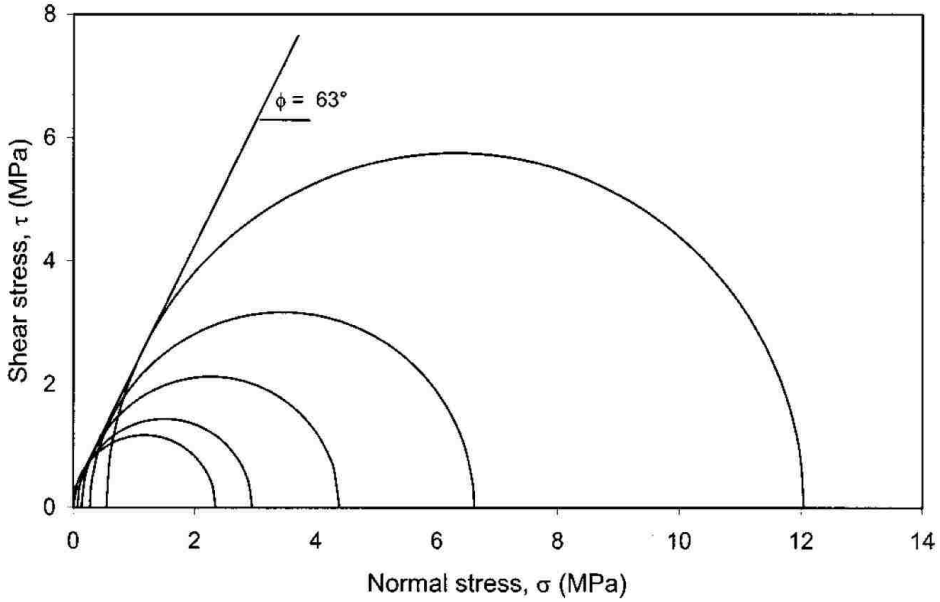

Figure 4.5. Mohr envelope of St. Peter Sandstone (Labuz et al., 1998)

4.2.2. Unusually High Friction Angle observed from the Triaxial Test Result. Another important contribution made by Watson (1938) is his comparative study on friction angles for both densely and loosely packed St. Peter sands. The triaxial test results for these two conditions are shown in Figures 4.6 and 4.7. The friction angles determined under these two conditions are 42˚ and 33˚, respectively, which are much lower than that for the original St. Peter Sandstone.

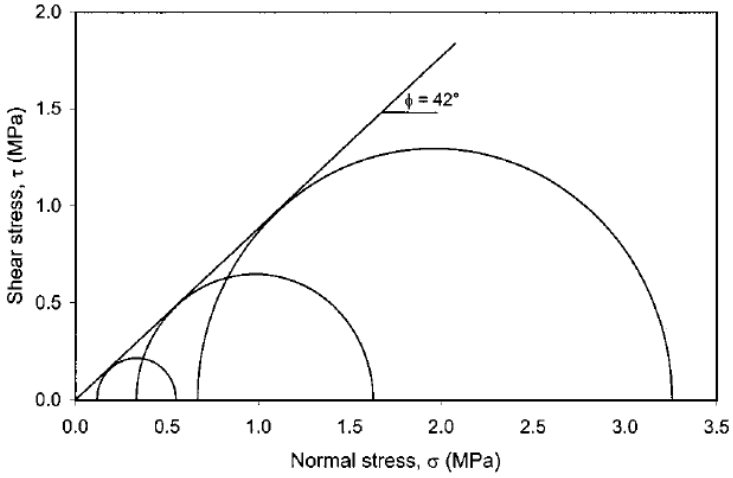

Figure 4.6. Mohr envelope for densely packed St. Peter sands (Watson, 1938)

The significance of this comparison study is that the high friction angle is a manifestation of the unique properties of St. Peter sandstone, which are very difficult to duplicate under laboratory conditions. One such property for St. Peter sandstone is an extremely low porosity, which varies within a very narrow range of approximately 24-30% (Thiel, 1935). If we assume an equal size particle structure model, a material with this porosity range is virtually incompressible (Graton and Fraser, 1935).

The friction angles for both densely and loosely compacted sands, are well within the

ranges of friction angles for other sands as shown in Appendix B (Holtz and Kovacs, 1981). However, the friction angle for St. Peter Sandstone is exteremely higher than recompacted sands.

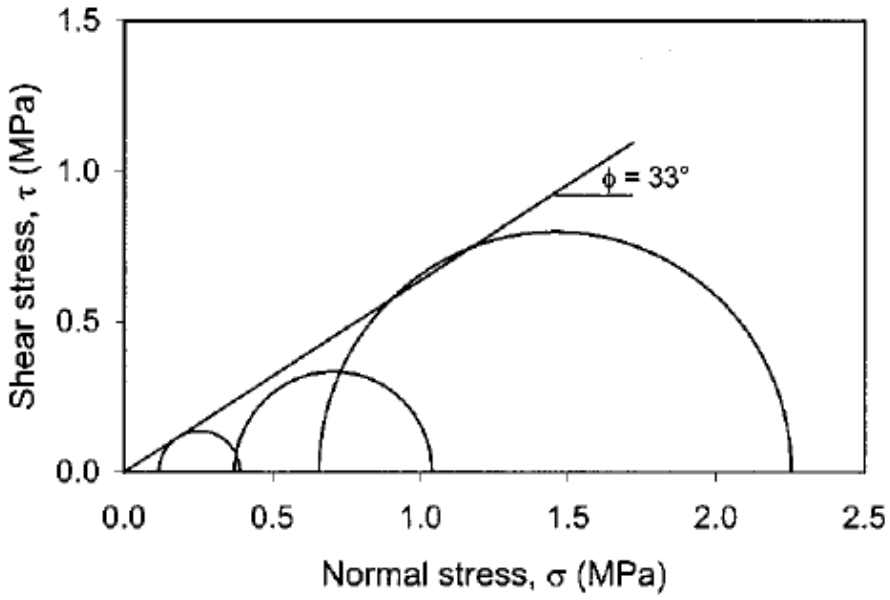

Figure 4.7. Mohr envelope for loosely packed St. Peter sands (Watson, 1938)

4.2.3. High Dilation rate associated with Direct Shear Tests. The friction angle of a rock material can be also determined by direct shear test. The concept of direct shear test is illustrated in Figure 4.8.

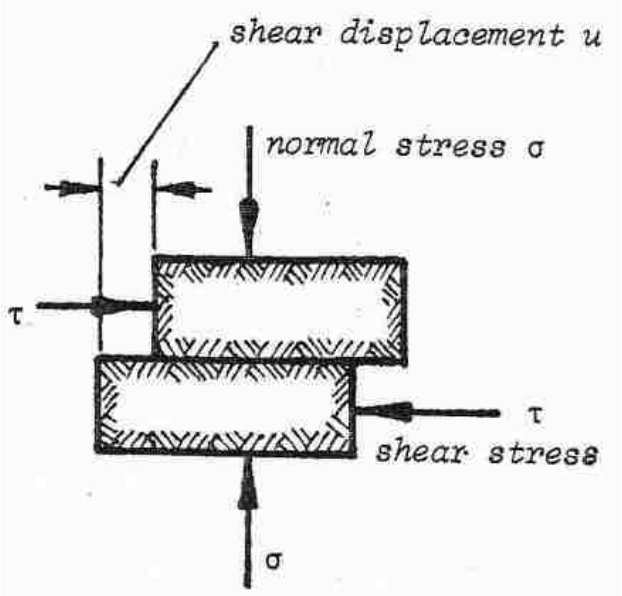

Figure 4.8. Direct shear test (Hoek and Bray, 1978)

The direct shear method was utilized by a number researchers to study the friction angle of St. Peter Sandstone (Dusseault and Morgenstern, 1978; and Dittes and Labuz, 2002). The test results by Dittes and Labuz (2002) for St. Peter Sandstone and recompacted sands are given in Figure 4.9. This figure shows that the friction angle obtained by the direct shear method for St. Peter Sandstone is 57˚, which is 6˚ lower than they determined using the triaxial test (Labuz et al., 1998). The friction angles for dense and loosely compacted sands are almost identical to those determined by Watson (1938). Dittes and Labuz (2002) investigated the volume change of St. Peter sandstone as well as recompacted (densely and loosely packed) St. Peter sands (Figure 4.10).They found a dilatancy behavior for St. Peter Sandstone. The rate of dilation for intact samples was considerably higher than dense recompacted samples.

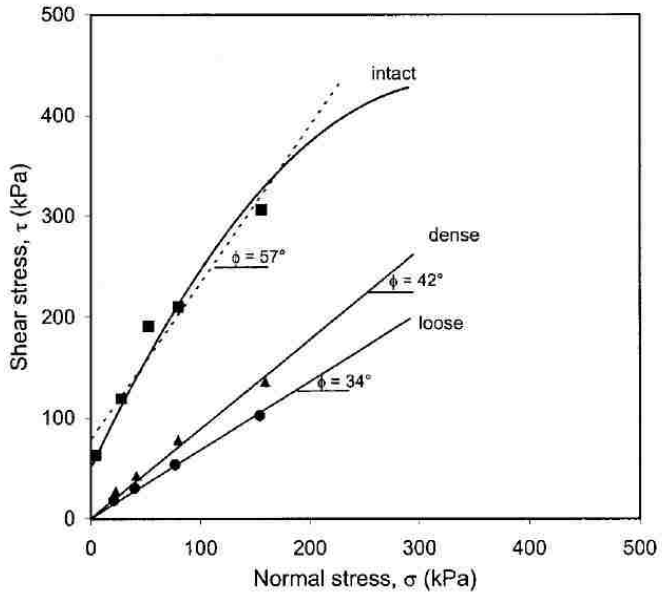

Figure 4.9. Failure envelops of St. Peer sandstone and sand in direct shear (Dittes and Labuz, 2002)

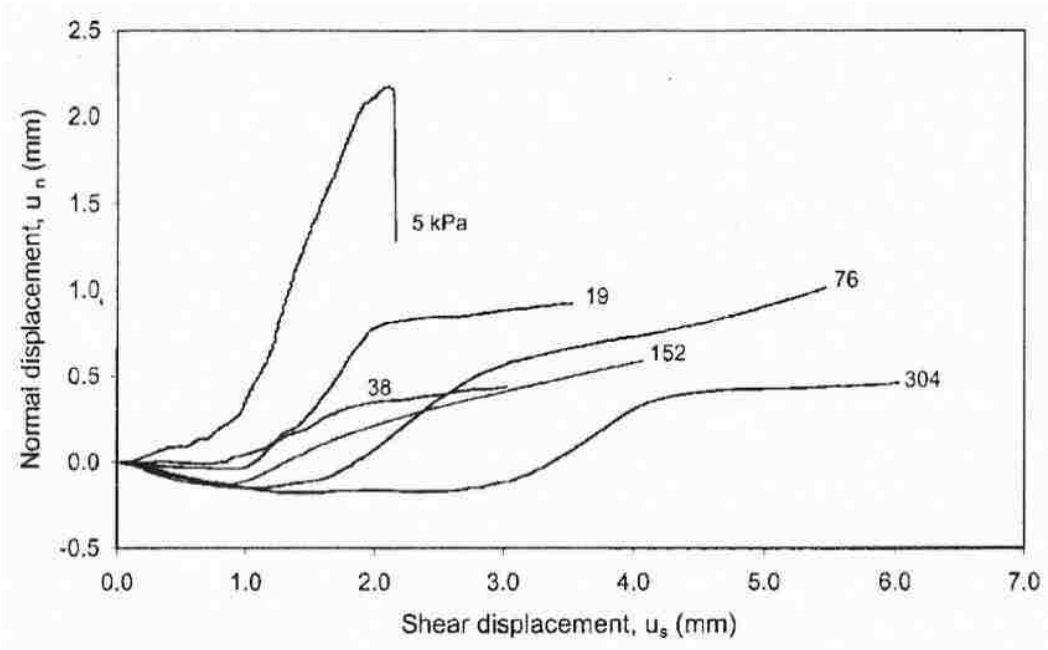

Figure 4.10. Dilation of intact St. Peter sandstone over range of normal stresses (Dittes and Labuz, 2002).

4.3. TEST APPARATUS

One of the major difficulties for the triaxial test of St. Peter Sandstone is that the triaxial test equipment is primarily designed for cylindrical specimens. However, the specimens used for St. Peter Sandstone are mostly cubic or rectangular. As discussed in Chapter 3, it is not a recommended practice to use cylindrical specimens for St. Peter Sandstone. In addition to the fact that they have to be hand trimmed and the hand trimming is a very difficult process, the main problem is that this process will inevitably create more disturbances to specimens and make the test results less reliable.

4.3.1 Utilizing a State-of-the-Art True Triaxial Test Apparatus. In order to solve this problem, it was decided to use a state-of-the-art, servo-hydraulic testing apparatus at Pennsylvania State University (Figures 4.11 & 4.12). The vertical load frame of the apparatus has a maximum force of 1MN and the horizontal frame can produce forces up to 800kN. Each load frame may be operated in displacement- or load-feedback servo control. Displacement control resolution is 0.1 micron for each axis and load resolution is <0.1kN. The apparatus is powered by a 20 GPM, 50 hp hydraulic power supply. Servo-controlled load point displacement rates of 0.01 micron/s to 2 cm/s are possible. Machine stiffness is roughly 4 MN/cm and therefore ideal for friction and fracture studies.

4.3.2. Loading Platens. To accommodate the specimens with the square cross section for the test, two loading platens.

Loading platens, which allow the test to be carried out under drained conditions were specially designed and manufactured (Figure 4.13). The square part of the platen that contacts the specimen has a dimension of 50 x 50mm and the circular loading end has a diameter of 44 mm.

4.3.3. Sealing Specimen Assembly. Figure 4.14 shows how the loading platens are attached to a specimen. Before the triaxial test, each of these assemblies has to be tightly sealed, a critical step for a successful triaxial test. Figure 4.15 is an illustration of how a test specimen is sealed with the loading platens before the test

Figure 4.11. The triaxial test apparatus utilized for this investigation

4.4. TEST DESIGN CONSIDERATIONS

4.4.1. Field Observations. An important observation at the Pattison mine is that failures are often associated with the areas of St. Peter Sandstone containing coarse grains. A typical example is pinch-out failures (Figure 4.16). The pinch-out failure is a term used by mine workers to describe fractures that initiate at the intersection of the cap rock roof and sandstone pillars. If the problem is not properly handled, it could develop into a very serious problem resulting in significant pillar damage. Figure 4.17 is a close look at initial pinch-out formation.

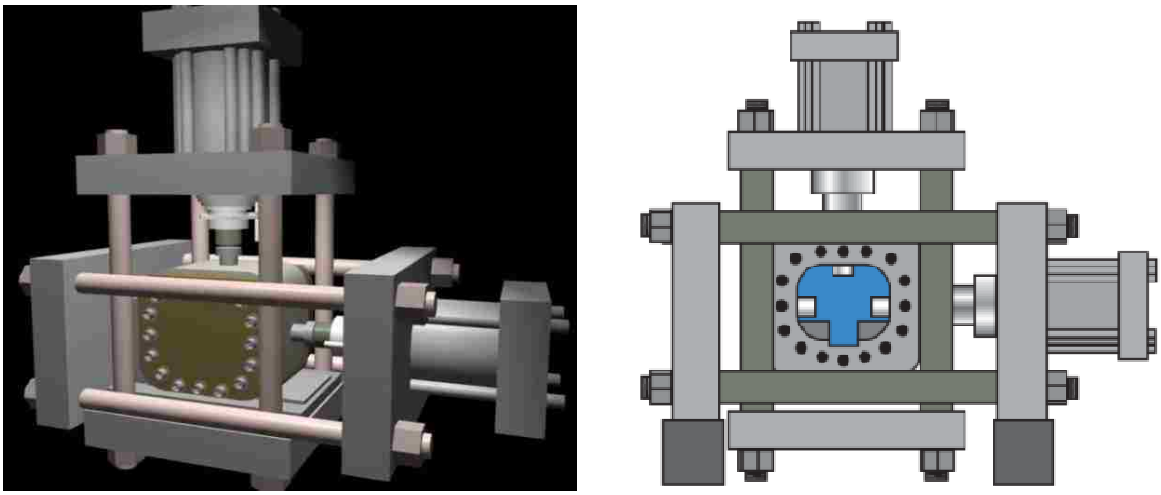

a) b)

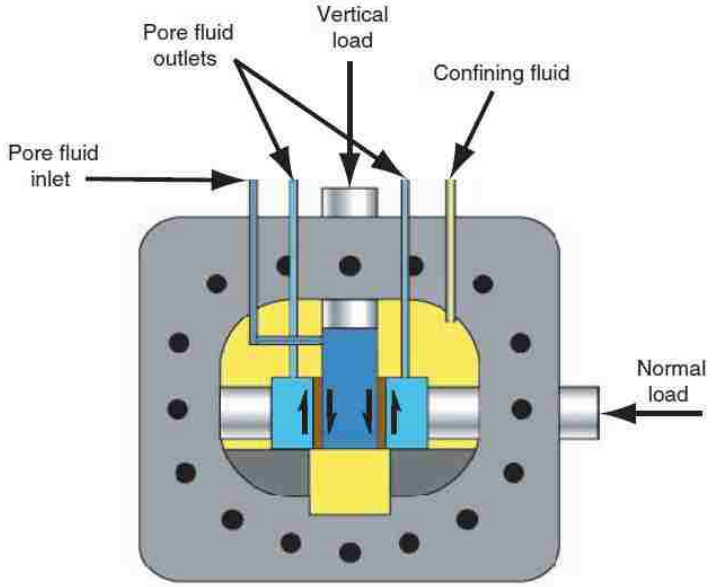

c)

Figure 4.12. (a) Three-dimensional illustration of true-triaxial pressure vessel and biaxial load frame b) two-dimensional illustration of true-triaxial pressure vessel and biaxial load frame c) the cross section of pressure vessel

4.4.2. Porosity and Structure of St. Peter Sandstone. The significance of pinch out failure observation is that it raised a fundamental question for St. Peter sandstone research:

what is the role of sand particle structure on the strength of St. Peter Sandstone?

The structure of St. Peter Sandstone can be characterized using different parameters. A basic and well established approach is the porosity associated with St. Peter sandstone at the time when this research started.

In the field of geotechnical engineering, the porosity is defined by the following equation:

$$n = \frac{V_v}{V} \tag{4.1}$$

Where n is porosity, V_v is the volume of void, which includes voids occupied by both air and liquid, and V is the total volume. The volume for solid material is usually expressed by V_s, and the total volume is the summation of the volume of void and volume of solid, that is

$$V = V_s + V_v \tag{4.2}$$

The porosity for St. Peter sandstone falls into a narrow range of approximately 24.5-30.5% (Thiel, 1935), which, according to our study, also fairly characterizes the porosity of St. Peter sandstone at the mine site in Clayton, Iowa.

Figure 4.13. Two loading platens, which allow the drained condition test, were specially designed and manufactured for this research.

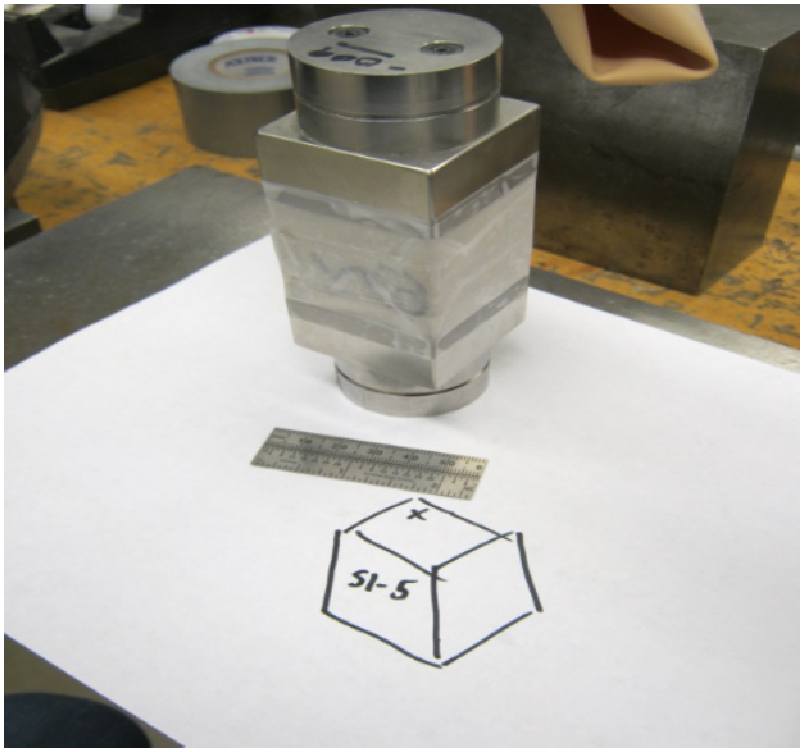

Figure 4.14. Loading platens with an attached specimen

a) Specimen assembly in latex jacket

b) Seals along loading platens

Figure 4.15. Sealing a specimen assembly for the triaxial test

Figure 4.16. Pinch-out failure, severe fractures developed between pillars and cap rock roof.

4.4.3. Structure Characteristics of 6AR and 1S Samples. In order to study the role of the sand particle structures, two sample blocks with the distinctive difference in porosity were identified, which are block 6AR and block 1S. The porosities for these two groups are 24.4% and 30.1%, respectively, which are very close to the lower and upper limits of the porosity range identified by Thiel (1935).

The thin section images for the samples from these two groups are presented in Figure 4.18. It is clear from these images that the particle structures for these two group samples are very different. There are two major differences. The first one is the particle size. The sand particles for 1S are significantly larger than those in the 6AR sample. The second difference is the size distribution. The 1S sample lacks fine sand particles while 6AR sample has a range of particle sizes.

Figure 4.17. A close look of at initial pinch-out failure formation

The grain size distribution curves for these two group samples in Figure 19 provide further quantitative information for the structural features observed from the thin section images. First, there is a relatively large distance between the two curves, which signals a distinctive difference in particle size. If the median is used to characterize the particle size, they are 2 and 3 mm for 6AR and 1S groups, respectively.

The difference is 50%. A comparison of these two curves also show that 1S sample

group contains almost no particles finer than 0.1 mm while the 6AR group has a long tail which reaches beyond 0.02 mm.

a) A thin section image of a 6AR sample

b) A thin section image of a 1S sample

Figure 4.18. Thin section images of the 6AR and the 1S samples.

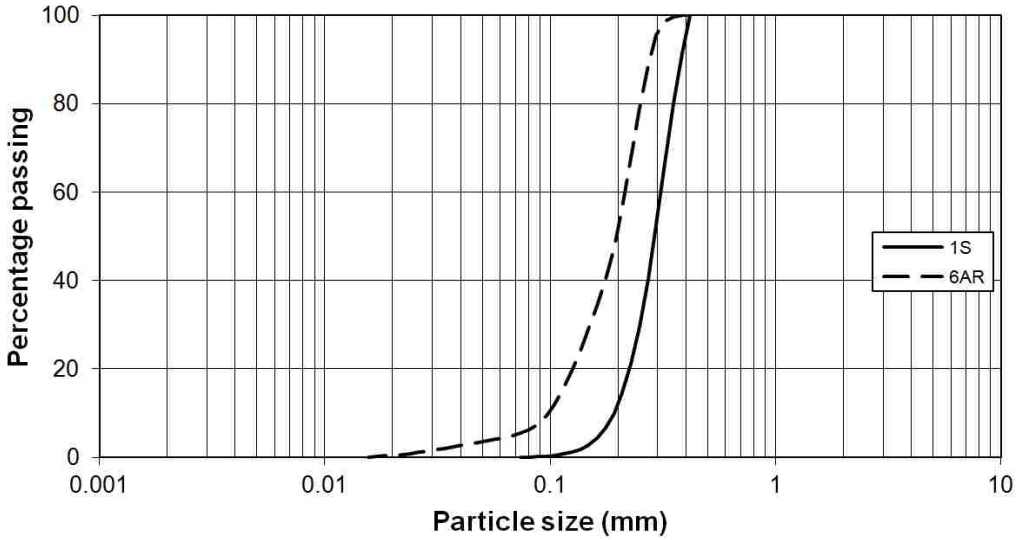

Figure 4.19. The grain size distributions for the 6AR and the 1S samples.

In addition to the structural characteristics, the other important consideration in utilizing 6AR and 1S sample blocks for this comparison study is that both blocks are sufficiently large to allow the preparation of multiple 50 mm size specimens.

A total of 14 such specimens were prepared from the 1S block and 11 were prepared from the 6AR block. This consideration is critical for obtaining a meaningful result since the St. Peter Sandstone‘s properties vary from location to location, as well as vertically at the same location. Utilizing the specimens from the same sample block assures identical properties for these specimens.

4.4.4. The Uniaxial Compressive Strength for 6AR and 1S Specimens. Among the specimens prepared from 6AR and 1S blocks, 8 from each group were utilized for the uniaxial compressive test. The result is summarized in Table 4.1. The average strength for 6AR specimens is about 32% higher than the strength for the 1S specimens.

4.4.5. Specimens Prepared for Triaxial Test. The remaining 50 mm specimens prepared from these two sample blocks were used for the triaxial test, including 5 1S

specimens and 3 6AR specimens. The specimens used for the triaxial test are shown in Figure 20. In addition to 6AR and 1S specimens, two 12AR specimens were included. The dimensions of these specimens are given in Table 4.2.

Table 4.1. The uniaxial compression test result for 6AR and 1S specimens

Group ID	Individual results (MPa)	Mean (MPa)	Std. (MPa)
6AR	1.80 2.13 3.60 3.82 4.14 4.21 7.00 10.63	4.67	2.88
1S	2.20 3.00 3.25 3.43 3.50 3.66 3.81 5.32	3.52	0.88

Table 4.2. Dimensions of the specimens utilized for the triaxial test

Sample ID	Dimension (mm)			Height to width Ratio
	Width	Depth	Height	
1S-2	51	51	70	1.38
1S-1	51	51	81	1.60
1S-3	51	51	67	1.33
1S-4	47	48	50	1.05
1S-5	47	46	67	1.44
6AR-1	51	51	57	1.13
6AR-3	51	51	54	1.06
6AR-2	51	51	48	0.95
12AR-2	48	51	65	1.36
12AR-1	50	50	74	1.48

The triaxial test is a critical part of this research because of its unique test condition and the information that it can provide under this test condition. In particular, there are three specific purposes in utilizing this technique. The first one is to explore the effect of the particle structure on the basic mechanical and strength properties of St. Peter Sandstone. This will be done by comparing the mechanical responses of 6AR and 1S specimens during the triaxial test. The mechanical response here refers material strength, stress-strain relations, failure characteristics, and friction angles. Next, the uniaxial compressive strength for 6AR

and 1S specimens will be further studied in light of the triaxial result. There are two specific reasons for this study: first the stress conditions under the triaxial test are much closer to in-situ situations, and second, the result from the triaxial test is much more stable. Finally, the engineering implications of the differences in mechanical responses between St. Peter Sandstone and the conventional will be studied.

4.5. ANALYSIS OF THE TEST RESULT

The results of the triaxial test in terms of the confining pressures and the corresponding axial stresses at failure are presented in Table 4.3. There were four confining pressure levels utilized for the triaxial test, which are 0.66, 2.06, 3.44 and 6.87. Among the 10 tests conducted, one failed due to a jacket leaking problem.

4.5.1. Effect of Confining Pressure on St. Peter Sandstone Strength. For convenience in comparing the effects of the confining pressure, the confining stresses and axial stresses at failure, 1S and 6AR specimens were regrouped Table 4.4. The average uniaxial compressive strengths for 1S and 6AR specimens were added to the table as the reference level. Figure 4.21 is a graphical expression of the data presented in Table 4.4 Two features can be captured immediately from Figure 4.21. First, the strengths increase very fast at the initial stage, shown by steeply raised curves at this stage.

a) 1S specimens for triaxial test

b) 6AR specimens for triaxial test

C) 12AR specimens for triaxial test

Figure 4.20. Specimens utilized for the triaxial test

Table 4.3. Confining stresses and axial stresses at failure

Sample ID	Dimension (mm)	Confining Stress (MPa)	Axial Stress at failure (MPa)
1S-2	51×51×70	0.66	20.23
1S-1	51×51×81	2.06	25.76
1S-3	51×51×67	3.44	31.75
1S-4	47×48×50	6.87	41.50
1S-5	47×46×67	6.87	42.10
6AR-1	51×51×57	0.69	25.74
6AR-3	51×51×54	3.45	46.23
6AR-2	51×51×48	6.87	88.73
12AR-2	48×51×65	0.70	14.37
12AR-1*	50×50×74	6.88	------

*A jacket leak occurred in this experiment

In order to measure the effect of the confining pressure on the axial stress at failure, the rate increase of the axial stress at failure was defined as

$$RAS = \frac{\sigma_a - \sigma_0}{\sigma_c} \tag{4.3}$$

where RAS stands for rate increase of axial stress, σ_a is the axial stress at failure, σ_0 is the uniaxial compressive strength, and σc is the confining pressure

Table 4.4. A comparison of the axial stress at failure for 6AR and 1S specimens

Confining stress (MPa)	Axial stress at failure (MPa)	
	1S Group	6AR Group
0.0	3.52	4.67
0.66	20.23	25.74
2.06	25.76	------
3.44	31.75	46.23
6.88	41.80	88.73

The rate of increase for 1S and 6AR specimens can be calculated based on the data presented in Table 4. For the confining pressure of 0.66 MPa, they are 25 and 32 for 1S and 6AR specimens, respectively. The rate increase in this range is very significant. To appreciate this effect, just calculate the strength increase for a 6AR block by adding just 10 psi confining pressure. The strength increase is 320 psi.

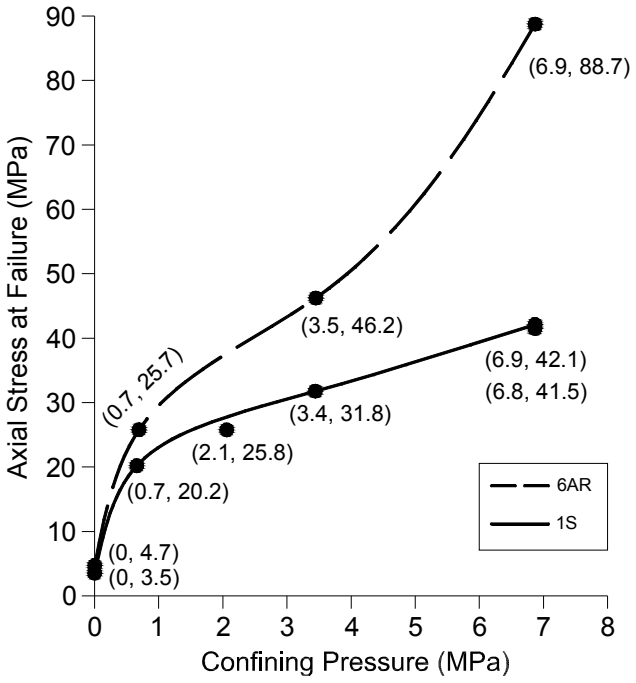

Figure 4.21. Axial stresses at failure vs. confining pressures for 6AR and the 1S specimens

The other important feature is that the strength increase for 6AR specimens are much quicker than that for 1S specimens. The strength of 6AR specimen at the confining pressure of 6.9 MPa is 88.7 MPa, more than twice the strength for 1S specimens. It is interesting to note that there are two 1S specimens tested with the same confining pressure of 6.9 MPa and

the axial stresses at failure for these two specimens are almost identical, which are 41.5 and 42.1 MPa.

4.5.2. Effect of Confining Pressure on Sandstone Behavior. The significant strength increase is fundamentally due to the change of material behaviors under the triaxial test condition. As discussed in section 4.1, the triaxial test has two major effects: it increases the strength and changes the material behavior from brittle to ductile. This is also true for St. Peter Sandstone as shown in Figure 4.22.

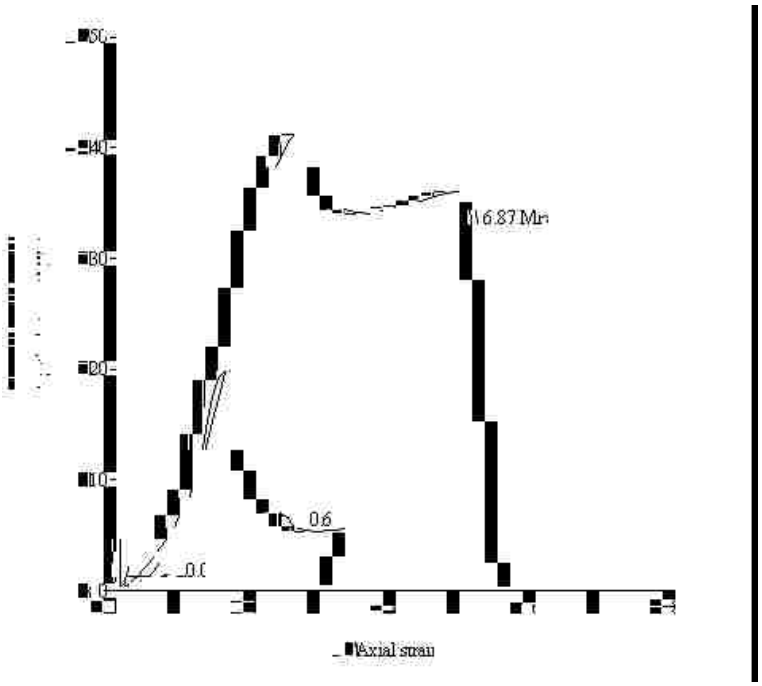

Figure 4.22. Change of material behavior of St. Peter Sandstone under triaxial test condition

There are three curves in the figure: a stress-strain curve resulting from the uniaxial compression indicated in the figure by 0 confining pressure and two curves obtained from the triaxial tests. These two curves cover the complete test circle, that is they also include the

post-failure behavior of the specimens being tested. The confining pressures for these two tests are 0.66 and 6.87 MPa, respectively.

The stress-strain curve for the uniaxial compression test is steep and short, which indicates that the tested specimen is brittle and the strength is low. The mechanical response changes drastically once the confining pressure is added. In addition to a rapid increase of the strength as discussed in Section 5.1, the shapes of these two curves are also different. The two curves start to increase nonlinearly, however, they attain approximately linear behavior until yild point is reached. It can also be seen the rate of increase in the linear portion of the curves is much steeper in comparison with non-linear section. The slopes for the increasing section, however, are still much gentler than that for the uniaxial compression test.

The most valuable part of these two curves is the post failure section. It shows the residual strength associated with St. Peter sandstone. It can be seen from the curves that the specimens after the initial failure (passing the peak strength) can still "hang" there with the support of the residual stress before a complete failure. The difference between these two curves is that the residual stress is much lower for the specimen with the lower confining pressure. The level of the residual stress for the specimens with the higher confining pressure is much higher and can stay there much longer.

The stress-strain curves for 6AR specimens at 4 confining pressure levels, 0.00, 0.66, 3.44, and 6.88 MPa, are shown Figure 4.23. All curves with non-zero confining pressures have very similar shapes, including the post failure sections. This characteristic shows that the failure is no longer significantly affected by local anomalies. Rather, it is governed by its own structure, which is further proof of the reliability of the strength data obtained from the triaxial test.

The stress-strain curves for 1S specimens at 5 confining pressure levels, 0.00, 0.66, 2.66, 3.44, 6.88 MPa, are given in Figure 4.24. There are two notes about these curves. First, there are two tests for the confining pressure of 6.87 MPa. The result in this figure is one of them, and the other one was given in Figure 4.22 earlier. A comparison of these two curves is given in Figure 4.25. The axial stresses at failure and the residual stresses for these two curves are almost identical.

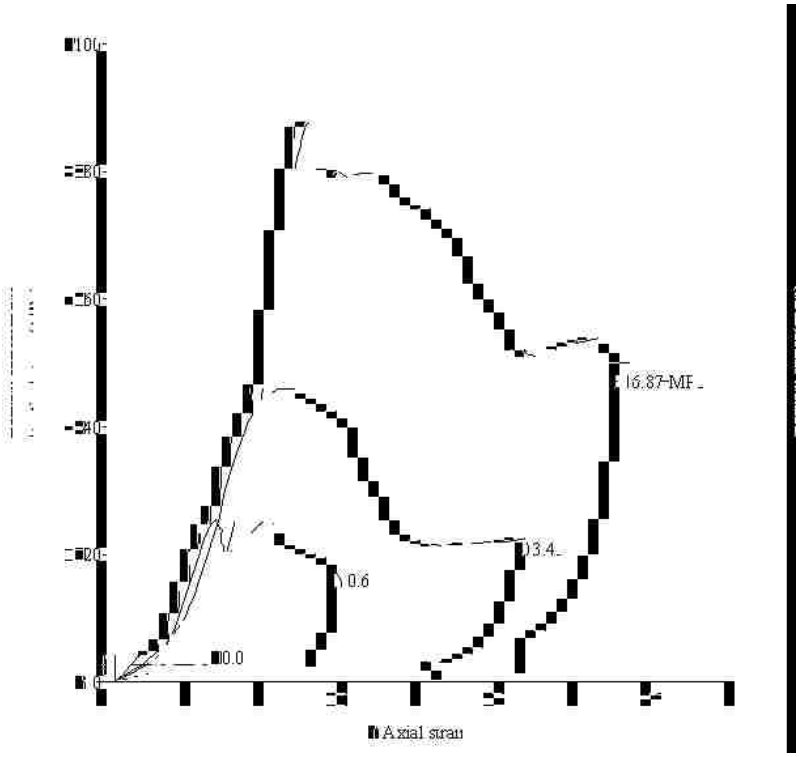

Figure 4.23. Axial stress-strain curves for 6AR specimens under different confining stresses

The second note is the similar pattern of these curves. Although the stress-strain curves in Figure 4.24 do not follow an almost identical pattern as those for 6AR specimens, they are actually very similar if compared individually by pairs. To illustrate this effect, four pairs are presented in Figure 4.26

4.5.3. Failure Mode Observed from the Triaxial Test. In Chapter 3 the failure mode associated with the uniaxial compression test was discussed. The main characteristics for the failure mode associated with the uniaxial compression test are summarized as follows:

•There are two main failure formations: vertical splitting and steeply dipping shearing (Figure 3.8). Vertical splitting is a result of cohesionless property, local anomalies, and the test conditions. Steeply dipping shearing is caused by the high friction angle. Random failure locations, which can be either locally or crossing the entire specimen body. Random failure pattern is a manifestation of the important role of local anomalies. Vertical splitting and random failure patterns are important factors responsible for the large variations of the uniaxial compressive strength.

4.5.3.1. Volumetric dilation. A phenomenon that can be observed after each triaxial test is the increase of the specimen volume or volumetric dilation. Such an example is given in Figure 4.27, where specimen 1S-5 is shown before and after the triaxial test.

It is seen from the figure that the specimen is confined within the platen before the test. As discussed earlier, the dimensions of the platen is 50 x 50 mm and the cross section for the specimen is 46 x 47 mm. However, the cross section of the specimen after the test is expanded beyond the boundary of the platen.

Based on the original dimension of the specimen and its appearance after the test, the expansion in each cross section direction is estimated between 4 –7 mm.

The volumetric dilatation is a basic phenomenon associated with specimens under the triaxial test. It is caused by fracture growth inside the specimens after the axial stress reaches a certain level during the triaxial test. Figure 4.28 is an illustration of this process for oolitic limestone (Elliott, 1982).

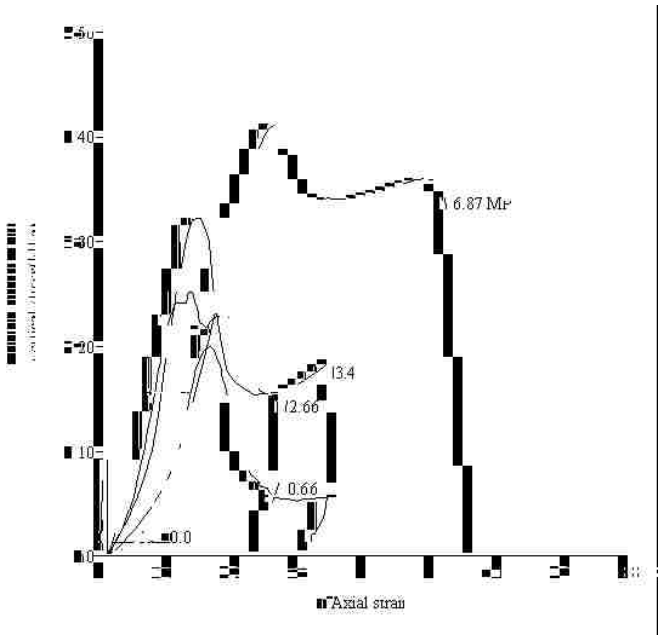

Figure 4.24. Axial stress-strain curves for 1S specimens under different confining stresses

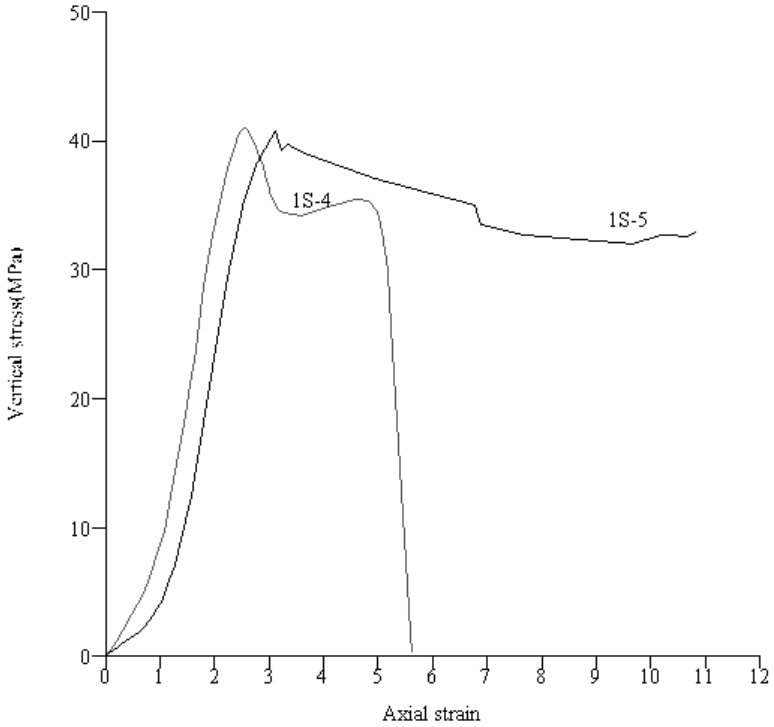

Figure 4.25. A comparison of the axial stress-strain curves for specimens 1S-4 and 1S-5 which were tested with the same confining pressure of 6.78MPa.

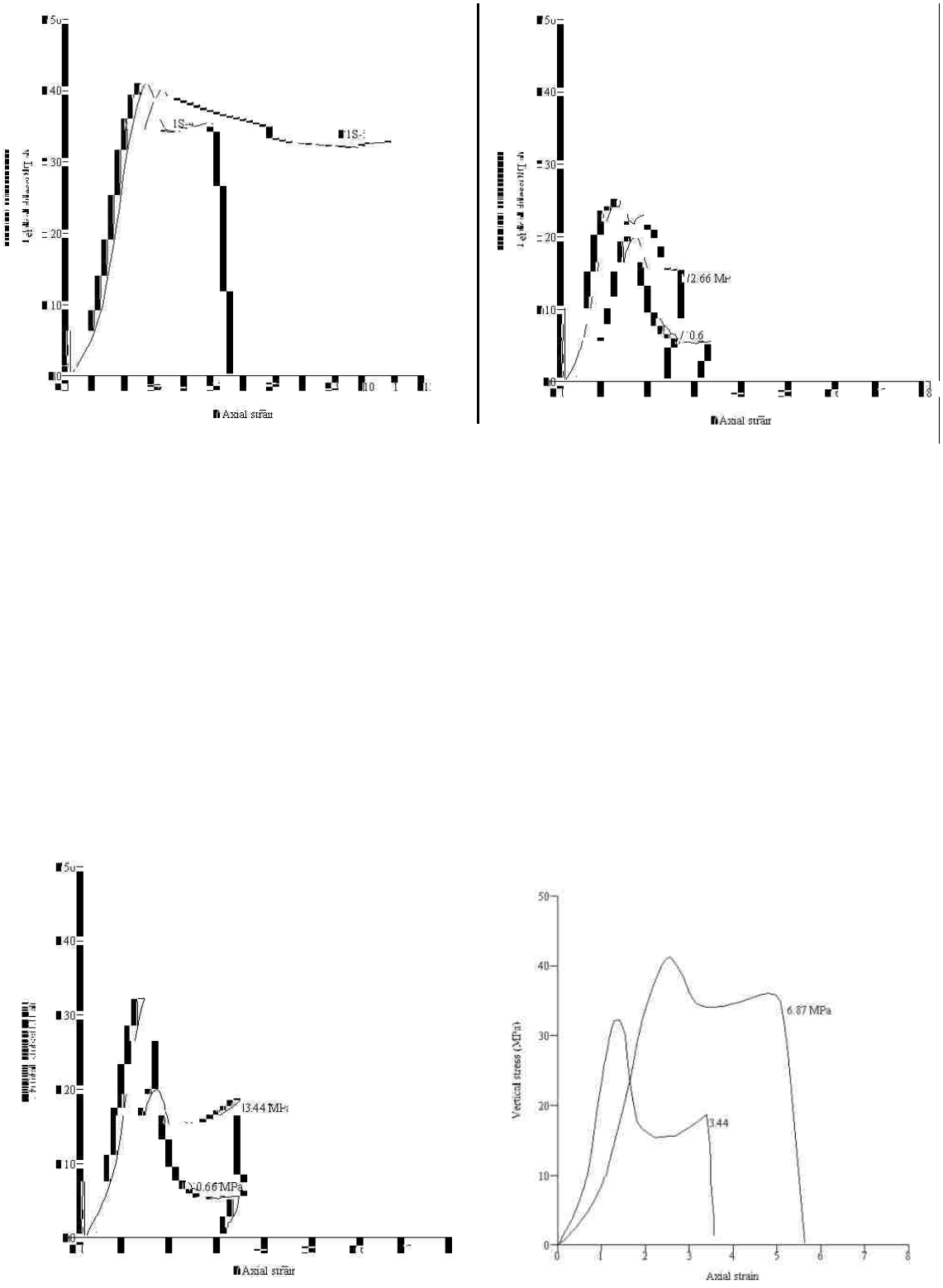

Figure 4.26. Comparing the axial stress-strain curves of 1S specimens by pairs

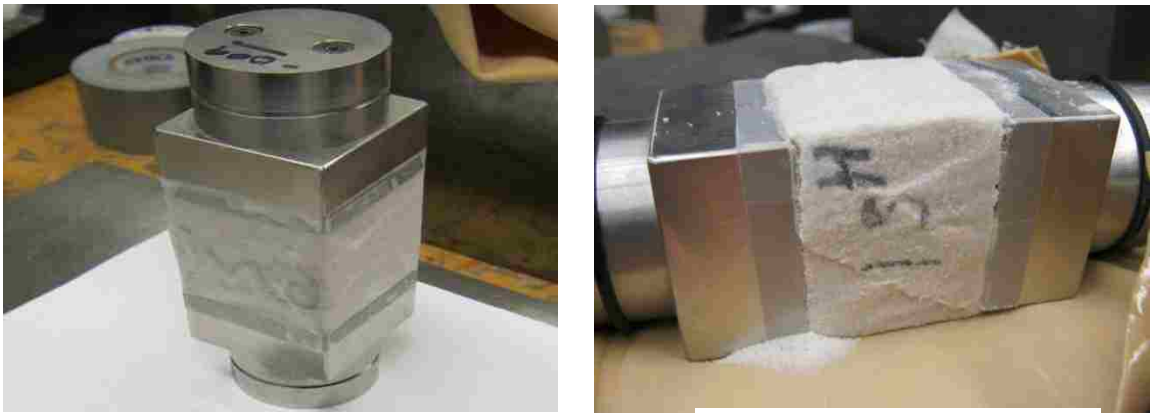

a) Before test b) After test

Figure 4.27. Specimen 1S-5 before and after the triaxial test

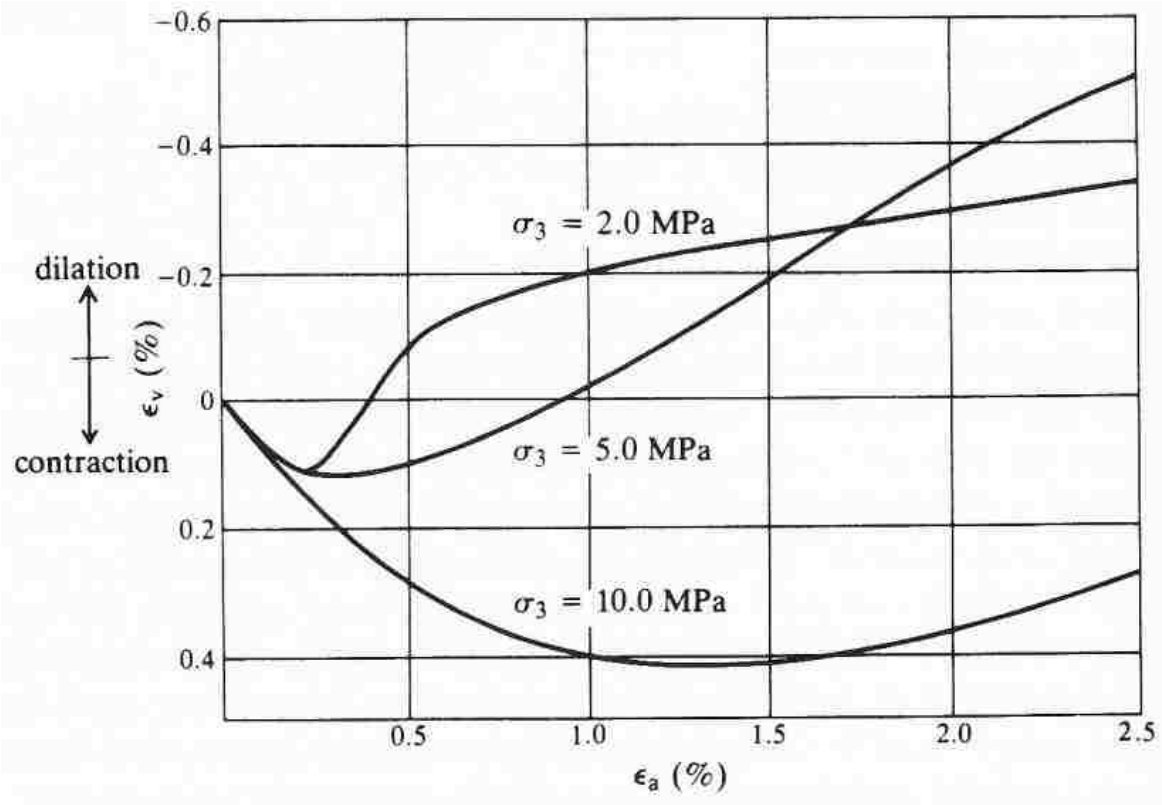

Figure 4.28..Results of triaxial compression tests on an oolitic limestone with volumetric strain measurement (after Elliott, 1982)

Volumetric dilation was observed for all specimens after the triaxial test. Three additional examples are shown in Figure 4.29. The original cross sections for these three specimens are 51 x 51 mm for both 6AR-1 and 6AR-2, and 48 x 51 mm for 12AR. It is clear that all these specimens expanded horizontally. For instance, the new cross section for 6AR-1 is 53 x 53 mm. If we consider a compression of 2.5% in the vertical direction (axial strain) as indicated in Figure 4.23, the volumetric increase for this specimen is 5.3%.

4.5.3.2. A Uniform failure formation featured with pyramid cones. This significant volumetric dilation is an indication of heavy fracturing processes that took place within St. Peter Sandstone specimens. Figure 4.29 shows volumetric dilation for several specimens.

Figure 4.29. Specimens after the triaxial test.

There are three parts in the Figure 4.30. The middle one is the main body of the specimen, which was wrapped by scotch tape immediately after the test to maintain the broken parts in place. The pyramid shaped sandstone piece on the right is the cone from the

upper end of the specimen with the present view. This end was actually the bottom of the specimen during the test. The “pyramid” was found when the specimen was lifted. The loose sands in the plastic were originally part of the main body and they came loose when the specimen was removed. The small piece on the other side is the core from the other end.

Figure 4.31 is a close look at the pyramid. The failure formation as observed from specimen 12AR is not a rare phenomenon. In fact, it is the formation observed from all test specimens. Figure 4.32 is the test result for specimen 6AR-1 and Figure 4.33 is for specimen 1S-

Figure 4.30. Failure formation associated with specimen 12AR -2.

A distinctive difference between the failure modes resulting from the uniaxial compression test and the triaxial test is that the severe impact caused by the uncertainties created by local anomalies for the uniaxial compression test is essentially not a problem for the triaxial test. The uncertainties caused by the cohesionless property is significantly

diminished under triaxial test condtions. In this sense, the axial stress at failure determined by the triaxial test is a much more stable and reliable indication of the strength of St. Peter Sandstone. Therefore, the triaxial test should be conducted if possible.

Figure 4.31. A close look of the pyramid core at specimen 12AR-2

4.5.3.3. Steep failure angle. Figures 4.30 through 4.33 show that all failure surfaces are defined by a very steep angle, which can be evaluated by either the shape of the pyramids or the shape of the inside walls of the specimens. The estimated angle is in the range of 75˚-80˚ based on the height/width ratio of 4-5 for the slopes measured in this study. This angle is very close to the one observed from the uniaxial test, which yields a theoretical friction angle of 60˚-70˚.

Figure 4.32. Failure formation associated with specimen 6AR -1.

Figure 4.33. Failure formation associated with specimen 1S-1.

4.5.3.4. Ductile behavior of specimens after the triaxial test. The change of the material behavior from brittle to ductile under the triaxial test can be observed not only from the change of stress-strain curves, but also from the change of the appearance of the test specimens. For the uniaxial compression test, if we carefully examine those broken pieces individually, the integrity for many of them still remains at a very good level similar to those of the large pieces in Figure 4.35. For the specimens under the triaxial test, the situation is very different. There are significant amounts of loose sands. The crushed pieces are smaller and also much rounder. For those remaining large pieces, they are actually very fragile and are easily disaggregated by any disturbance. Figure 4.36 shows the appearances of specimen 1S-5 immediately after the test and after it was moved to the storage disk. Even though extra attention was paid during the moving process, the specimen disintegrated into small pieces. This led to the procedure of wrapping all samples in scotch tape to prevent their disintegration.

4.5.4. Analysis of Friction Angle associated with St. Peter Sandstone. A particular advantage of the triaxial test for St. Peter sandstone study is that it allows the friction angle to be determined quantitatively under a well-controlled laboratory condition.

4.5.4.1. Friction Angles for St. Peter Sandstone determined by this Investigation. The Mohr circles and the failure envelopes for 6AR and 1S specimens are shown in Figures 4.36 and 4.37. It is evident that the friction angle for 6AR specimens is much higher, shown by the much steeper slopes for its failure envelope.

For a non-linear Mohr envelope, the friction angle changes with the location. The average friction angle for a range of the failure envelope can be defined in many ways. In this research, the average friction angle for a specific range is defined as the angle of the secant line for that range. There are several advantages for adopting this definition: it is simple, easy

to use, and has no ambiguity.

Figure 4.34. A typical specimen appearance after the uniaxial compression test

a) Immediately after the test

b) after removing the specimen

Figure 4.35. specimens after triaxial test and after removing the specimen

Based on this approach, the upper range friction angle is defined as the angle of the secant which intersects the Mohr envelope at the shear stress level of 5 MPa. The friction angles which are determined in Figures 4.36 and 4.37 are therefore the upper range friction angles for 6AR and 1S specimens, which are 73˚ and 69˚, respectively. Similarly, the lower

range friction angle is defined as the angle of the secant which intersects the Mohr envelope at the shear stress level of 10 MPa. The lower range friction angels for 6AR and 1S specimens are shown in Figures 38 and 39, which 68˚ and 56˚, respectively. The average friction angles for 6AR and 1S specimens are 71˚ and 63˚, respectively.

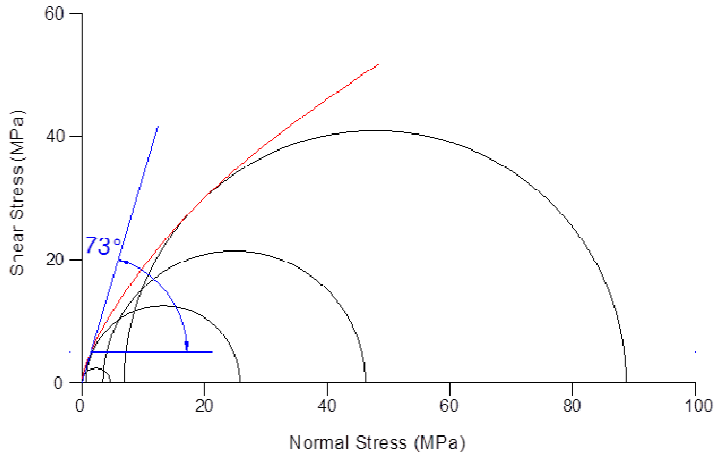

Figure 4.36. Internal frication angle measured at shear stress of 5 MPa for 6ARspecimens

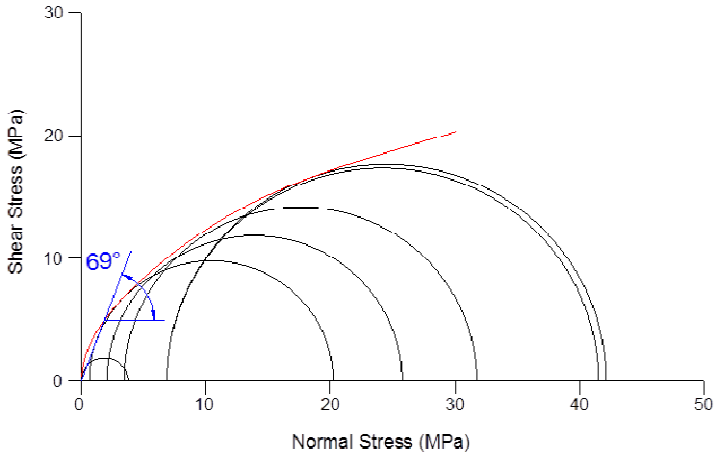

Figure 4.37. Internal frication angle measured at shear stress of 5 MPa for 1S specimens

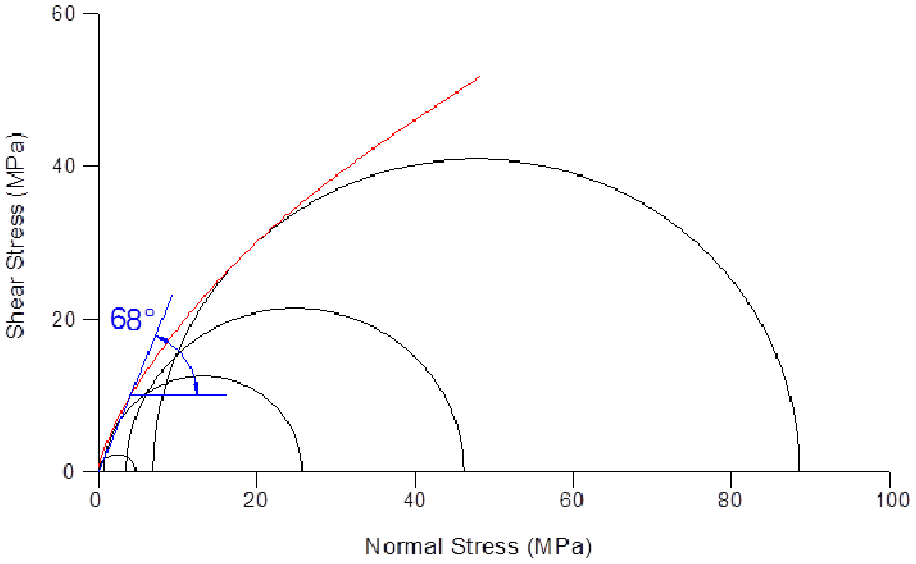

Figure 4.38. Internal frication angle measured at shear stress of 10 MPa for 6AR specimens

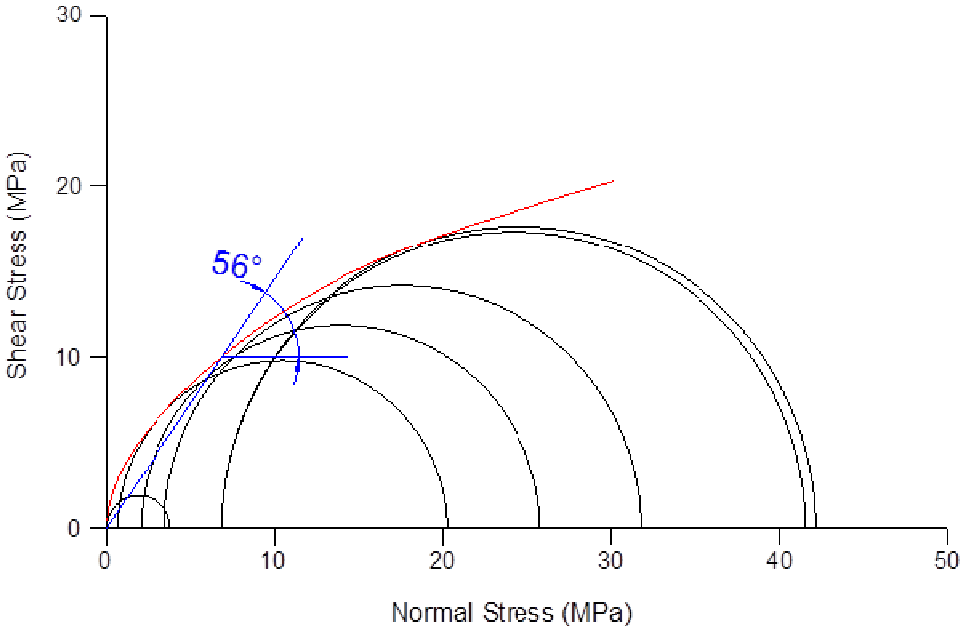

Figure 4.39. Internal frication angle measured at shear stress of 10 MPa for 1S specimens

4.5.4.2. A summary of friction angles for St. Peter sandstone determined by major studies. The friction angles determined by the Mohr's envelope method from this and previous studies are summarized in Table 4.5, which range from 56˚ to 73˚. It is noticed that 56˚ is the low end friction angle for specimens with the highest porosity, while 73˚ is the high end friction angle for specimens with the lowest porosity. The average friction angle determined by Watson (1938) and Labuz et al. (1998) is 63˚, which is the same for 1S specimens tested in this research. With the consideration that the average 71˚ is associated with specimens that have the lowest porosity for St. Peter Sandstone, it appears that 63˚ is a representative figure for St. Peter Sandstone while it may fall on the conservative side with given our test results.

Table 4.5. Friction angle determined by Mohr's envelope method

Specimen source	Friction angle (degree)			Reference
	Low end	High end	Average	
6AR, Clayton, IA	68	73	71	
1S, Clayton, IA	56	69	63	
Twin cities, MN	59	69	63	Watson, 1938
Twin cities, MN			63	Labuz et al., 1998

Finally, it is important to recognize that the high friction angle in the 60˚s is an inherent property of St. Peter Sandstone that can be determined by different means and that the Mohr envelope is just one of them. The direct shear, as discussed earlier, can also reveal this property. The most direct means to observe this property is to look at the tested specimens. As it is demonstrated in the previous chapter and this chapter, the steeply dipping failure formations which are observed from both the uniaxial compression and triaxial compression tests are the best evidences for the high fiction angle for St. Peter Sandstone.

4.6. PRACTICAL IMPLICATIONS OF TRIAXIAL TEST CONDITIONs

The triaxial test on St. Peter Sandstone specimens has shown that the axial stress at failure increases rapidly with the increase of confining pressures. A question that has not been answered so far is the implication of this phenomenon for ground control and engineering problems in rock mechanics.

4.6.1. The Effect of Confining Pressures on General Geological Materials. In order to answer this question, the results of several classical studies on the triaxial test are presented in Figures 4.40-4.43. Figures 4.40 and 4.41 are the mechanical responses of sandstone and norite under the triaxial compression test. These studies were carried out by Bieniawski (1972) and were used by Goodman (1989) for illustrating the effects of confining pressure. The study in Figure 4.42 shows the results of triaxial compression tests on Tennessee Marble which was performed by Wawersik and Fairhurst (1970) and was utilized by Brady and Brown (1993) for demonstrating the behavior of isotropic rock material in multiaxial compression. The study in Figure 4.43 displays results for the triaxial test for Carrara marble, which was conducted by Karman (1911) and was used by Jaeger and Cook (1979).

Table 4.6. A comparison of RAS for St. Peter sandstone and conventional geological materials

Rock type	σ_0 (MPa)	σ_c (MPa)	σ_a (MPa)	RAS	Reference
Sandstone	69.18	6.29	110.00	6.5	Bieniawski , 1972
Norite	251.57	6.29	327.04	12.0	Bieniawski , 1972
Tennessee marble	130.00	20.70	195.00	3.1	Wawersik and Fairhurst, 1970
Carrara marble	137.00	21.38	207.55	3.3	von Karman, 1911
St. Peter sandstone, 1S specimens	3.52	0.66	20.23	25.3	
St. Peter sandstone, 6AR specimens	4.67	0.66	25.74	31.9	

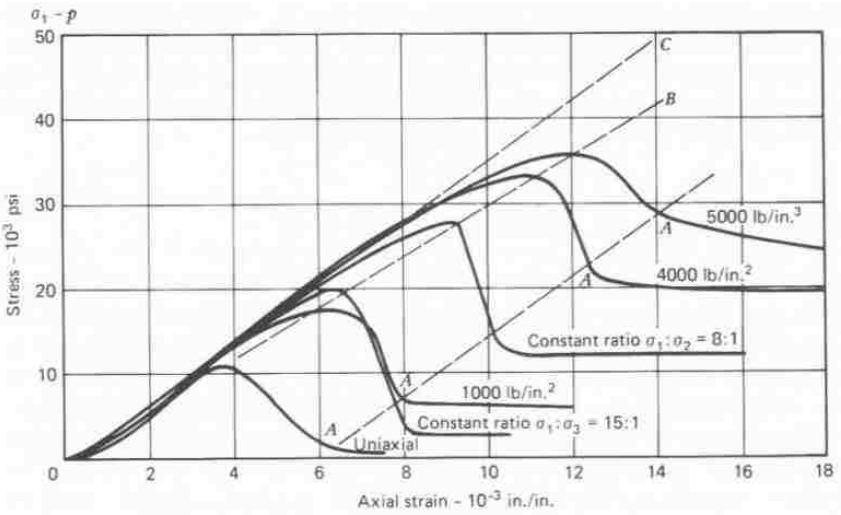

Figure 4.40. Stress difference versus axial strain curves as a function of confining pressure in triaxial compression experiments on sandstone (Bieniawski , 1972)

To compare the effect of the confining stress on the axial stress at failure for the rock materials illustrated in Figures 4.40-4.43 with the effect exhibited by St. Peter sandstone, the RAS, the rate increase of axial stress as defined by Eq. 4.3 was calculated for these materials and compared with the RASs for St. Peter Sandstone in Table 4. 6.

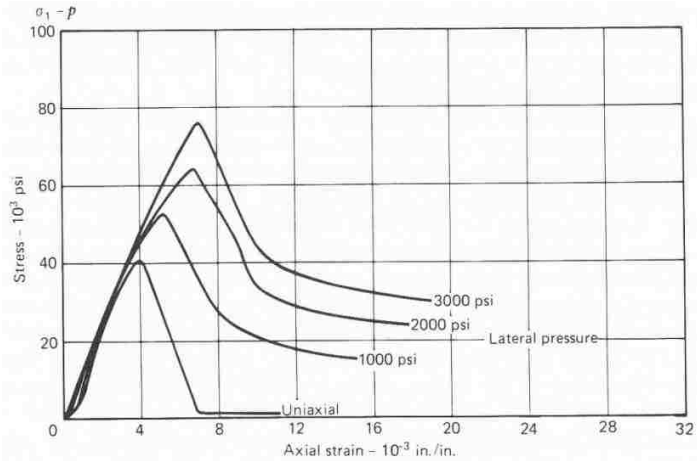

Figure 4.41. Stress difference versus axial strain curves as a function of confining pressure in triaxial compression experiments on norite (Bieniawski,1972)

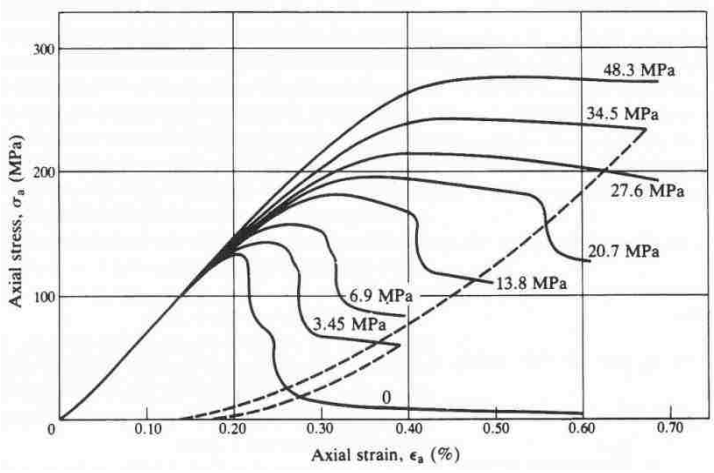

Figure 4.42. Complete axial stress-axial strain curves obtained in triaxial compression tests on Tennessee Marble at the confining pressures indicated by the numbers on the curves (Wawersik and Fairhurst, 1970).

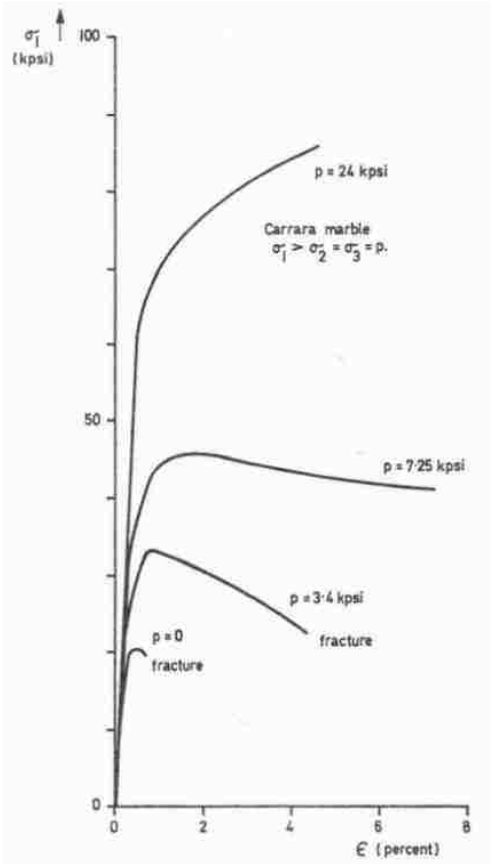

Figure 4.43. The results of triaxial tests on Carrara marble (von Karman, 1911).

It is clear from the table that the rate increase (RAS) for St. Peter Sandstone is much higher than that for four conventional geological materials in Table 4.6. The rate increase for St. Peter sandstone ranges from 25.3 to 31.9. In contrast, it is much lower for conventional geological materials. For Tennessee marble and Carrara marble, they are only 3.1 and 3.3, respectively. It is interesting to note that the rate increases for these two marbles are very similar. The rate increase for sandstone is somewhat higher, which is 6.5. The rate increase for Norite is 12, which is the highest for the conventional geological materials, but is still significantly lower than that for St. Peter Sandstone.

The rate increase range of 25-32 for St. Peter Sandstone implies that, for every unit increase of confining pressure, the strength measured by the axial pressure will increase by 30 units. The extremely high rate increase for St. Peter sandstone suggests that the most efficient means to improve the strength of St. Peter sandstone is to apply the necessary confining pressure.

4.6.2. The Implication of Triaxial Test Conditions for Ground Control Problems. The effect of confining pressures is of fundamental importance for ground control practices in St. Peter sandstone mines. In particular it concerns two outstanding issues: rock reinforcement and pillar design.

At Pattison mine, the most significant ground control problem is pinch-out failures and pillar damages caused by pinch-out failures. Conventionally these problems were treated by rockbolts. Rockbolting is the basic technique for stabilizing underground openings. The operational principle of the technique is to increase the integrity of the rockmass by locking the rock blocks weakened by discontinuities together. An important precondition assumed by using this technique is that those rock blocks, or seams to be locked by rockbolts, are strong enough to stand the locking force. St. Peter Sandstone, as discussed, is cohesionless and is,

therefore, extremely vulnerable to local stress concentration. Because of this, rockbolting, which is a very efficient ground control technique for almost all conventional mines may not be the best choice for these specific sandstone problem. As an example, Figure 4.44 shows that the rockbolts and steel strips were used to reinforce a pillar, attempting to stop a progressive failure of the pillar originally caused by the pinch-out problem. The method, however, did not work.

Figure 4.44. An attempt to stop a progressive pillar failure by rockbolting and steel stripping.

In addition to rock reinforcement, the other potential important application of the confining pressure effect is pillar design. The rate increase index, RAS, may provide the designer useful information for assessing pillar strength. Figure 4.44 shows the application of shotcrete for increasing pillar strength.

Figure 4.45. Stopping initial failures by applying a thin layer of shotcrete.

4.7. CONCLUSIONS

The triaxial compression test provides additional information for a further understanding of the basic mechanical and strength properties of St. Peter Sandstone, which in many ways is much more fundamental and important than uniaxial compressive tests.

The study carried out by this investigation on the triaxial test for St. Peter Sandstone is pioneering in several fronts and has revealed much important information for understanding the basic mechanical and strength properties of St. Peter sandstone.

4.7.1. Axial Stress-axial Strain Curves for St. Peter Sandstone. This is the first report of axial stress-axial strain curves for St. Peter Sandstone under the triaxial test conditions. The axial stress-axial strain curves obtained from triaxial tests are the record of the failure process, the basic information that allows one to analyze rock properties. In this regard, this study fills an important gap for the study of St. Peter Sandstone.

The axial stress-axial strain curves obtained from our study clearly shows the effect of confining pressure: the rapid increase of the axial stress at failure is correlated with an increase of confining pressure. It also clearly shows the change of the material behavior from brittle to ductile because of the increase of confining pressures. The most interesting feature of the axial stress-strain curves obtained from our study is the remarkable similarity for the

same group specimens, which is an illustration that these specimens experience a very similar failure process.

The similarity is also a strong indication of the stability of the test result. The following example is a further demonstration of the stability associated with the triaxial test. For the 1S group, two specimens, 1S-4 and 1S-5, were tested under the same confining pressure of 6.88 MPa and the axial stresses at failure obtained for these two specimens are 41.5 and 42.1 MPa, respectively. The difference is only 0.6 MPa, 1.4% of their average strength. From the similarity of their stress-strain curves in Figure 4.24, it is known that this small difference is by no means an accidental match.

4.7.2. Failure Formations Observed from Test Specimens. Another important contribution of this research is revealing and analyzing the failure formation of specimens after failure, which is the first effort on this front for St. Peter Sandstone. The failure formation observed from the triaxial test is the result of the failure process recorded by the axial stress-axial strain and preserves the physical evidence for further exploring the failure process.

The failure pattern for the triaxial compression test is very different from that exhibited for the uniaxial compression test. For the uniaxial compression test, there are two dominant failure formations, vertical splitting and steeply dipping shearing. However, the pattern of failure is totally random, which is largely controlled by local anomalies. Failures can occur either locally or crossing specimens with unpredictable combinations of two failure formations. The failure pattern for the triaxial is almost identical: a pyramid shape cone is formed at each end of the specimen as shown in Figure 4.27. This uniform appearance indicates that the failure process under the triaxial test conditions is no longer heavily affected by local anomalies. Rather, it is primarily governed by its inherent mechanical

properties. In this regard, the strength assessed from the triaxial test is a much more reliable indication of the strength of St. Peter Sandstone than the strength data obtained from the uniaxial compression test.

A very important feature of the failure pattern observed from the triaxial test is the steep failure angles in the range of 70˚-80˚ degrees, which is a further confirmation of the extremely high friction angles associated with St. Peter Sandstone. The other important feature which can be observed from the specimens after the triaxial test is the change of the material behavior. For the uniaxial compression test, the failure is brittle which is shown not only by a very quick failure process, but also by the fact that the "debris" from the fractured specimens is often still quite strong. For the specimens after the triaxial test, the situation is very different. The debris has no strength at all. Most of them are small and round. The large pieces, such as the core, are in fact very fragile and are easily broken into small pieces once it is disturbed. Specimen 1S-5 discussed earlier is a good example in this regard. The specimen remained as one piece immediately after the test and before the test platens were removed (Figure 4.36 a). However, it disintegrated into very small pieces after the platens were removed (Figure 4.36 b).

4.7.3. Effect of Particle Structure of St. Peter Sandstone. One of the most important contributions of this investigation is the demonstration that the strength of St. Peter Sandstone is primarily governed by its particle structure. This is done by comparing the mechanical response of specimens from two sample groups, 6AR and 1S. The porosities for these two sample groups are 24.5% and 30.5%, which define the porosity range for St. Peter Sandstone.

The study shows that the strength for 6AR group, the group with the low porosity, is much higher than that for 1S group, the group with the high porosity. At the confining

pressure of 6.87 MPa, the strength for 6AR group is 89 MPa which is more than twice of the strength for 1S group, which is 42 MPa, at this confining pressure. The friction angle is also much higher for 6AR group, which ranges from 68˚ to 73˚ with an average of 71˚ while it ranges from 56˚ to 69˚ with an average of 63˚ for 1S group.

The mechanical responses in terms of the axial stress-axial strain curves for these two groups are also very different. For the 1S group, the residual stress decreases much faster at the low confining pressures and is quite steady at the high confining pressures. The behavior for the 6AR group is almost opposite. Its residual stress is steady at low confining pressure, but decreases much faster at high confining pressure. Despite the fact that the residual stress for the 6AR group has a significant drop at the high confining pressure, it is still higher than the peak strength for the 1S group.

Because of the critical influence of the particle structure on the strength of St. Peter sandstone, it is important to identify the specimen structure before the test so that the strength data can be analyzed in context.

4.7.4. Effects of Confining Pressure. In order to measure the effect of confining pressures on the stress at failure for different materials, an index of rate increase of the axial stress at failure, RAS, was defined. RAS provides a quantitative measurement of the increase of the axial stress at failure for each confining pressure unit. A study of RAS for both St. Peter Sandstone and conventional geological materials shows that the RAS for St. Peter Sandstone is much higher than that for conventional geological materials. This study provides a theoretical base for rock reinforcement and pillar design under St. Peter Sandstone condition.

5. PARTICLE STUCTURE OF ST. PETER SANDSTONE

5.1. INTRODUCTION

A primary research objective set for this investigation is to determine the role of the particle structure on the basic mechanical and strength properties of St. Peter Sandstone. This research was first promoted by field observations that failures often started from the locations where sand particles are coarse and poorly graded (uniform gradation).

During the uniaxial and triaxial compression test, the role of the particle structure for St. Peter sandstone was investigated by comparing two groups of specimens, 6AR and 1S, which exhibit distinctive difference in porosity. The porosities for these two groups 6AR are 24.5% and 30.5%, respectively, which represent two extremes of the porosity associated with St. Peter sandstone. The test results show that 6AR specimens are much stranger than 1S specimens. The friction angle for 6AR specimens is also considerably higher.

In this chapter, the mineralogical structure of St. Peter Sandstone will be studied in terms of mineral composition, density, porosity and particle size distribution.

It is important to note that the mineralogical study carried out in this chapter is significantly different from the conventional approach. First the samples utilized for study are not randomly selected. Rather they are from two groups with distinctive structures. As such, all mineralogical features for these two group specimens can be compared objectively. Furthermore, a focus for this study is to identify the relations between the mineralogical properties so that one may be able to interpret these properties from one to another. Finally, a goal of this study is to establish a physical model for the particle structure of St. Peter sandstone, which can be used to explain and to explore the basic mechanical and strength properties of St. Peter sandstone.

5.2. MINERALOGICAL COMPOSITION

St. Peter formation is a pure silica sand and this is especially true for the northern part of states (Thiel, 1935). The chemical characters of St. Peter sands from different areas are presented in Table 5.1.

Table 5.1. Comparison of the chemical characters of St. Peter sandstone from different areas (Thiel, 1935)

State	No. of analyses	SiO_2	Al_2O_3	Fe_2O_3	CaO	MgO	Loss on ignition	Total
Minnesota	3	98.79	0.64	0.21	0.15	……	0.09	99.88
Wisconsin	3	98.01	0.55	0.66	0.43	0.10	……	99.75
Illinois	5	99.72	0.11	0.05	0.56	0.04	……	99.95
Missouri	22	98.87	0.35	0.19	0.13	0.08	0.34	99.96
Arkansas	18	99.02	0.27	0.17	0.07	0.002	0.25	99.77
Oklahoma	1	99.22	0.32	0.14	0.18	trace	0.003	99.86

During this investigation, three samples were sent to Advanced Materials Characterization Laboratory (AMCL), Missouri University of Science and Technology, for the mineralogical composition analysis. The equipment that was utilized for the test is Philips MPD X-Ray Diffraction. Mortar and pestle were used to crush each sample. Coning and quartering were used to obtain representative samples. The test result shows that the silica content for all three samples are greater than 99% (Table 5.2). The detailed test result is given in Appendix C.

Table 5.2. Silica content for St. Peter sandstone samples from Clayton, Iowa

Sample ID	SiO_2
1S	>> 99%
6AR	>> 99%
3AS	>> 99%

The main purpose of the mineralogical composition test is to determine the degree of sand purity in terms of its silica content. This study served two purposes for this investigation. First, we can directly use the density of silica for various volume-weight related calculations if the sand can be considered pure silica. Secondly, there will be no scientific base for sand particles being interpenetrative each other when the sand has such a high degree of purity. penetrative surface fabric is a dominant theory used for explaining the phenomenon of high friction angles associated with St. Peter sandstone.

5.3. DENSITY

The density of St. Peter Sandstone was studied in this investigation. The objective of this study was to determine the correlation between porosity and density. The focus for this study, again, was 6AR and 1S samples.

The density for each specimen was determined by measuring its weight and bulk volume. Digital calipers were utilized for the volume measurement. An important reason to use this measurement method is to minimize the disturbance to the specimens as they were to be used for other tests. Two measures were taken in order to minimize errors associated with this measurement method. First the size of the specimens used for the test is relatively large. No specimens with a size less than 50 mm were used. Secondly, six specimens were tested for two main groups (6AR, 1S) so that the quality of the measurement can be judged statistically. Table 5.3 is a summary of the specimens used for the test as well as the test results. Table 5.4 is a density comparison for specimens from three sample groups. It is noted that the density for the 6AR group is almost 8% higher than the density for the 1S group.

Table 5.3. Densities of St. Peter Sandstone from Clayton, Iowa

Sample ID	Dimension (mm) (L×W×H)	Volume(Kmm^3)	Weight(g)	Density(g/cm^3)
Waterjet	91×90×94	769.86	1513.00	1.967
6AR-1	77×74×85	484.33	1003.28	2.040
6AR -2	53×51×63	170.29	339.04	1.954
6AR- 3	52×50×48	124.80	255.44	2.068
6AR -4	56×53×57	169.18	349.36	2.092
6AR -5	51×51×52	135.25	263.70	1.946
6AR- 6	54×53×60	171.72	332.83	1.922
1S- 1	52×50×70	182.00	338.84	1.857
1S -2	52×49×82	208.94	402.79	1.936
1S- 3	51×51×81	210.68	388.82	1.827
1S- 4	52×50×94	244.40	446.38	1.815
1S -5	52×52×48	129.79	244.88	1.876
1S -6	50×52×87	226.20	413.58	1.833

Table 5.4. A comparison of densities for different sample groups

Sample ID	Density for individual specimens (g/cm^3)	Mean (g/cm^3)	Stand. Dev.
6AR	2.040 1.954 2.068 2.092 1.946 1.922	2.004	0.072
1S	1.857 1.936 1.827 1.815 1.876 1.833	1.857	0.044
Waterjet	1.967	1.967	---

5.4. PARTICLE SIZE DISTRIBUTION FOR ST. PETER SANDSTONE

The knowledge of the particle size distribution for St. Peter Sandstone is important in different ways. First it is the property that has a dominant effect on other basic properties, such as density porosity, permeability. A thorough understanding of these properties is of fundamental importance for St. Peter Sandstone research. Secondly, it is also critical for characterizing the particle structure of St. Peter Sandstone and for further exploring the structure related phenomena, such as high friction angle associated with St. Peter Sandstone. Finally, it is also of great practical importance. As discussed earlier, failures in the field often start from the locations where sand particles are coarse and uniformly distributed. The research on particle size distribution will provide the useful information to explain the

problem and shed light on how to deal with the problem.

5.4.1. A General Discussion of Particle Size Distribution for St. Peter Sandstone. According to Thiel (1935), St. Peter sands have a very uniform distribution. About 90% of the sands fall within the range of 1/8 – 1/2 mm. The finer and coarse grades are in very small amounts. As an example, Figure 5.1 shows the grade size distribution of a series of channel samples taken at vertical intervals of ten feet, from an outcrop of the St. Peter near Blue Mound, Wisconsin (Thiel, 1935). There are two distinctive characters which can be observed from this figure. First the particles that are smaller than 1/16 mm are less or significantly less, in most cases, than 0.3% except the last interval. Second, the amount of coarse sands, which is greater than 1/2 mm, is about or less than 5%. However, the top two intervals are not following this rule.

5.4.2. Particle Size Distribution for Samples from Clayton, Iowa. In this investigation, the particle size distribution was analyzed for both 6AR and 1S samples. A Microtrac S3500 size analyzer from the Department of Material Science and Engineering, Missouri University of Science and Engineering, was utilized for this study. Samples were carefully disaggregated from 6AR and 1S blocks. Conning and quartering were used to prepare representative sample. A total of ten 6AR samples and ten 1S samples were prepared and analyzed for their particle size distributions. The test results for 6AR and 1S samples are presented in Figure 5.2 and Figure 5.3, respectively.

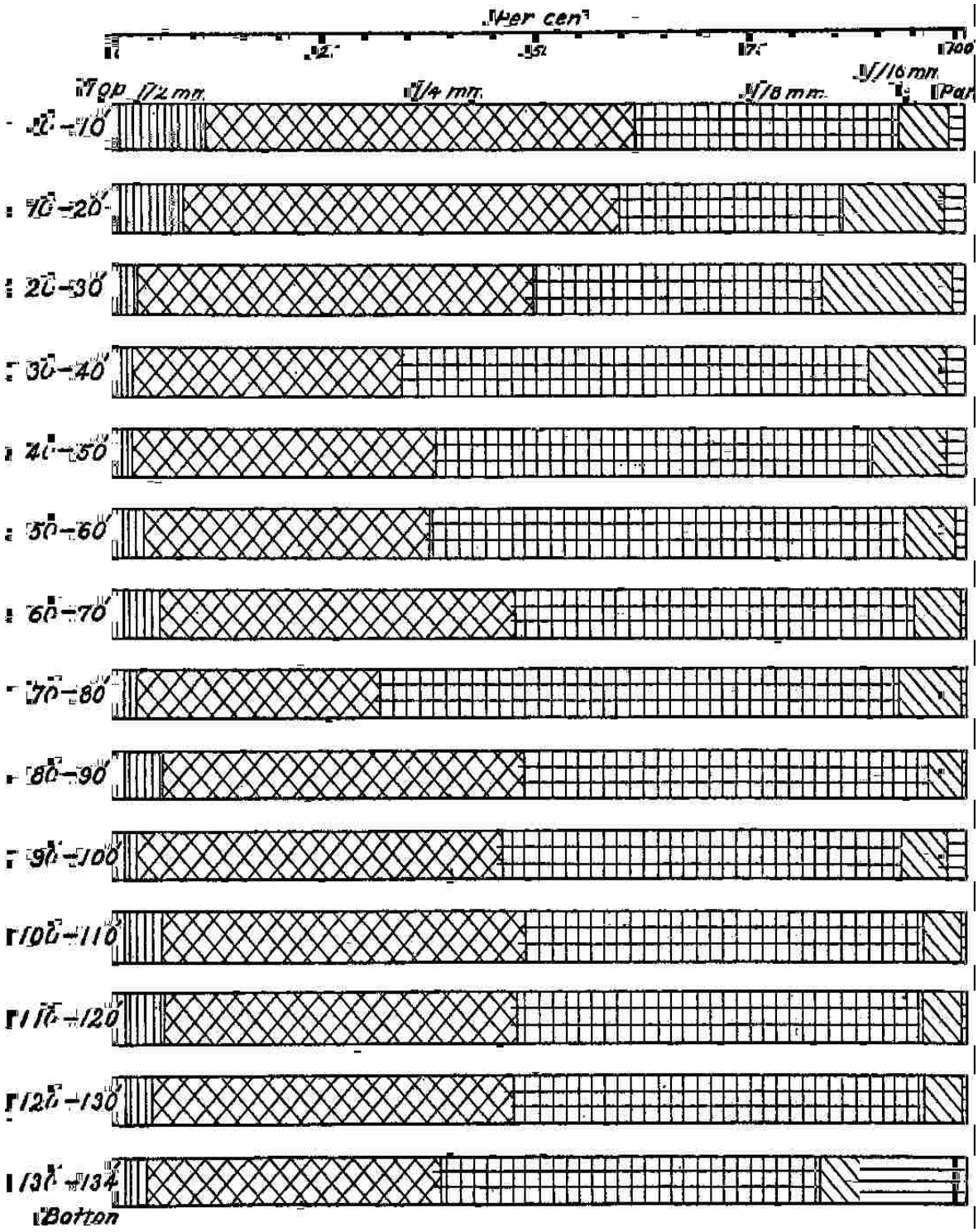

Figure 5.1. Textural analysis in percent by weight of samples of St. Peter sandstone from an exposure near Blue Mound, Wisconsin (Thiel, 1935)

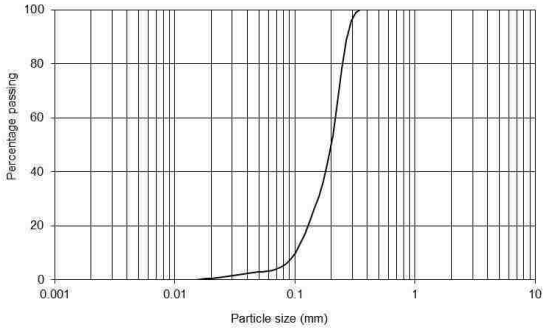

Sample ID: 6AR-1-1

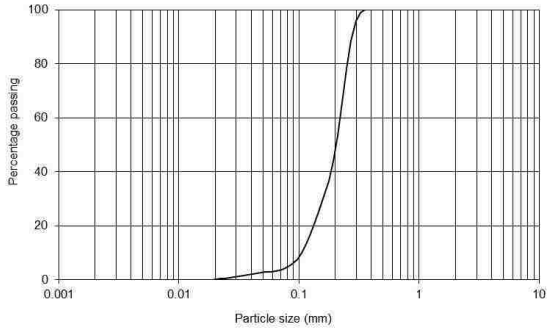

Sample ID: 6AR-2-2

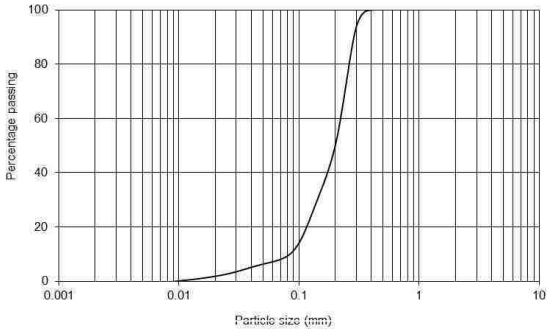

Sample ID: 6AR-4

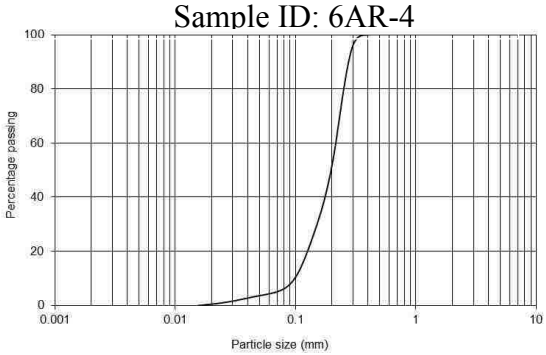

Sample ID: 6AR-6

Figure 5.2. Particle size distribution for 6AR samples

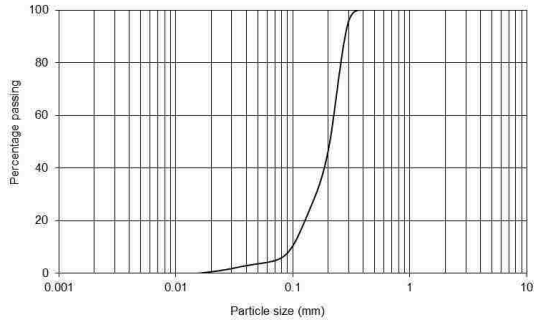

Sample ID: 6AR-6

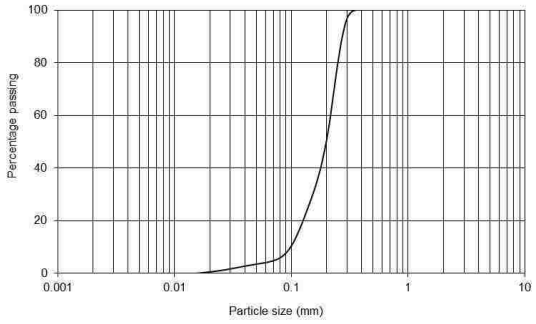

Sample ID: 6AR-7-1

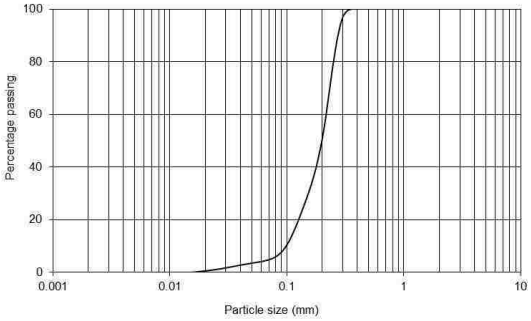

Sample ID: 6AR-7-1-1

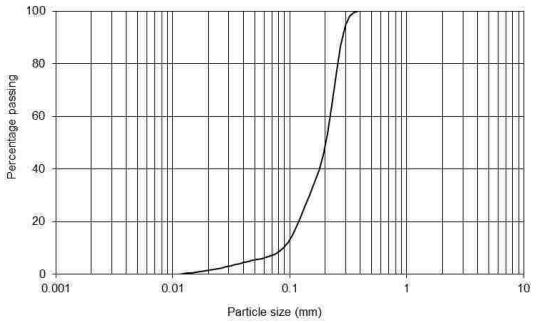

Sample ID: 6AR-8-1

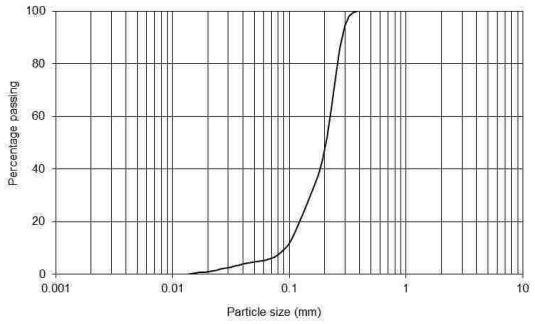

Sample ID: 6AR-9-1

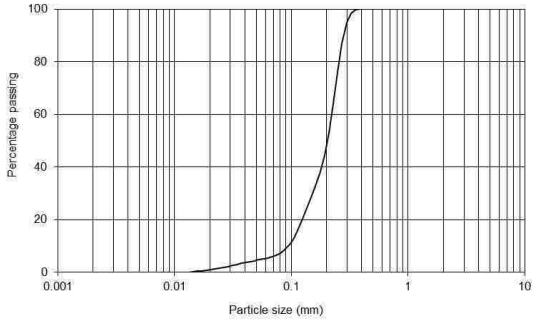

Sample ID: 6AR-10-1

Figure 5.2. (cont.) Particle size distribution for 6AR samples

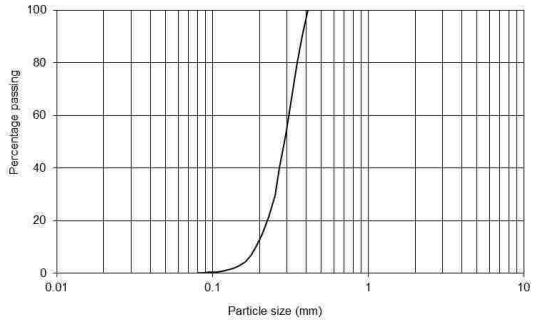

Sample ID: 1S-1(5-4-2012)

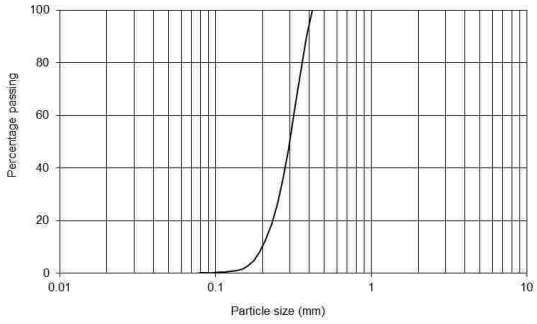

Sample ID: 1S-2-(5-3-2012)

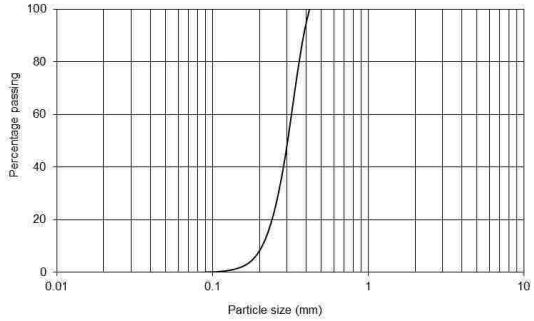

Sample ID: 1S-2-3(5-3-2012)

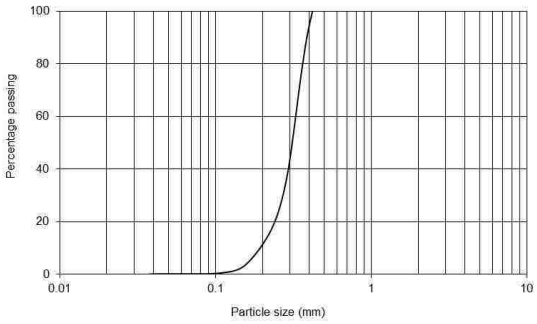

Sample ID: 1S-3-(5-3-2012)

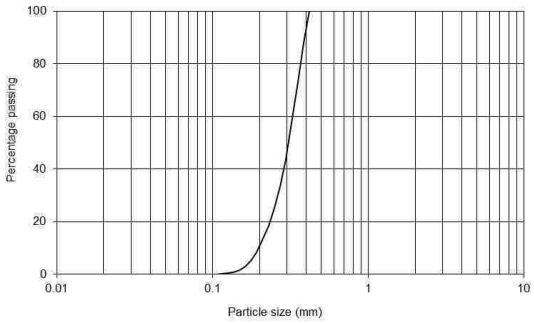

Sample ID: 1S-4-(5-3-2012)

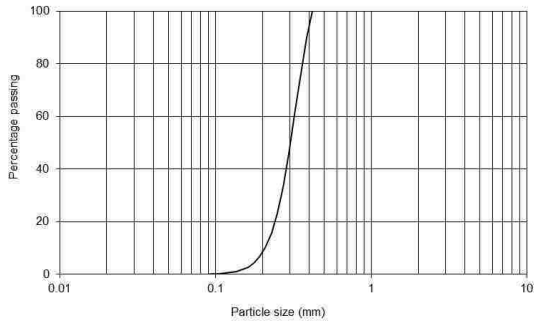

Sample ID: 1S-5-(5-3-2012)

Figure 5.3. Particle size distributions for 1S samples

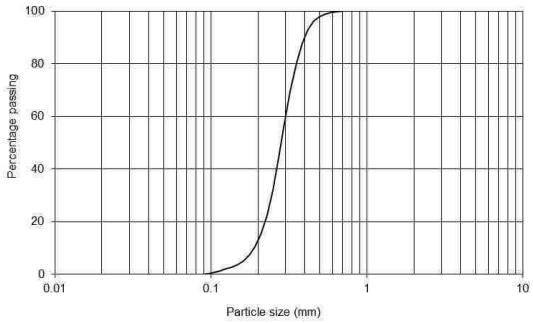

Sample ID: 1S-1-(10-8-2012)

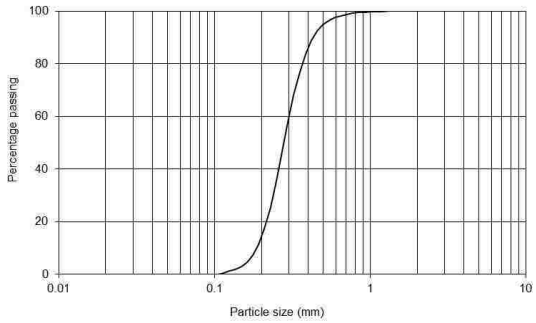

Sample ID: 1S-1-(9-12-2012)

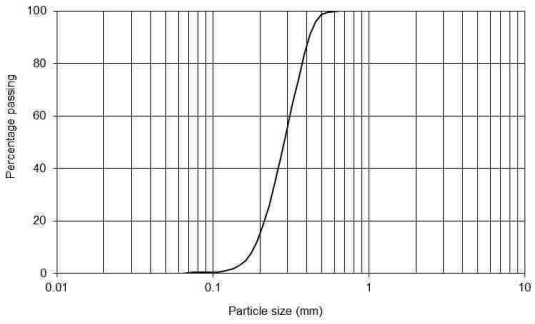

Sample ID: 1S-7-(9-12-2012)

Figure 5.3 (cont.) Particle size distribution for 1S samples

A quick examination of these figures shows that the particle size distribution curves for each sample group are very similar. To facilitate the discussion, the indexes that characterize these distribution curves are summarized for 6AR and 1S samples in Tables 5.5 and 5.6, respectively.

Before a further discussion of the characteristics of the particle size distribution curves associated with 6AR and 1S samples, it is necessary to have a brief discussion on the parameters which are conventionally used for characterizing these distribution curves.

In the field of geotechnical engineering, a symbol, Dn, often denotes particular screen

size that n% materials can pass. For instance, D_{10} refers to a screen size that 10% of materials can pass by weight. Physically it is an indication of the size that (1-n)% materials will be larger.

Table 5.5. Grain size parameters for 6AR samples

Sample ID	D_{10} (mm)	D_{50}(mm)	D_{60} (mm)	C_u	Min(mm)	Max(mm)
6AR-1-1	0.101	0.200	0.210	2.08	0.016	0.348
6AR-2-2	0.105	0.200	0.210	2.00	0.020	0.352
6AR-3	0.087	0.200	0.210	2.41	0.010	0.419
6AR-4	0.100	0.200	0.210	2.10	0.017	0.419
6AR-6	0.100	0.200	0.210	2.10	0.017	0.384
6AR-7-1	0.100	0.200	0.210	2.10	0.017	0.352
6AR-7-1-1	0.100	0.200	0.210	2.10	0.017	0.352
6AR-8-1	0.090	0.200	0.210	2.33	0.012	0.419
6AR-9-1	0.090	0.200	0.210	2.33	0.014	0.419
6AR-10-1	0.093	0.200	0.210	2.26	0.014	0.419
Median	0.100	0.200	0.210	2.10	0.017	0.402

D_{10} is also called effective size. In geotechnical engineering, it is a quick indication how coarse the material is and is used directly as a measurement of permeability. If we compare this index for 6AR and 1S samples, it can be understood that 1S samples are much coarser than 6AR samples. The medians of this parameter for 6AR and 1S are 0.1 and 0.2 mm, respectively.

For this research, a much more important application of this parameter is whether there is a significant presence of fine sand particles. As it has been discussed earlier about 90% of St. Peter sands fall within 0.125 and 0.500 mm. When D_{10} is only 0.1 mm for 6AR samples, it is immediately known that there are a significant amount of fine sand particles, and this can be clearly seen in Figure 5.4.

Figure 5.4 is a combination of two typical particle distribution curves, one for 6AR and one for 1S samples. The arrangement in Figure 5.4 allows a direct comparison of the size

distribution for these two groups of samples. For 1S sample, D_{10} is at 0.2 mm and the smallest particles are about 0.1 mm. For 6AR sample, D_{10} is at 0.1 mm and it has a long tail, ending at 0.02 mm. The importance of this structure feature will be discussed in later sections.

Table 5.6. Grain size parameters for 1S samples

Sample ID	D_{10} (mm)	D_{50}(mm)	D_{60}(mm)	C_u	Min(mm)	Max(mm)
1S-1(5-4-2012)	0.190	0.280	0.310	1.63	0.081	0.419
1S-2-(5-3-2012)	0.200	0.300	0.310	1.55	0.081	0.419
1S-2-3(5-3-2012)	0.200	0.300	0.320	1.60	0.096	0.419
1S-3-(5-3-2012)	0.200	0.310	0.330	1.65	0.040	0.419
1S-4-(5-3-2012)	0.200	0.310	0.329	1.55	0.114	0.419
1S-5-(5-3-2012)	0.200	0.310	0.320	1.60	0.096	0.419
1S-1-(10-8-2012)	0.190	0.280	0.300	1.58	0.096	0.837
1S-1-(9-12-2012)	0.180	0.280	0.310	1.72	0.114	1.408
1S-7-(9-12-2012)	0.180	0.280	0.310	1.72	0.068	0.704
Median	0.200	0.300	0.310	1.60	0.096	0.419

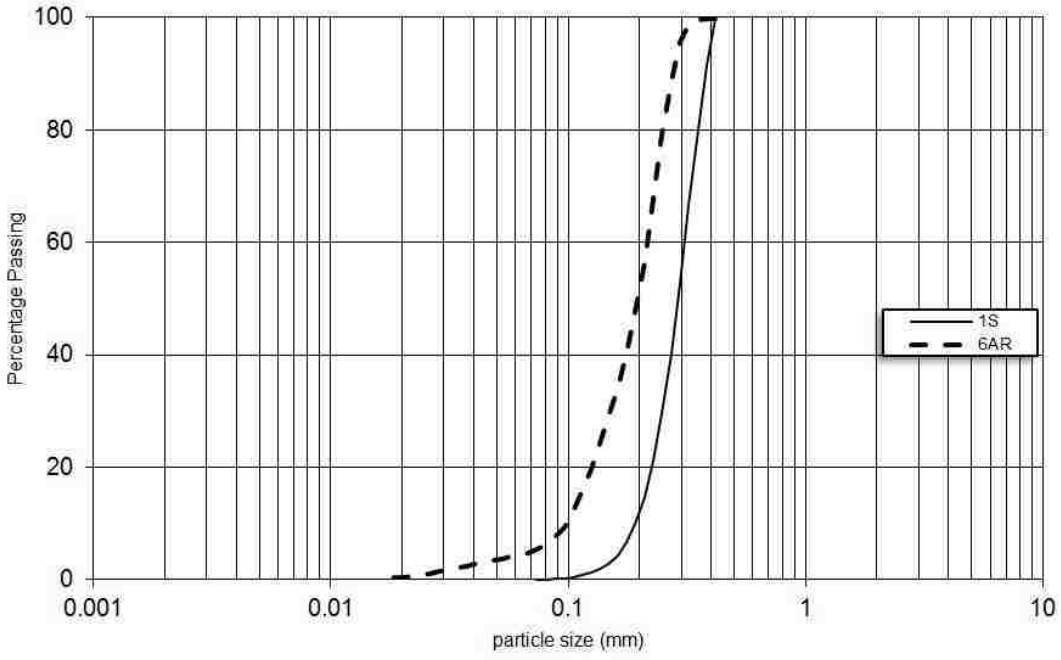

Figure 5.4. A comparison of particle size distributions for 6AR and 1S samples

The other important parameter used in Tables 5.5 and 6 is D_{50}. From the definition of this notation explained earlier, it is immediately known that this parameter represents the median of sand particle, an indication of a representative or an average size. The difference is very significant for 6AR and 1S samples. For 6AR samples, it is 0.2 mm and for 1S samples, it is 0.3 mm, which is 50 larger than that for 6AR samples, a quantitative confirmation of the size difference observed from thin section images (Figure 5.5). It is also interesting to note from the thin section images that it lacks fine particles for 6AR sample, a confirmation of the particle size analysis.

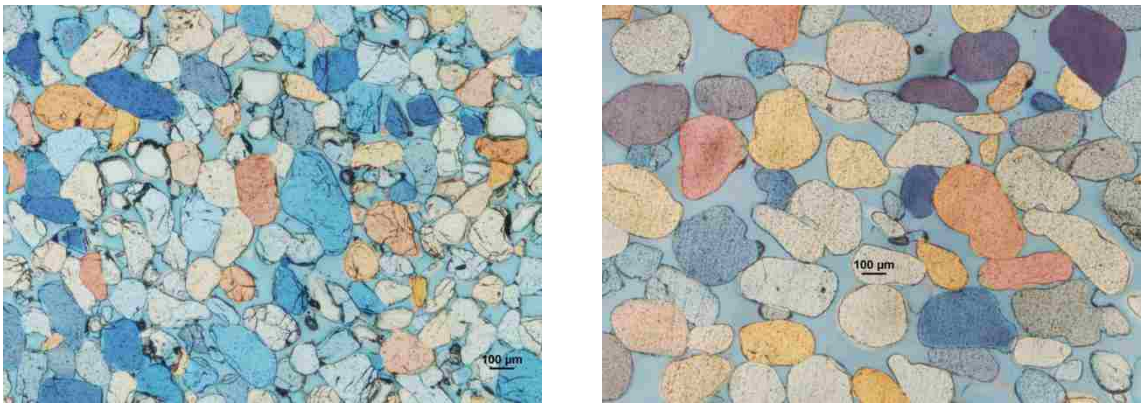

a) Thin section image of 6AR b) Thin section image of 1S sample

Figure 5.5. Thin section images of the 6AR and the 1S samples.

The uniformity coefficient is defined as a ratio of $D_{60}/D_{10,}$. It represents the uniformity of the particle size distribution. A small value means that particles are narrowly distributed. For 6AR and 1S samples, they are 2.1 and 1.6. For general geological materials, even for sand materials, the values of 1.6 and 2.1 are considered extremely low, that is, the sand particles for both 6AR and 1S samples are confined within a very narrow range.

5.4.3. A General Discussion of Particle Size Distribution for St. Peter Sandstone.

The study of the characteristics of the particle size distributions associated with 6AR and 1S specimens also provides valuable information on how to reliably characterize the particle size distribution of St. Peter Sandstone. For the sake of discussion, it is interesting to compare the distribution parameters obtained in this research (Table 5.7) and those obtained from the earlier work (Tables 5.8 and 5.9) .

Table 5.7. A comparison of grain size parameters for 6AR and 1S sample

Sample ID	Effective size, D_{10} (mm)	Median Diameter D_{50} (mm)	D_{60} (mm)	Uniformity Coefficient Cu	Minimum Diameter (mm)	Maximum Diameter (mm)
6AR	0.100	0.200	0.210	2.10	0.016	0.419
IS	0.200	0.300	0.310	1.60	0.088	0.419

In Tables 5.8 and5. 9 there are two parameters, coefficient of sorting and coefficient of skewness, which have not been discussed. Although these parameters are not the subjects for any further discussion, their meanings are briefly explained here for a completion of the discussions related to these two tables. Coefficient of sorting is defined as Squr(D75/D25), The function of this parameter is very similar to that of uniformity coefficient, which measures the uniformity around median. Coefficient of skewness measures skewness of the density function of grain sizes.

The medians for 6AR and 1S samples are 2.00 and 3.00 mm. In Tables 5.8 and 5. 9, if we ignore the special cases, such as 0.463 mm at Illinois, 0.161 mm at Missouri, and 0.114 mm at Willow River, the medians for 6AR and 1S define the range for St. Peter Sandstone.

The uniformity coefficients for 6AR and 1S samples are 2.10 and 1.60. The uniformity coefficients for 6AR and 1S samples are in the range of the uniformity

coefficients listed in these two tables. The uniformity coefficient of 1S, 1.60, is the lowest among the listed values. There are several values, which are larger than 2.10. This should not be considered unusual. In fact, four out of ten 6AR samples have the uniformity coefficients higher than 2.10, which are 2.26, 2.30, 2.30, and 2.40.

Table 5.8. Summary of the textural characteristics of St. Peter s of the Upper Mississippi Valley. Based on computed averages from 96 samples (after Thiel, 1935)

Geographic Location	Median diameter	Coefficent of sorting(SO)	Coefficient of skewness (SK)	Effective size in millimeters	Uniformity coefficient
Gadelonia	0.241	1.39	1.02	0.165	2.12
Castle Rock	0.192	1.31	1.17	0.106	1.64
Chatfield	0.239	1.42	1.01	0.124	2.39
Chimney Rock	0.309	1.45	1.26	0.107	2.24
Decorah, Iowa	0.233	1.45	0.99	0.117	2.34
Mendota	0.235	1.41	1.09	0.142	1.99
N. Minneaoopolis	0.235	1.48	0.96	0.107	2.65
St. Paul Park	0.178	1.32	1.20	0.119	2.28
Zumbrota	0.201	1.32	1.06	0.114	2.00
Pretson	0.225	1.47	0.97	0.119	2.23
S. Minneaoopolis	0.219	1.55	0.94	0.089	3.02
Rochester	0.207	1.38	1.12	0.121	2.00
Mound Park	0.197	1.37	1.07	0.121	1.92
Washington Co	0.281	1.27	1.11	0.175	3.66
Blue Mound, WI	0.235	1.33	1.04	0.125	2.38
Ripon, WI	0.236	1.32	1.09	0.139	1.93
South Geen Co, WI	0.221	1.33	1.14	0.133	1.90
Willow River, WI	0.281	1.25	0.97	0.175	1.71
Average	0.222	1.39	1.07	0.122	2.25

The effective sizes for 6AR and 1S are 0.100 and 0.200. The effective sizes for 6AR and 1S are in the margins of the values showed in Tables 5.8 and 5.9 if the value associated with Illinois is ignored. There are several numbers that are slightly less than 0.10 mm. For 6AR samples, there are three samples having the effective sizes lower than 0.100 mm. The lowest one is 0.087 mm.

Table 5.9. Summary of the textural characteristics of St. Peter sandstone from its northern margin in Minnesota and Wisconsin to south-central Arkansas (after Thiel, 1935)

Geographic Location	Number of samples	Median diameter in millimeters	Coefficient of sorting (SO)	Coefficient of skewness (SK)	Effective size in millimeters	Uniformity coefficient
Minnesota	72	0.216	1.42	1.03	.114	2.34
Wisconsin	24	0.223	1.33	1.06	.124	2.31
Illinois	11	0.463	1.34	0.93	.279	1.74
Missouri	8	0.161	1.25	1.11	.151	1.59
Arkansas	11	0.241	1.28	1.10	.149	1.75

The characteristics of the size distributions associated with 6AR and 1S provide two base lines for comparison purposes. For instance, it is known from Table 5.9 that St. Peter Sandstones in Minnesota and Wisconsin are similar to 6AR samples from Clayton, Iowa, which the particle size close to the lower range of St. Peter Sandstone.

These two base lines can also be utilized to check the reliability of the previous research. For instance,. the effective size and the median 0.175 mm are of 0.281 mm for respectively for samples from Washington Co. In other words, the size characteristics of samples from Washington Co are very similar to 1S. If D50/D10 is used, the uniformity coefficient approximated 1.606. However, the uniformity coefficient was reported 3.66 (Table 5.8). This is a contradictory result since the sorting coefficient is 1.27, which is an extremely low value for St. Peter Sandstone. It is an indication that the size distribution curve is very steep for its central part. According to the above analysis, this value should be 1.66, instead of 3.66.

5.5. POROSITY MEASUREMENT FOR ST. PETER SANDSTONE, CLAYTON, IOWA

Porosity is a basic parameter for characterizing the particle structure of St. Peter Sandstone. In this research a special effort was made to accurately measure porosity because

of the fundamental importance of this parameter for this research. In addition to the buoyancy technique, a conventional method used for this purpose, the porosities were also studied in terms of petrographic images and density-volume relations.

5.5.1. Porosities of St. Peter Sandstone for St. Paul-Minneapolis Area. It is beneficial to review previous research on this topic briefly. The study of porosity, however, appears to be very limited in the past. The only systematic study we could find is the one carried out by Kamb (1932) and the result of this study is presented in Table 5.10.

Table 5.10. Porosities of St. Peter Sandstone (after Thiel, 1935)

Sample No	Stratragraphic position (in feet)	Geographic location	Percentage of Porosity (%)
1	5 from top of formation	Gov't Dam, Minneapolis	27.2
2	15 from top of formation	Gov't Dam, Minneapolis	27.2
3	20 from top of formation	Gov't Dam, Minneapolis	24.6
4	50 from top of formation	Gov't Dam, Minneapolis	26.8
5	65 from top of formation	Gov't Dam, Minneapolis	30.1
6	100 from top of formation	Gov't Dam, Minneapolis	29.5
7	40 from top of formation	Battle Greek Park, St. Paul	29.6
8	20 from top of formation	Newport, Minnesota	28.8
9	15 from top of formation	St. Paul Park, Minnesota	28.1
10	30 from top of formation	North Minneapolis	31.1
		Average	28.3

The porosities in the table were determined by a volumetric method suggested by Russell (1926). The tests were performed on St. Peter sandstone. Acetylene tetrachloride was used as the immersion liquid.The data in the table are all from St. Paul-Minneapolis area and are listed according to the depth locations of these samples. The minimum porosity is 24.6% and the maximum is 31.1%. It appears that the porosities for shallow locations are smaller than those for deeper locations, except sample No. 10, which is quite shallow (30 ft below top), but has the highest porosity of 31.1%.

5.5.2. Porosity Measurement by Liquid Saturation Technique. The liquid saturation technique is used to measure the effective porosity for rock samples (Torsæter & Abtahi, 2000). With this technique, samples are first vacuumed inside a dessicator by a vacuum pump and then saturated by fluid immersion in a vacuum for a period of at least 1 hour (Figure 5.6). The saturated samples are then weighed. In this study a 2 % potassium chloride (KCL) solution was used to saturate the samples. Figure 5.6 shows the saturation process for the samples used in this investigation.

Before the vacuuming process, samples were dried in an oven at approximately 105˚ Celsius for no less than 24 hours.

The bulk volume of each sample was also measured. The volume of voids is determined by the following equation

$$V_V = \frac{W_{sat} - W_{dry}}{\gamma_{fluid}} \tag{5.1}$$

Where Vv is the volume of voids, Wsat is the weight of saturated samples, Wdry is the weight of dry samples, and γfluid is the density of the fluid.

The porosity can then be calculated by the following equation,

$$n = \frac{V_V}{V} \tag{5.2}$$

Where n is porosity and V is the sample volume.

Figure 5.6. Samples are saturated by fluid immersion in a vacuum using liquid saturation method.

In this research three samples were measured for their porosities using the liquid saturation technique, including two 6AR samples and one 1S sample, and the results are given in Table 11. A comparison of the porosities for 6AR and 1S samples is given in Table 5.12.

Table 5.11. Porosity of St. Peter Sandstone, Clayton, Iowa, using liquid saturation technique method

Sample ID	Dimension (mm)	Volume (cm^3)	Weight -dry (g)	Weight -Sat. (g)	Void (cm^3)	Porosity (%)
6AR-3	51×51×50	129.98	249.302	280.462	30.81	23.7
6AR-6	50×51×51	130.11	253.194	285.652	32.14	24.7
1S-3	48×50×38	92.29	172.485	200.549	27.78	30.1

5.5.3. Porosity Measurement based on Petrographic Images. In this research, thin section images, as those presented in Figure 5.5, were utilized for porosity measurement.

A thin section is a thin layer of a rock sample that is ground to a thickness of 30 microns. The cross area dimension for a thin section is typically 26 mm × 46 mm.

There are mixed opinions about the efficiency of method for estimating volumetric pore content. For instance, it was stated in ISRM suggested methods (ISRM, 1981) that

> "*Microscopic techniques used to determine volumetric content of mineral grains, do not provide a sufficiently accurate estimate of volumetric pore content and experimental techniques are required*."

Table 5.12. Porosities determined by liquid saturation method for St. Peter Sandstone

Sample ID	Porosity (%)	Mean (%)
6AR	23.7 24.7	24.2
1S	30.1	30.1

A mathematical verification for this method was provided first. Assume that a sample has a cross section area of A with a thickness of D. The sample consists of m number of thin sections with a thickness of Δd for each thin section such that D = Δd x m. Let Avi denote the void area for the ith thin section, where i = 1, 2, 3, ……, n. The porosity for this sample is

$$n = \frac{V_V}{V} = \frac{\sum_{i=1}^{m} A_{vi} \Delta d}{A \Delta d \times m} \tag{5.3}$$

Where n is the porosity, V is the sample volume, and VV is the void volume. Assume that the image size is significantly larger than the grain size and grain particles are randomly distributed in the volume. As such, the void for each thin section should be statistically identical, that is,

$$A_v \Delta d = A_{v1} \Delta d = A_{v2} \Delta d = ... = A_{vm} \Delta d \tag{5.4}$$

Where Av is the void area for each thin section. Considering Eq. 4, Eq. 3 can be rewriting as

$$n = \frac{V_V}{V} = \frac{\sum_{i=1}^{m} A_{vi} \Delta d}{A \Delta d \times m} = \frac{\sum_{i=1}^{m} A_v \Delta d}{A \Delta d \times m} = \frac{A_v \Delta d \times m}{A \Delta d \times m} = \frac{A_v}{A} \tag{5.5}$$

Eq. 5.5 simply states that porosity can be expressed by the ratio of void area to total area measured from microscopic images.

In this investigation four thin section samples, two for 6AR and two for 1S, were utilized to study their porosities. Each thin section sample was divided into 15 image areas to assure the image resolution. Such an example is given in Figure 5.7 which contains 15 thin section images for a 6AR thin section sample.

The porosity for each thin section image is determined by the following procedure:

- The image is loaded on the computer screen,
- Each sand particle was traced with the help of Element, a Nikon developed imaging software package,
- The traced area is calculated by Element and the result is imported to a spreadsheet,
- The total particle areas were calculated after all sand particles in the thin section image were traced and the corresponding areas were determined by NIS Element software developed by Nikon, and
- The void area in each petrographic image was calculated by subtracting the total grain areas from the total image area.

As an example, the porosities determined by this method for 15 thin section images in Figure 5.7 are listed in Table 5.13

Table 5.13. Porosities determined for 6AR samples by using thin section images

Image ID	Porosity (%)
6AR-1	24.0
6AR-2	24.9
6AR-3	22.7
6AR-4	23.5
6AR-5	25.5
6AR-6	22.2
6AR-7	23.4
6AR-8	20.5
6AR-9	21.2
6AR-10	20.1
6AR-11	24.3
6AR-12	24.3
6AR-13	24.8
6AR-14	27.4
6AR-15	22.8
Average	23.4
Standard deviation	1.9

The final measurement results for four thin section samples are summarized in Table 14. The average porosities for 6AR and 1S samples are 24.30 and 30.49, respectively, which are very close to results determined by the Buoyancy method. The porosities for 6AR and 1S samples determined by the liquid saturation method method are 24.2% and 30.1%, respectively.

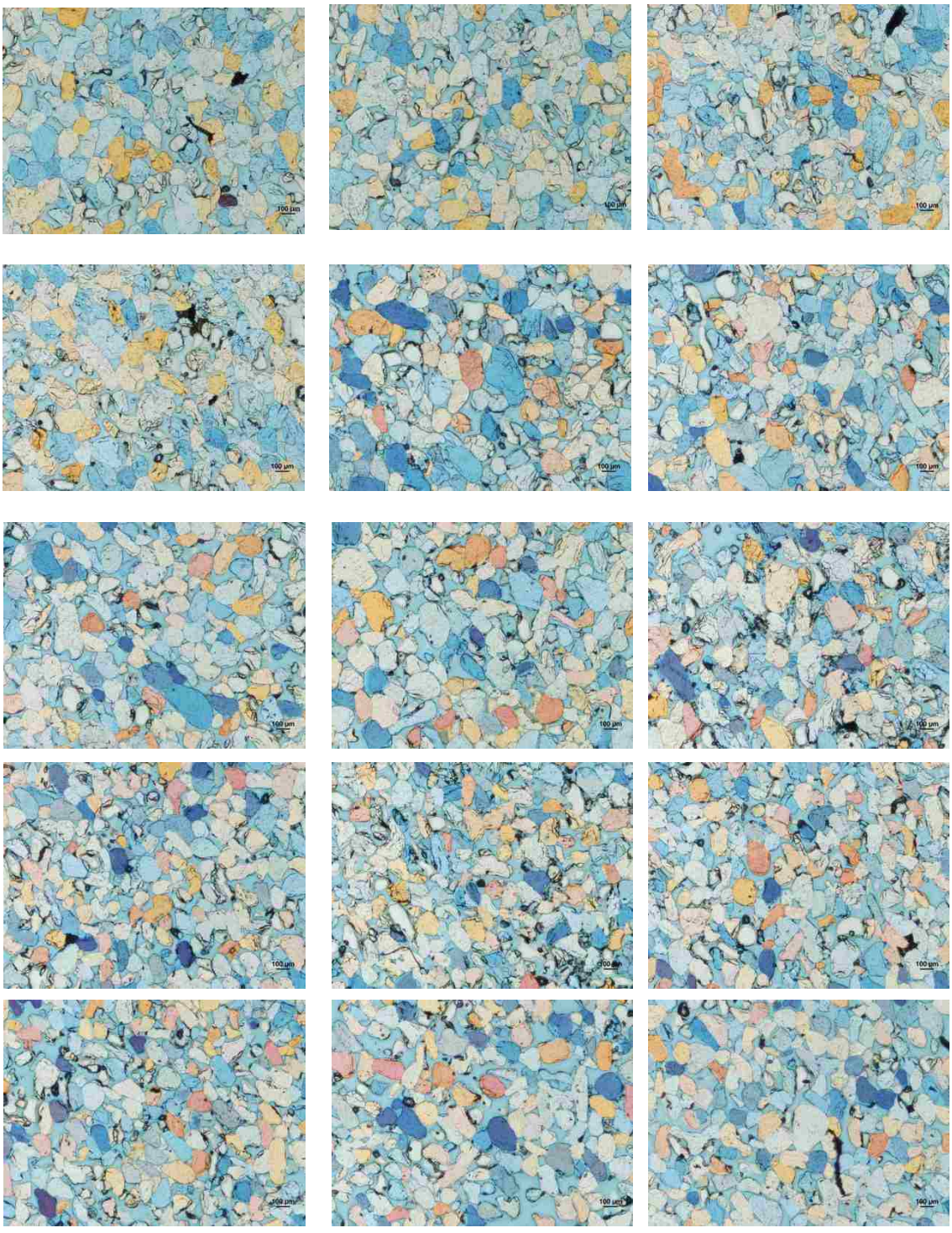

Figure 5.7. Thin sections that are used for porosity measurement in this research

5.5.4. Porosity Estimation based on Dry Density of Samples. As discussed in section 5.1, St. Peter Sandstone can be considered as pure quartz. Because of this, porosities for St. Peter Sandstone samples can be estimated in terms of the specific gravity of quartz and the densities of these samples. Mathematically, this relation can be expressed by the following equation,

$$n = \frac{G_s \gamma_w - \gamma_d}{G_s \gamma_w} \tag{5.6}$$

Where Gs is the specific gravity, which is 2.65 for quartz, γ_w is the density of water, which is 1, and γd is the dry density. The densities for 6AR, 1S and waterjet were discussed in section 5.2 and were given in Table 5.3. The average densities for these sample groups and the corresponding porosities are listed in Table 5.15.

Table 5.14. Porosities of St. Peter sandstone determined based on petrographic images

Block name	Individual Results (%)	Average Porosity (%)
6AR	23.4, 25.2	24.30
1S	30.0, 30.98	30.49

Table 5.15. Porosities determined based on sample densities

Sample group	Density (g/cm^3)	Porosity (%)
6AR	2.004	24.41
1S	1.857	29.89
Waterjet	1.967	25.77

5.5.5. A Summary of the Porosity Measurement Results. The porosity of St. Peter Sandstone was measured by three different approaches: liquid saturation technique, petrographic images, and dry density of samples. The results, as displayed in Table 5.15, are remarkably similar. The standard deviation for 6AR samples is only 0.1% and for 1S samples

is only 0.3%.

The results presented in Table 5.16 are significant for three particular reasons. First it demonstrates extremely high reliability of the porosities determined from this research as the results given by three independent methods with different measurement mechanisms are most identical.

Table 5.16. A comparison of porosities determined by three approaches

Sample group	Porosity (%)				
	Liquid Saturation	Petrographic	Density	Average	Std.
6AR	24.2	24.3	24.4	24.3	0.10
1S	30.1	30.5	29.9	30.2	0.31

Secondly, it demonstrates that the porosity for St. Peter Sandstone can be reliably determined by any of the three methods. The importance of this finding is that it provides flexibility for determining this important parameter. It is important to emphasize that the highly consistent results obtained from this research is also due to attention to details. For instance, only large samples were used for the volume measurements in order to reduce the impact of measurement errors. Breaking the thin section sample into 15 image areas to assure high image resolutions is another example of such attention to detail.

Finally, the consistent result is a validation of the quality of all related work, including volume measurements, density determination, test procedures with the liquid saturation technique, and working procedures with petrographic images.

5.6. RHOMBOHEDRAL PACKING – A PARTICLE STRUCTURE MODEL FOR ST. PETER SANDSTONE

In order to study the structural effect of St. Peter Sandstone, rhombohedral packing

was selected to model the particle structure of St. Peter Sandstone. The expermintal results of this research was used. Figure 5.8 is a three dimensional view of this model which consists of even size spheres packed with the rhombohedral pattern.

Figure 5.8. Rhombohedral packing.

Rhombohedral packing was originally discussed by Graton and Fraser (1935). The selection of the rhombohedral packing as the structure model for the St. Peter sandstone is based on three considerations. First the rhombohedral packing offers the closest porosity for the St. Peter sandstone. The porosity for the St. Peter sandstone is in a range of 24 – 31%. The porosity for the rhombohedral packing is in the middle of the porosities typically associated with the St. Peter sandstone, 25.95%. Secondly, the rhombohedral packing has the most stable structure among all even-sphere models. It is incompressible because it reaches

the minimum porosity that can be achieved by even-sphere models. This characteristic is representative for the St. Peter sandstone. The third consideration is that the rhombohedral packing is the basic model for densely packed soils. In comparison with soil samples, the St. Peter sand is much more closely resembled by the model if we consider the roundness and narrowly distributed size of these sand particles.

Graton and Fraser (1935) conducted a detailed model study on the porosity and permeability of rocks (Graton and Fraser, 1935). The model consists of the geometrically systematic arrangement of uniform spheres. With this model, not only the porosity for the assumed grain structure can be studied, but also the stability of the associated structure can be evaluated. Six typical cases were identified in this study, which are Case 1 – cubic packing, Case 2 – orthorhombic packing, Case 3 – rhombohedral packing, Case 4 orthorhombic packing, Case 5 –tetragonal-spheroidal packing, and Case 6 – rhombohedral packing (Figure 9). Among these six cases, two pairs of cases have identical internal arrangements. The first pair is Case 2 and Case 4 and the second pair is Case 3 and Case 6. As a result, only four cases are independent. The porosities for these four independent cases are listed in Table 5.17.

It is known from the table that cubic packing is the loosest packing and rhombohedral packing is the tightest. Among these four independent cases, rhombohedral packing offers the most stable structure

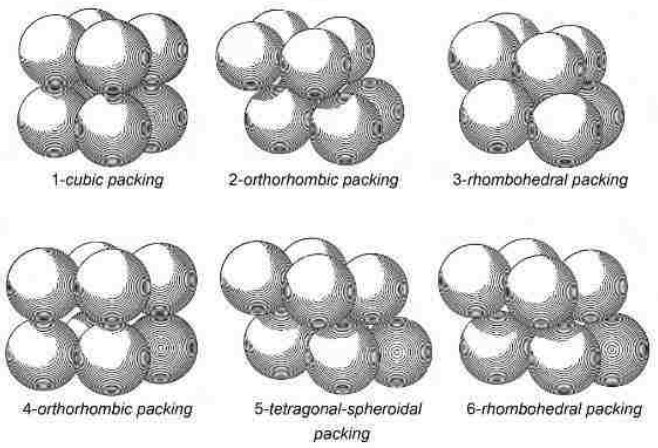

Figure 5.9. Six typical packing patterns of uniform spheres (after Graton and Fraser, 1935).

Table 5.17. Porosities for six typical packing patterns of uniform spheres (Graton and Fraser, 1935).

Case #	Packing case	Porosity (%)
Case 1	*cubic packing*	47.64
Cases 2 & 4	*orthorhombic packing*	39.54
Case 5	*tetragonal-spheroidal packing*	30.19
Cases 3 & 6	*rhombohedra packing*	25.95

The even-sphere models have been used extensively in soil mechanics due to the fact that the porosity range of 26.0% - 47.6%, predicted by this modeling approach fits very well for soils. The question arises as to why a highly simplified modeling approach is well suited for soils which are known for varying particle shapes and particle size distributions. The answer lies in the balancing of two opposite effects: high uniformity in size distribution and varying particle shape. Generally speaking, the size of soil particles spreads over a wide range, which tends to decrease the porosity. The irregular shape of soil particles, on the other hand, increases the porosity. These two totally opposite effects are apparently neutralized in terms of their impacts on the porosity.

The proposed model provides a quantitative means to estimate the porosity in terms

of the grain size distribution for the St. Peter Sandstone. The model provides a theoretical explanation of the porosity range typically associated with the St. Peter sandstone, which is 24.5 – 30.5% (Ge et al.; 2014a). This was verified by the St. Peter Sandstone data from Clayton, Iowa. Based on the proposed model, as well as the typical grain size distribution, it was hypothesized that the porosity for the shallowly buried St. Peter Sandstone is not a random phenomenon. Rather, it was suggested that it is significantly affected by the smaller grains fraction.

5.7. CONUCLUSIONS

Both field observations and the laboratory studies discussed in Chapters 3 and 4 have suggested an important role played by the particle structure of St. Peter Sandstone and a need of an in-depth understanding of this particle structure. The study discussed in this chapter was the first step to explore this particle structure and its effect. The significance of this study is discussed as follows.

5.7.1. Porosity Measurement for ST. Peter Sandstone

- The porosities for 6AR and 1S sample groups were determined by three different methods, which are liquid saturation technique, petrographic image and density approach.
- The measurement results can be used as a calibration data base for related studies, because of the accuracy of the measurement and the special status of the porosities associated with these two sample groups.
- It was demonstrated that the porosity of St. Peter sandstone can be determined accurately by three methods with different measurement mechanisms.
- It was mathematically verified that an accurate porosity measurement can be achieved by using two dimensional petrographic images.

- The demonstration of the reliability of these three methods provides researchers much more flexibility to study the porosity of St. Peter sandstone.

5.7.2. Particle Size Distribution

- The the particle size distributions was determined for for 6AR and 1S groups.
- Study of the particle size distributions for 6AR and 1S samples reveals the physical cause of the porosity difference between two sample groups: the existence of fine particles. 6AR samples have a significant amount of fine particles that can fill large gaps while 1S samples are completely devoid of fine particles.
- The measurement results can be used as a calibration data base for related studies, bcause of the accuracy of the measurements and the special status of the porosities associated with these two sample groups. In fact, it becomes one of the key parameters to examine the consistency and reliability of previous research result. For instance, as it was discussed in section 5.3, it was found that the uniformity coefficient for the sandstone from Washington Co. in Table 5.8 should be around 1.66 instead of 3.66 showed in the table.

5.7.3. Rhombohedral Packing. A particle structure model for St. Peter Sandstone

A particle structure model, rhombohedral packing, was proposed for St. Peter sandstone. The model in this research was utilized to examine several important structure related effects, including

- The porosity variance (24% - 31%) for St. Peter sandstone,
- High friction angle associated with St. Peter sandstone, and
- Hertzian fractures observed from St. Peter sandstone.

5.7.4. Size distribution – Porosity – Density Relation. One of the most important contributions resulting from this study is the demonstration of the close correlations among size distribution, and porosity and density. The significance of this work can be summarized as follows:

- It provides an inside view of the particle structure: samples dominated by coarser particles lack of fines and samples dominated by smaller particles have a fair amount of fines. It is this difference that causes the differences in porosity and density. This explains why there exist close correlations among size distribution, porosity, and density.
- The close correlations demonstrated in this research provide a powerful tool, which allows one to cross check the research results on these basic mechanical properties of the St. Peter Sandstone. For instance, St. Peter Sandstones from Minnesota should have a very similar property to 6AR based on the size distribution characteristics in Table 5.9. However, it looks like 1S samples based on the porosities in Table 5.10. Clearly, the data from these two tables are inconsistent.
- The close correlations demonstrated in this research allow one to interpret the other parameters from the one he has the confident.

Based on the close correlation between the strength and porosity, the size distribution-porosity-density relation can be extended to the size distribution-porosity-density-strength relation, which will be extremely useful information for ground control.

6. ADVANCED STUDY ON MICROSTRUCTURE OF ST. PETER SANDSTONE

6.1. INTRODUCTION

An important part of this research is to utilize thin section and Scanning Electron Microscopy (SEM) techniques to study the microstructure of St. Peter Sandstone.

The most significant result of this study is the discovery of the systematical presence of Hertzian fractures on St. Peter Sandtone. This discovery provides not only critical information for understanding the microstructure of St. Peter Sandstone, but also important information for resolving a number of outstanding scientific issues. In this chapter, the concept of herzian fractures is discussed in section 6.2 in brief. The observation of hertzian fractures on St. Peter Sandstone's grains are given in this chapter.

6.2. CONCEPT OF HERTZIAN FRACTURES

When a hard spherical indenter is pressed against the flat surface of a brittle material, they are initially in contact only at a single point. As the load increases, the contact point becomes a contact circle. When the vertical stress at the contact area is sufficiently high, ring shaped fractures will initiate, near the edge of the contact area, and extends down a small distance before widening into a fully developed cone (Zeng et al., 1992).

Although extensive research has been conducted on the theory of Hertzian fractures, the complete profile of naturally formed Hertzian fractures on geological materials in general and St. Peter sandstone in particular has not been observed.

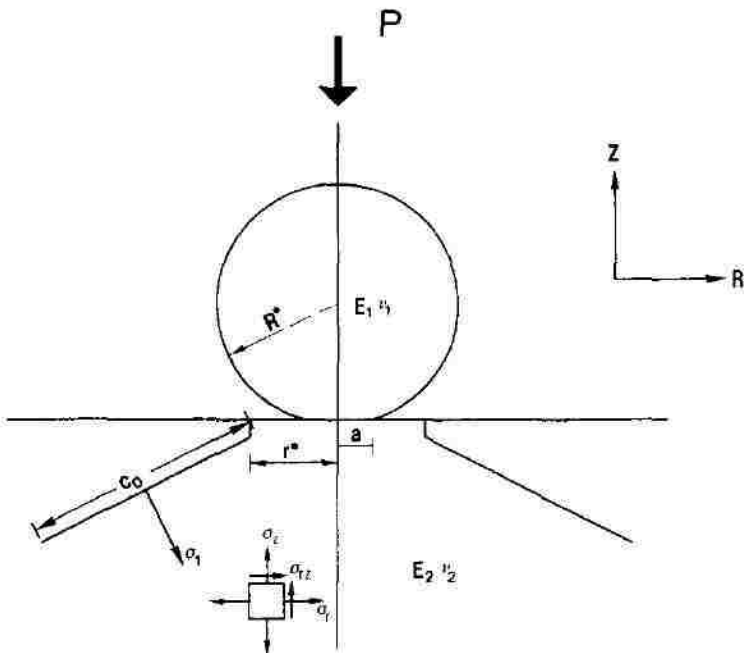

Figure 6.1. a schematic view of Hertzian fractures (Zeng et al., 1992)

6.3. HERTZIAN FRACTURES OBSERVED FROM ST. PETER SANDSTONE

6.3.1. Basic Features of Hertzian Fractures associated with St. Peter Sandstone.

A phenomenon discovered in this research is the systematical presence of Hertzian factures on St. Peter sands (Figure 6.2). The following is a brief discussion of such an example.

As discussed in section 6.2, Hertzian fractures are the mechanical response of brittle materials, shown as the cracks generated immediately outside of contact locations. In Figure 2, the dark lines that radiate away from the particle contact locations and along the particle surface are Hertzian fractures. It is noticed from Figure 6.2 that the presence of Hertzian fractures are systematic. Hertzian fractures were developed symmetrically at the both sides of every contact locations, regardless the sized of sand particles.

Hertzian fractures are the sign of the high stresses developed at the contact locations. This is evident not only by the fact of fractures, but also by the continuity of highly stressed

areas shown by those bright locations. By following the location of these bright spots one will immediately know how stresses are transmitted within the structure. It is noted that there are two typical locations for bright spots: the interior area of the particle and the particle contact locations. This is because these locations are confined three dimensionally and, therefore, can carry out most stresses.

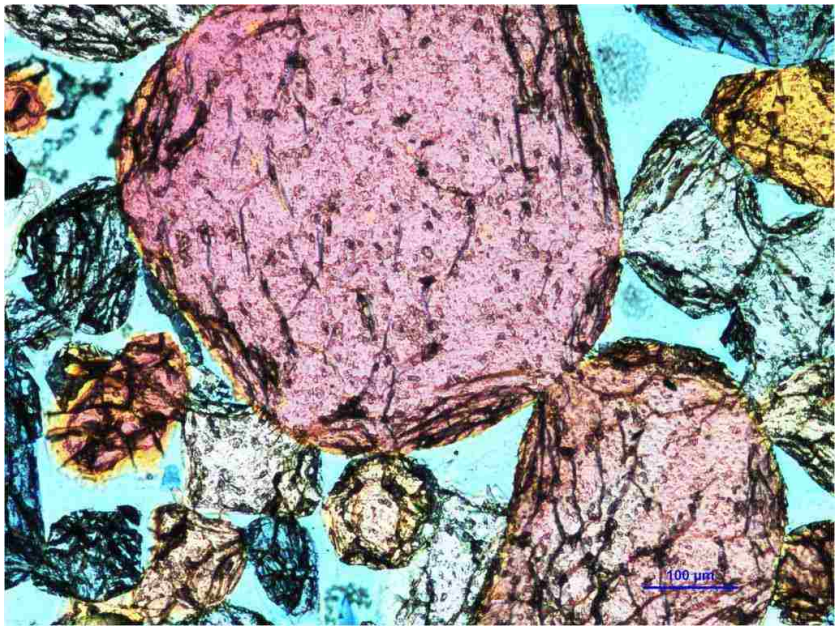

Figure 6.2. Hertzian fractures observed on a thin section image of St. Peter Sandstone from Clayton, Iowa.

A very important conclusion which can be drawn from pattern of Hertzian fractures is that all sand grains are highly stressed regardless of their sizes. For instance, if all sand particles, which are in direct contact with the largest sand particle located in the center of Figure 6.2 are examined, it can be observed that every grain is highly stressed regardless how large or small it is. The other important observation is that all contact locations are smooth. There are no signs of any forms of penetration at these contact locations.

6.3.2. Stress Trajectories. Figure 6.3 is another example of Hertzian fractures observed from St. Peter sandstone, where well-developed stress trajectories in both horizontal and vertical directions can be observed. With regard to horizontal stress trajectories, one can observe this trajectory either through the contact locations for the grains in the upper line (Grains denoted by A, B, C), or the grains in the middle line or the bottom line. For the vertical stress trajectory, the contact location of grains in the middle, marked by C, D, and E, is the clearest one. The vertical stress trajectories can be traced also from the sand grains on both sides of this thin section image.

6.3.3. Stress Trajectories and Highly Stressed Small Sand Grains. Stress trajectories can be also observed in Figure 6.4. There are different ways to look at the stress trajectories associated with the sand grains on this thin section image. One can start from the large pink grain located on the right where one can trace the flows of the stress trajectories from the right tip of this grain, or from the bottom of the grain or from the top of the grain. The other one is to start from the large blue sand grain which is on the top of this pink one. A clear stress trajectory can be seen, which begins from this blue sand and points to the left-lower corner direction. The end of this stress trajectory on the image is two blue color grains. It is interesting to note that there is a very small grain at the bottom tip of the last blue grain. From the pattern of the Hertzian fractures on the large grain, it is known that the stress is high at this contact location.

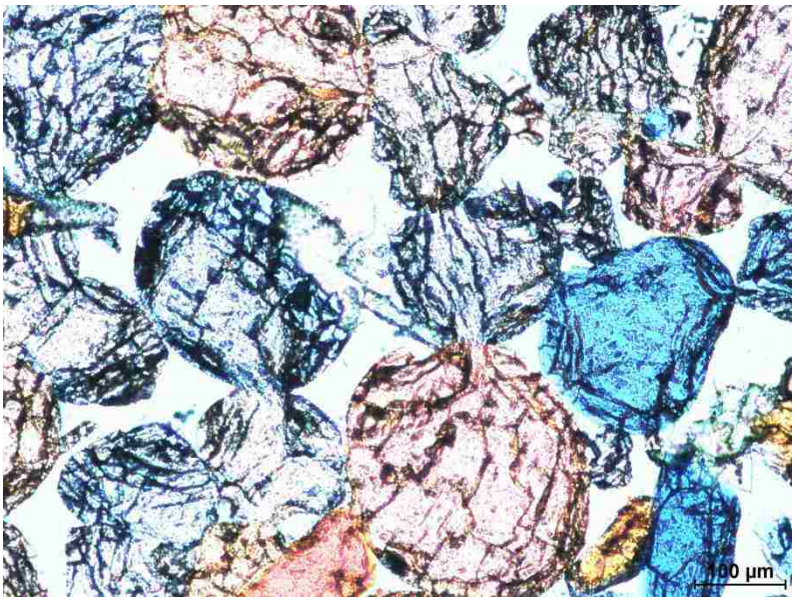

Figure 6.3. Stress trajectories manifested by Hertzian fractures.

There are many ways to look at the stress trajectories associated with the sand grains on Figure 6.5. One may start from the large pink grain located at the bottom of the image and trace two stress trajectories upward starting from the contacts with two blue grains. It is interesting to note that there is a very small grain (light brown color) between these two trajectories. From the pattern of the Hertzian fractures on two much larger sand grains which sandwiched this small sand particle, it is known that this small sand grain is highly stressed.

There are many ways to look at the stress trajectories associated with the sand grains on Figure 6.6. First one may examine the contacts with the large blue grain located on the right and see how the stress trajectories radiate to other directions through these contacting grains. The most interesting phenomenon that can be observed in this image, however, is that small grains, are also highly stressed. For example, one can consider the grain located immediately above the big blue sand. Each of these two is in contact with three grains. From

the fracture pattern observed on the surrounding grains, it is known that these two small sand grains are highly stressed.

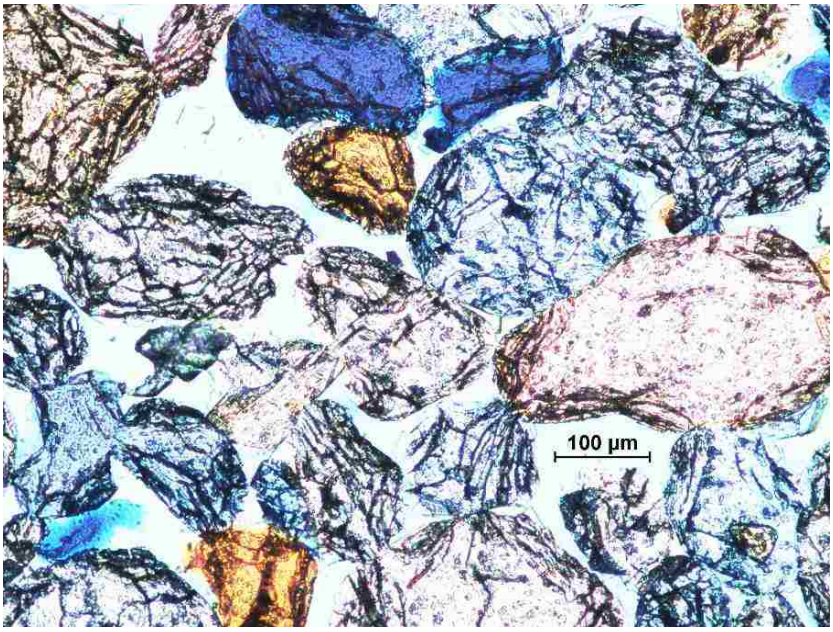

Figure 6.4. Stress trajectories and a highly stressed sand grain

The main phenomenon observed in Figure 6.7 is that small grains are also highly stressed. Consider the small sand grain under a pink sand in the middle. It is noticed that this small grain is surrounded by four larger ones. From the pattern of Hertzian fractures on these grains, it is known that this small grain is highly stressed. It is also interesting to note that the small blue grain on the left side, is also highly stressed based on the pattern of the Hertzian fractures on the two adjacent larger grains.

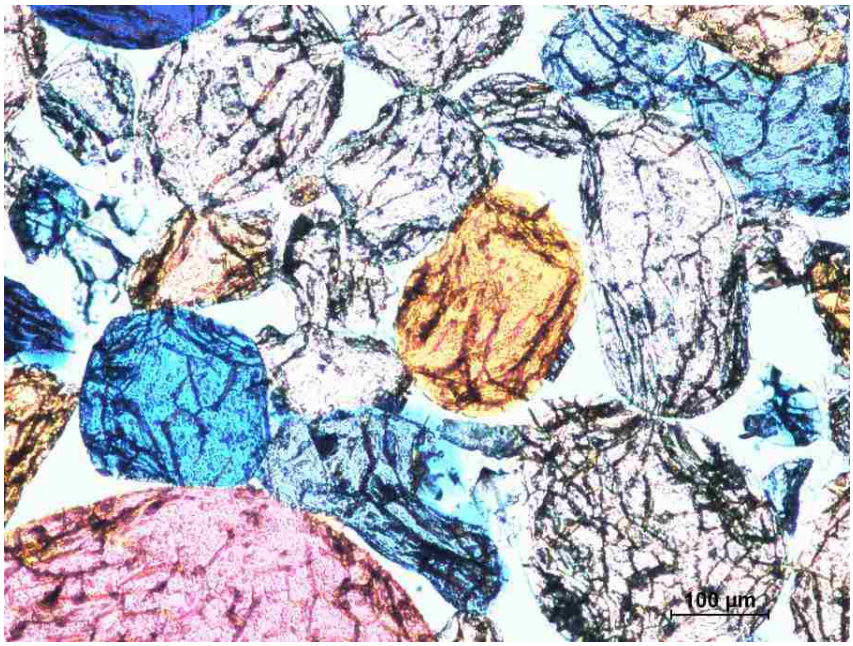

Figure 6.5. Stress trajectories and a highly stressed small sand grain.

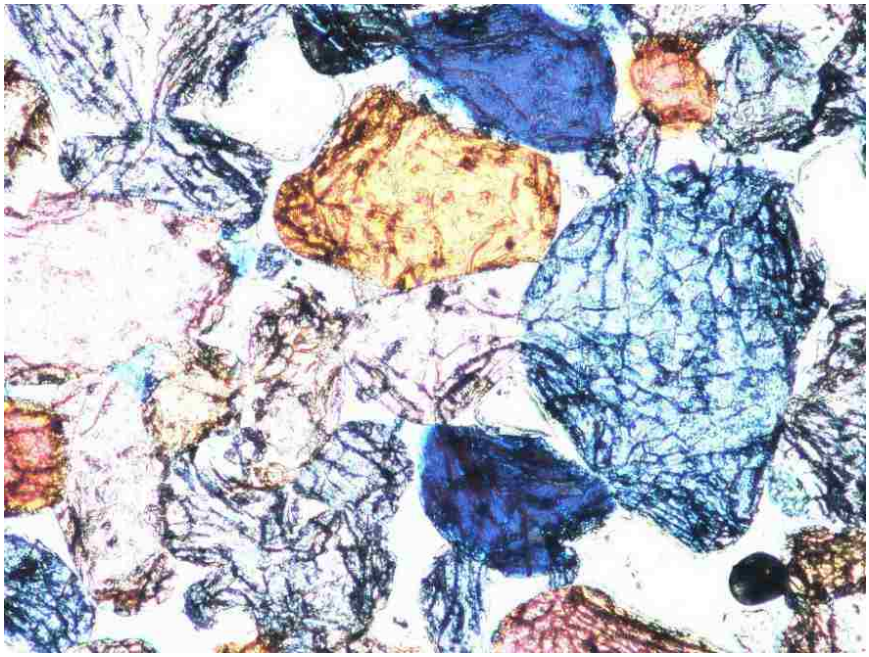

Figure 6.6. Stress trajectories and highly stressed small grains.

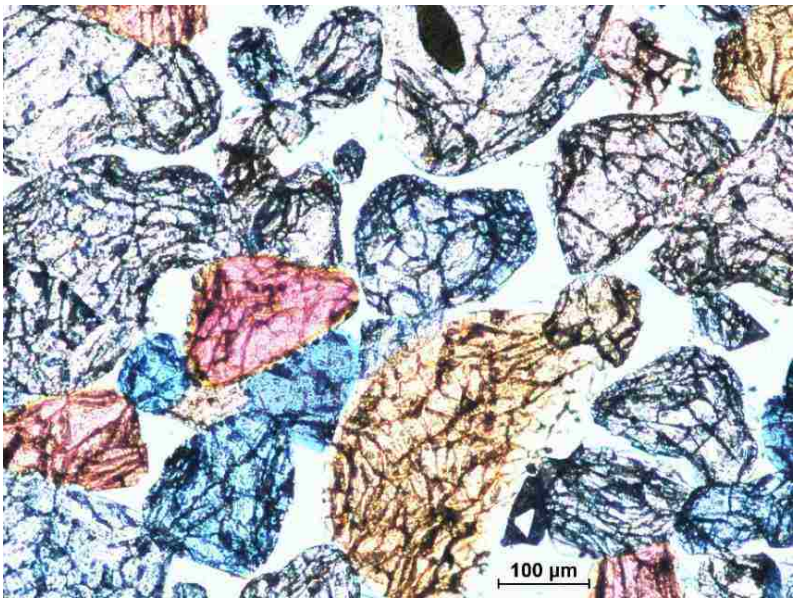

Figure 6.7. Stress trajectories and a highly stressed small grain.

6.4 .CAUSE OF HIGH FRICTION ANGLE

A property that is unique of the St. Peter Sandstone is its extremely high friction angle, in the range of 60˚- 70˚, which is 15˚ - 20˚ higher than the upper limit of the friction angle for general geological materials, which is about 45˚ - 50˚.

6.4.1 Theory of Penetrative Surface Fabric (Locked Sand Theory). Understanding the mechanics of the high friction angle associated with St. Peter sandstone is significant from both a scientific and an engineering points of view. A dominant theory on the mechanics of the high friction angle is “locked sand”, which was originally proposed by Dusseault and Morgenstern (1979). According to the theory, the high friction angle is the result that sand particles are locked each other due to interpenetrative surface fabric. Figure 6.8 is an example used by Dusseault and Morgenstern (1979).

The theoretical background for the interpenetrative surface fabric is intergranular fabric classification that is used by geologists. The one given in Figure 6.9 was developed by Taylor (1950), which is the first classification scheme for grain contacts. This classification

scheme was based on observations on the thin section images of five sandstones from two deep wells in Wyoming. Grain contacts were classified as floating, tangential, long contact, concavo-convex, and sutured (Figure 6.9). Grains that have no contacts are considered as floating grains. Sutured contacts are featured with wavy to jagged lines.

In this classification, floating and tangential grain contacts are attributed to original packing of grains. Long contacts are considered as the result of original packing with pressure or cement. Sutured contacts are considered as a result of pressure. In other words, this classification is based on progressive change from original packing to increased pressure, which is an indication of an increasing degree of consolidation.

6.4.2. Contact Surfaces Observed from Thin Section and SEM Images. It is clear from both the development process and the intended applications that caution has to be taken on the the usage of this classification system.

First the system was developed for general sandstone formations which, in general, have multiple and complex compositions. Therefore, the response of the material changes progressively from tangential to sutured contacts. St. Peter Sandstone, however, is fundamentally different from the conventional sandstone in that it is pure quartz. Hence, the stress response for St. Peter Sandstone will be very different. For instance, there is no mechanics for developing sutured contacts as the materials on both sides of all contacts have the identical property.

Furthermore, it is important to emphasize that the intergranular fabric classification is primarily used for assessing the stress condition. Tangential to sutured contacts are merely the reflection of the associated stress condition. For St. Peter sandstone, as illustrated in

Figures 6.2 – 6.7, most of contacts are tangential. It is clear that it would be a major mistake if one conisders these grains were not subjected to any pressure.

If all contacts in Figures 6.2-6.7 are carefully considered, it is not difficult to draw a conclusion: all contacts are smooth and most of them are flat. There are no any signs of interpenetrative contacts. The SEM images of St. Peter sandstone in Figure 6.10 provide the further evident in this regard.

St. Peter grains have a predominantly frosted surface. The texture of frosted surfaces can be seen clearly in Figure 6.10c. The texture of contact surfaces is very different from that of frosted surfaces, and Figure 6.10d is a typical example. In addition to the fact that the contact surface is very smooth, its boundary is also smooth and clear. The smooth surface and boundary for contact surfaces are the results of high contact stress existed during long geological years.

With these two features in mind, it is not difficult to find many contact locations in Figure 10b. One may also notice in Figure 6.10b , that there are a number of spots appeared to be impacted by external forces. Both the surfaces and boundaries of these spots are not smooth. Clearly these are not contact surfaces even though the surfaces are not frosted.

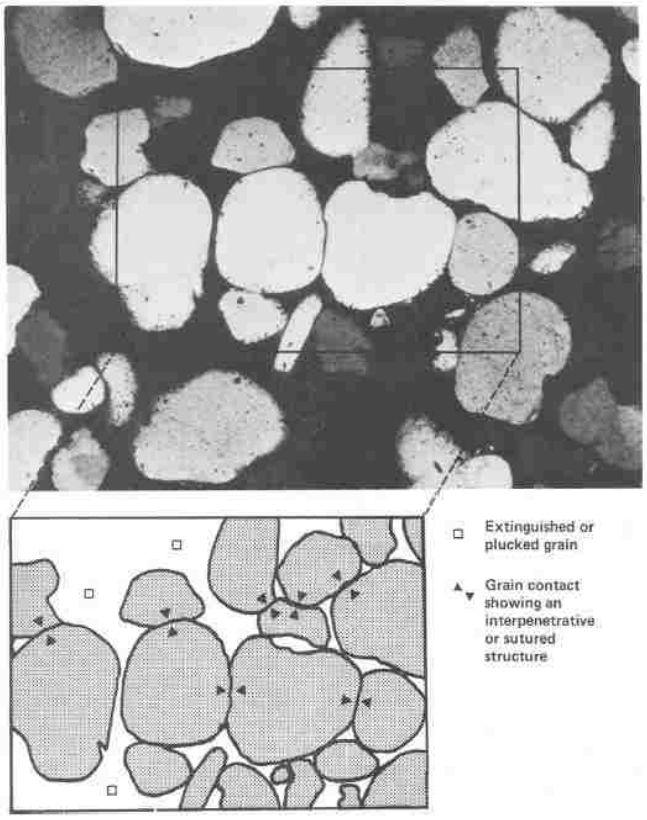

Figure 6.8. Penetrative fabric of St. Peter sandstone (Dusseault and Morgenstern, 1979)

6.4.3. A Hypothesis on High Friction Angle for St. Peter Sandstone. Both thin section and SEM images have shown that contact surfaces of St. Peter sands are smooth and cannot be characterized by interpenetrative. Therefore, the locked sand theory is not applicable to St. Peter Sandstone. Instead, the pattern of the Hertzian fractures, and especially stress trajectories manifested by Hertzian fractures, seem to suggest that St. Peter sands are locked structurally. A structure induced friction model was proposed by Ge et al. (2014b) to explain the cause of the high friction angle for St. Peter sandstone. The concept of this model is illustrated in Figure 6.11.

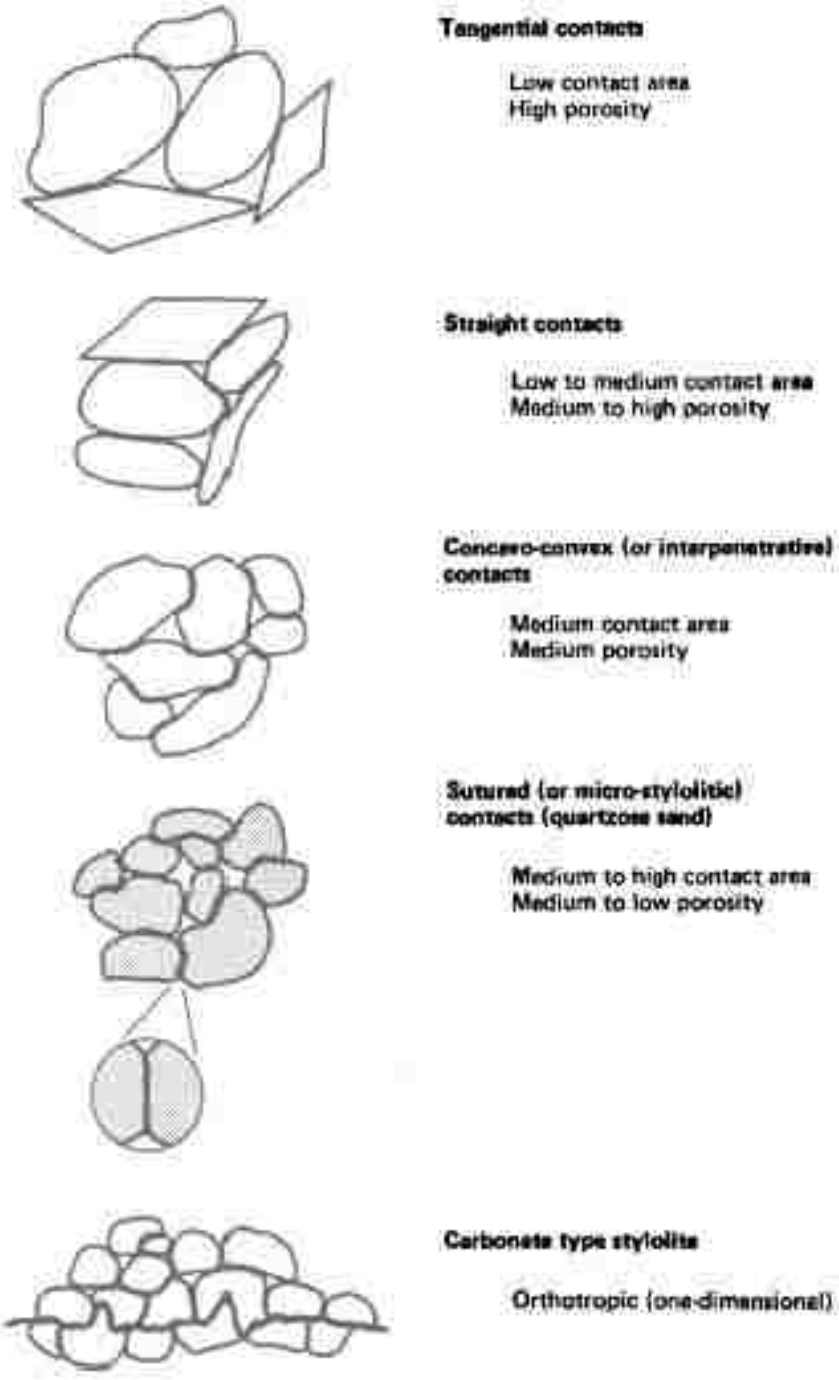

Figure 6.9. Taylor's intergranular fabric classification Taylor (1950)

a)

b)

c)

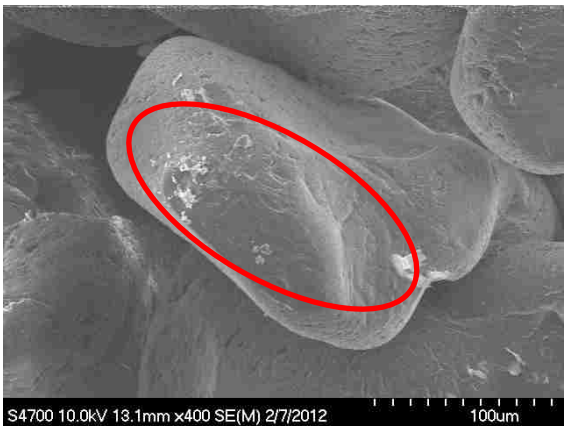

d)

Figure 6.10. SEM images of St.Peter sandstone

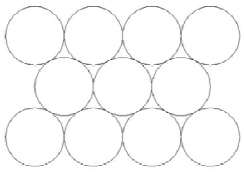

A) A 2-dimentional even-sphere model

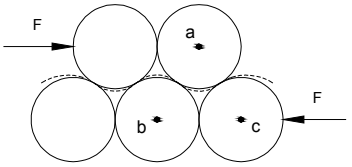

b) Movement caused by a shear force

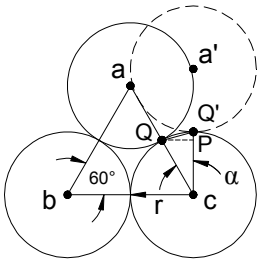

c) Movement of sphere a

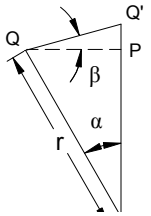

d) Average climbing slope of sphere a

Figure 6.11. 2D illustration of the particle movement during shear test

According to this model, the average climbing slope for a 2D model is 15˚, and for a 3D model is about 17˚, which are very close to what we have actually observed for St. Peter sandstone.

6.5. DEPOSITIONAL ENVIRONMENT FOR ST. PETER SANDSTONE

The depositional environment of the St. Peter Sandstone is a problem which has puzzled geologists since the discovery of the St. Peter Sandstone over 150 years ago. There are two campuses on the origin of St. Peter sandstone: marine and eolian. Two evidences used by eolian campus to support its theory are Hertzian fractures and cleavage plates (Winfree,1983; Johnson et al., 1989).

Johnson et al. (1989) stated that *"Hertzian cracks are commonly formed upon sand grains by gain-to-gain impacts during transport"*. The image in Figure 6.12, according to them, is *"full-circle Hertzian cracks formed on a quartz sand grain under experimental eolian conditions in a NASA wind tunnel. Scale bar equals 10 microns*". Assuming that the interpretation of the image in Figure 6.12 by Johnson et al. (1989) is correct, these are, nevertheless, not naturally formed Hertzian cracks. The Hertzian fractures observed in thin sections were formed naturally and the pattern of these Hertzian fractures is undeniable evidence that these Hertzian fractures were not the product of eolian related depositional environment.

The other evidence used for supporting eolian depositional environment is broken cleavages observed from St. Peter sands. Such an example is shown in Figure 6.13. As earlier, St. Peter sands are featured with frosted surfaces. For the areas that are not frosted, they are either contact surfaces or newly created by sampling. From the texture of the broken cleavages shown in Figure 6.13, these broken cleavages were most likely created during the sample collection process. Notice small and freshly broken chips on and around broken surfaces.

Figure 6.12. Full-circle Hertzian cracks formed on a quartz sand grain under experimental eolian conditions in a NASA wind tunnel. Scale bar equals 10 microns (Johnson et al., 1989).

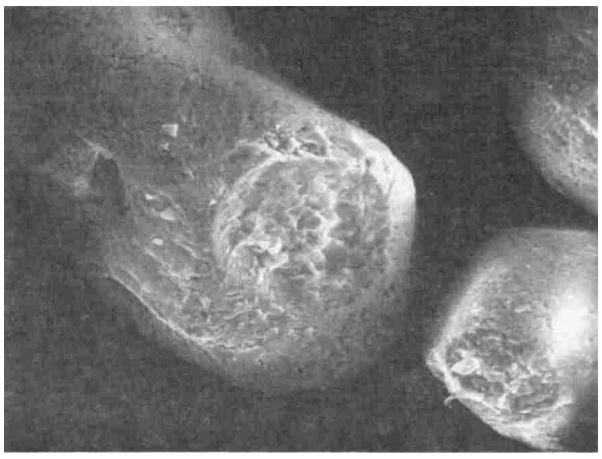

Figure 6.13. Broken cleavage plates on St. Peter sandstone (Winfree,1983)

6.6. CONCLUSIONS

The Hertzian fractures discussed in this research provide important information on particle structures of St. Peter Sandstone.

6.6.1. St. Peter Sandstone were Highly Stressed Regardless of their Sizes. First all St. Peter grains, regardless of their sizes, were highly stressed, which was demonstrated by systematically developed Hertzian fractures and networks of stress trajectories.The stress condition, manifested by Hertzian fractures, provides the answer/further information for a number of structure related effects:

- why the porosity of St. Peter Sandstone is near the lowest level indicated by rohmbohedral model,
- why St. Peter sandstone, a typical particle structure, behaves elastically, and
- why St. Peter sandstone shows a large dilation under a low normal stress during direct shear tests.

6.6.2. Contact Surface. The observations of thin sections and SEM images have shown that contact surfaces for St. Peter sands are smooth and are flat in most cases. The assumption of the penetrative surface fabric fundamentally contradicts the basic material property of St. Peter sandstone (pure quartz), as well as the stress condition indicated by Hertzian fractures. If the contact surface were penetrative, Hertzian fractures would be developed inside the contact areas. This is clearly not the case. All Hertzian fractures were developed outside of the contact areas.

6.6.3. High Friction Angle. Based on the analysis of contact surfaces for St. Peter Sandstone, it is known that the theory of locked sand is not applicable to St.Peter Sandstone.

Penetrative surface fabric assumption for St. Peter Sandstone is flawed. The high friction angle is due to the structure of St. Peter sands (Ge, et al., 2014).

6.6.4. Origin of Hertzian Fracture. The pattern of these Hertzian fractures is undeniable evidence that the Hertzian fractures were the product of a marine deposition process and had nothing to do with eolian related actions.

6.6.5. Origin of Broken Cleavage Plates. Based on the analysis of the surface for St. Peter sandstone, especially the characteristics of contact surfaces, it is known that these broken cleavages were most likely created during the sample collection process. It is not an evidence of eolian depositional environment.

7. CONCLUSIONS AND RECOMMENDATION

7.1. THE SUMMARY OF ACHIEVEMENTS OF THIS STUDY

As discussed earlier in this dissertation, fundamental understanding of the basic mechanical and strength properties of the St. Peter Sandstone is needed for solving the ground control problems that St. Peter Sandstone underground mines are facing. The objective of this work were: (i) characterizing the basic strength properties of St. Peter Sandstone; and (ii) elucidating the strength mechanics of St. Peter Sandstone by experimental evidences.

In order to characterize the strength of St. Peter Sandstone. Four particular issues needs to be addressed. Those were (i) developing a sample preparation method for St. Peter Sandstone; (ii) determining the optimum size sample needed to characterize the strength of St. Peter Sandstone; (iii)identifying the critical parameters that affect St. Peter Sandstone's strength; and (iv) developing a comprehensive assessment method for St. Peter Sandstone.

The second objective of this study was elucidating the strength mechanics of St. Peter Sandstone by experimental evidences. As discussed earlier, St. Peter Sandstone possesses extremely high friction angle. The high frication angle was attributed to surface contacts by pervious researchers (Dusseault and Morgenstern, 1979). Another important underlying problem for St. Peter Sandstone is its origin of the strength. This problem is not only critical from rock mechanics standpoint, but also related to a number of geological problems such as depositional environment of St. Peter Sandstone and the origin of Hertzian cracks observed on St. Peter sandstone's grain.

To accomplish the above mentioned objectives, extensive laboratory and theoretical studies were carried out.

Uniaxial Compressive testing: The uniaxial compressive strength is a basic parameter for characterizing the strength of geological materials and used extensively for a variety of engineering design purposes in mining, civil, and geotechnical engineering. A comprehensive study was carried out for uniaxial compressive testing of St. Peter Sandstone. In this study, the results of this study, and the results from previous studies were analyzed. This part of study includes proposing a sampling technique for St. Peter Sandstone, investigating the effects of size and shape of sample on uniaxial compressive strength of St. Peter Sandstone, studying the elastic properties of St. Peter sandstone, and comparing the uniaxial compressive strength of cemented and uncemented specimens.

- It is not practical to use conventional sample preparation techniques that is used for rock mechanics studies. Therefore, based on this this study's experince, the first principle in preparing sample for St. Peter Sandstone, is minimizing distribunce during sample preparation.
- The failure modes of St. Peter Sandstone after uniaxial compressive testing were investigated. The study of failure modes of St. Peter Sandstone provides important information with regard to the strength properties of St. Peter Sandstone. The contribution of this part of our study is three-fold. The mechanics of two dominant failure modes namely vertical splitting, and steeply dipped shearing were studied. It was concluded that failure modes are linked to the basic mechanical properties of St. Peter Sandstone. Vertical splitting is caused by cohesionless property of St. Peter Sandstone, however, steeply dipped shearing is the result of high frication angle of St. Peter Sandstone. Secondly, steeply dipped shearing is another evidence of high friction angle of St. Peter Sandstone and it provides the quantitative

information regarding the friction angle calculation. Thirdly, the irregularities of failure locations of St. Peter Sandstone specimens indicates the sensitivity of failure location to anomalies, which is also the result of cohesionless property. The sensitivity to local anomalies as manifested by vertical splitting and irregularities of failure locations is one of the main reasons for high variance of uniaxial compressive strength.

- The size effect of specimens on uniaxial compressive strength of uncemented St. Peter sandstone was investigated in this research. The results of 95 tests of this study, as well as the results from previous studies were analyzed in this regard. The results indicate that the size effect for St. Peter Sandstone is different from what is observed for most geological materials. The size effect for St. Peter sandstone is the result of two factors: scaling and disturbance by sampling procedure. The effect of disturbance for smaller specimens is more pronounced. Thus, the smaller specimens are more prone to be disturbed during sample preparation procedure.
- The optimum size of 50 mm was determined based on different factors. Practical consideration, laboratory results, field investigation, and scaling and disturbance during sample preparation were taken into consideration.
- The shape effect for St. Peter Sandstone was not discussed by previous workers. Although the available data from previous studies that can be used in this regard is very limited, this is very important for characterizing the strength of St. Peter Sandstone. A practical implication is that height/width ratio of specimens should not be less than 1.

- The elastic proerties of St. Peter (Young's moduls, and Possion 's ratio) were also investigated in the course of this research. The contribuation of this study is the detailed study of stress-strain curves. The results of this study indiacte Stress- strain behavior of St. Peter Sandstone can be devided into three stages. The stress-strain behavior of St. Peter Sandstone is almost perfectly linear for the most test period. The stress-strain behavior of St. Peter Sandstone in the second stage also can be regarded linear. The third part of stress-strain curve is rupture.
- The results for the elastic properties of St. Peter Sandstone by previous studies were reviewed. The Young's modulus determined by previous studies are close to the results of this study.
- The uniaxial compressive strength of cemented St. Peter Sandstone was also investgated in this study. The uniaxial compressive strength of cemented St. Peter Sandstone is 5 to 8 times higher than uncemented St. Peter Sandstone.

The triaxial compressive tests were conducted on St. Peter Sandstone specimens of Iowa. The main contributions of this part of research are as follows:

- **Axial stress- axial strain curves for St. Peter sandstone.** It is the first time that axial stress-axial strain behavior of St. Peter Sandstone was investigated under different confining pressure. The results of axial-stress, stress-axail strain curves of this study indicate the effect of confining pressure on the mechanical behavior of St. Peter Sandstone. Confining pressure increases the axial stress at failure. It also changes the mechanical behavior from brittle to ductile. There exists remarkable similarity among axial-stress, axial-strain curves from the same group of specimens. This indicates specimens from

same group experience similar failure process. The results of triaxial compressive tests for St. Peter Sandstone indicate specimens from same group exhibit very similar mechanical response under same confining pressure. This is a further indication of stability of triaxial test results for St. Peter Sandstone.

- **Failure patterns**. It is the first time that failure mode for St. Peter Sandstone after triaxial tests were investigated. The failure patterns of triaxial test are different from what observed for uniaxial tests. The pattern for triaxial test is almost identical for all specimens. A pyramid shape cone formed at each end of specimen. It indicates that failure mode of triaxial test is not controlled by anomalies, rather it is governed by its inherent mechanical properties. Another important finding of failure pattern of triaxial test is steep failure angle which is a further confirmation of high friction angle for St. Peter Sandstone.
- **Effect of particle structure on strength of St. Peter sandstone.** One of the most important contributions of this investigation is the demonstration that the strength of St. Peter Sandstone is primarily governed by its particle structure. This is done by comparing the mechanical response of specimens from two sample groups, 6AR and 1S. The porosities for these two sample groups are 24.5% and 30.5%, which define the porosity range for St. Peter Sandstone.

  The study shows that the strength for 6AR group, the group with the low porosity, is much higher than that for 1S group, the group with the high porosity. The friction angle is also much higher for 6AR group. The

mechanical responses in terms of the axial stress-axial strain curves for these two groups are also very different. Because of the critical influence of the particle structure on the strength of St. Peter sandstone, it is important to measure the specimen‘s particle structural parameters such as porosity before the test.

- **Effects of confining pressure.** In order to measure the effect of confining pressures on the stress at failure for different materials, an index of rate increase of the axial stress at failure, RAS, was defined. RAS provides a quantitative measurement of the increase of the axial stress at failure for each confining pressure unit. A study of RAS for both St. Peter Sandstone and other geological materials shows that the RAS for St. Peter sandstone is much higher than that for conventional geological materials.

The particle structure of St. Peter sandstone was studied in terms of porosity, density, particle size distribution. The summary of findings of this research is as follows

- The porosity of St. Peter Sandstone were measured using three different methods which are liquid saturation technique, petrographic images and dry density approach. The results indicated that the porosity of St. Peter sandstone can be determined by these three methods. It was mathematically proved that porosity can be measured by two dimensional petrographic images.
- The particle size distribution of 6AR, and 1S groups were investigated in this research. The results of particle size distribution indicated the reason for porosity of two sample groups. The existence of fine particles in 6AR samples that filled the gaps between larger particles is the reseaon for

porosity difference.

- Rhomhedral packing was used to conceptualize the effect of finer grains on the porosity of St. Peter sandstone.
- One of most important contribution of this research was the demonstration of close correlation between particle size distribution, porosity and density. The samples dominated by coarse particle lacking fine materials are less densely packed in comparison with samples dominated by smaller particles having a fair amount of fines. This explains the correlation between size distribution, porosity and density. This correlation allows one to cross check the results of basic mechanic properties of St. Peter Sandstone.

Optical and Scanning Electron Microscopy were conducted on St. Peter Sandstone. The contact surfaces of St. Peter Sandstone grains were investigated in this study. Hertzian fractures observed on thin section images of St. Peter Sandstone. The principal conclusions drawn from these observations are as follows:

- All grains are stressed, this was demonstrated by systemic network of Hertzian fractures and stress trajectories. The can be helpful in understanding of porosity range for St. Peter sandstone and also high rate of dilation of St. Peter Sandstone under low confining pressure.
- Both optical microscopy and scanning electron microscopy images indicated that contact surfaces of St. Peter Sandstone are smooth in most cases. The assumption of penetrative surface fundamentally contradicts the basic material property of quartz, as well as stress condition indicated by Hertzain fractures. Therefore, penetrative surface fabric cannot be the reason for high friction angle of St. Peter Sandstone.

- The pattern of Hertzian fractures indicates that it cannot be the product of eolian depositional environment. Broken cleavage plates were most likely created during sample preparation. In other words, they cannot be evidence of eolian dispositional environment.

7.2. PRACTICAL GROUND CONTROL APPLICATION OF THIS RESEARCH FINDINGS

- Rock reinforcement. As it was mentioned earlier rock bolting has been the dominant way to reinforce conventional geological material such as coal, hard rock. However, this method is not useful for St. Peter Sandstone because of anchorage problems associated with the friable nature of it. The results of this study indicate that St. Peter Sandstone possesses very high friction angle. The confining pressure will significantly increase the strength of St. Peter Sandstone. Therefore, confining pillars with shotcrete is an effective way to reinforce the pillars.
- The role of particle structure on the strength of St. Peter Sandstone. As it was mentioned, one of the major finding of this research is that that the strength of St. Peter Sandstone is fundamentally governed by its particle structure. This was further manifested by direct relation between the strength, porosity, particle size distribution. This can provide useful information for ground control.

7.3. RECOMMENDATION FOR FUTURE WORK

The following recommendations are made for future research in terms of geotechnical properties of St. Peter Sandstone.

- The role of particle structure on the strength of similar friable sandstone s

such as Jordan sandstone can be investigated.

- The shape effect for St. Peter Sandstone specimens has not been investigated by previous studies. Although preliminary discussion provided by analyzing the data from previous studies. St. Peter Sandstone specimens can be prepared to study the effect of shape of specimens on the uniaxial strength of St. Peter Sandstone.
- Moisture content of rocks can significantly influence the strength of rocks. Experiments can be performed to investigate the effects of moisture on the strength of St. Peter Sandstone.
- The effect of Herzlian fracture on fracture mechanics of St. Peter Sandstone can be investigated.

APPENDIX A: THE DETAILS OF UCS TESTS CONDUCTED ON ST. PETER SANDSTONE SAMPLES TAKEN FROM CLAYTON, IOWA

Table A1. The details of ucs tests conducted on St. Peter Sandstone samples taken from Clayton, Iowa

Test Number	Sample ID	Size(mm)			Equivalent Width(mm)	Height to width ratio	UCS (Mpa)	Test Date
		Length	Width	Height				
1	6AR S1	16.51	16.00	16.26	16.26	1.00	0.50	5/12/2012
2	6AR S2	16.26	15.75	16.00	16.00	1.00	1.43	5/12/2012
3	6AR S3	16.00	15.75	15.49	15.75	0.98	0.81	5/12/2012
4	6AR S4	14.48	14.48	14.22	14.48	0.98	0.95	5/12/2012
5	1S S1	16.26	15.75	16.00	16.00	1.00	2.12	5/12/2012
6	1S S2	15.75	15.75	15.24	15.75	0.97	2.06	5/12/2012
7	BD*C1	13.27	14.13	14.64	13.69	1.07	1.30	6/8/2014
8	BD*C2	14.44	12.72	14.79	13.55	1.09	1.45	6/8/2014
9	BD*C3	12.38	13.25	13.04	12.80	1.02	0.81	6/8/2014
10	BD*C4	13.14	13.55	13.87	13.35	1.04	0.87	6/8/2014
11	BD*C5	13.62	12.66	13.68	13.13	1.04	1.03	6/8/2014
12	BD*C6	11.81	13.00	13.91	12.39	1.12	0.43	6/8/2014
13	BD*C7	12.92	12.75	14.25	12.83	1.11	1.22	6/8/2014
14	BD*C8	13.47	14.67	14.79	14.06	1.05	2.03	6/8/2014
15	BD*C9	13.39	14.32	14.80	13.84	1.07	0.23	6/8/2014
16	BD*C10	14.33	13.49	13.77	13.90	0.99	0.17	6/8/2014
17	BD*C11	13.20	12.40	13.44	12.79	1.05	1.29	6/8/2014
18	BD*C12	14.54	14.70	14.87	14.62	1.02	0.10	6/8/2014
19	BD*C13	14.26	13.08	14.51	13.66	1.06	0.24	6/8/2014
20	BD*C14	12.11	14.77	14.78	13.37	1.11	1.12	6/8/2014
21	BD*C15	12.11	14.77	14.78	13.37	1.11	0.31	6/8/2014
22	BD*C16	13.14	14.17	14.69	13.65	1.08	5.38	6/8/2014
23	6ARC-1	23.11	21.08	23.88	22.10	1.08	0.55	5/12/2012
24	6ARC-3	25.15	23.88	23.88	24.38	0.98	0.72	5/12/2012
25	6ARC-4	24.13	23.37	23.88	23.62	1.01	0.71	5/12/2012
26	6ARC-6	25.40	23.88	23.88	24.64	0.97	0.24	5/12/2012
27	6AR 1-1	25.15	24.38	35.81	24.64	1.45	6.06	5/12/2012
28	6AR 1-2	24.89	24.38	36.07	24.64	1.46	7.27	5/12/2012
29	6AR 1-3	25.40	24.89	35.81	25.15	1.42	11.78	5/12/2012
30	6AR 1-4	24.89	24.64	36.32	24.64	1.47	6.36	5/12/2012
31	1S C-1	25.65	24.89	21.84	25.15	0.87	1.95	5/12/2012
32	1S C-2	25.91	25.40	21.84	25.65	0.85	1.22	5/12/2012
33	1S C-3	26.16	25.65	21.84	25.91	0.84	1.31	5/12/2012

Test Number	Sample ID	Size(mm)			Equivalent Width(mm)	Height to width ratio	UCS (Mpa)	Test Date
		Length	Width	Height				
34	1S C-4	24.64	23.62	22.10	24.13	0.92	0.82	5/12/2012
35	1S 1-2	25.40	24.38	39.37	24.89	1.58	1.78	5/12/2012
36	1S 1-6	25.15	23.88	34.04	24.38	1.40	1.33	5/12/2012
37	1S 1-7	25.15	24.13	34.29	24.64	1.39	2.31	5/12/2012
38	BD*B1	28.37	25.72	25.77	27.01	0.95	1.83	6/8/2014
39	BD*B2	28.18	26.16	28.70	27.15	1.06	4.22	6/8/2014
40	BD*B3	26.74	25.21	26.83	25.97	1.03	4.98	6/8/2014
41	BD*B4	26.20	27.27	27.76	26.73	1.04	5.04	6/8/2014
42	BD*B5	25.01	26.75	27.94	25.86	1.08	3.79	6/8/2014
43	BD*B6	26.56	26.03	26.90	26.29	1.02	2.90	6/8/2014
44	BD*B7	26.63	26.19	25.84	26.41	0.98	2.23	6/8/2014
45	6AR +	38.86	35.05	33.27	36.83	0.90	0.82	5/12/2012
46	1S 2-1	39.62	37.85	37.34	38.61	0.97	2.43	5/12/2012
47	BD*A1	39.52	39.23	39.62	39.38	1.01	4.95	6/8/2014
48	BD*A2	39.18	39.89	39.57	39.53	1.00	8.13	6/8/2014
49	BD*A3	40.01	39.81	40.21	39.91	1.01	2.81	6/8/2014
50	BD*A4	39.12	37.57	37.41	38.34	0.98	4.62	6/8/2014
51	BD*A5	38.19	38.12	38.04	38.16	1.00	9.18	6/8/2014
52	BD*A6	40.31	40.83	39.42	40.57	0.97	2.76	6/8/2014
53	BD*A7	38.59	40.21	40.69	39.39	1.03	0.82	6/8/2014
54	BD*A8	38.13	39.22	39.66	38.67	1.03	3.33	6/8/2014
55	BD*A9	38.11	39.48	39.90	38.79	1.03	4.60	6/8/2014
56	BD*A10	39.94	38.76	40.75	39.34	1.04	3.74	6/8/2014
57	BD*A11	38.29	38.59	39.99	38.44	1.04	4.37	6/8/2014
58	BD*A12	38.93	40.23	39.72	39.58	1.00	15.02	6/8/2014
59	BD*A13	39.56	39.09	39.60	39.32	1.01	2.91	6/8/2014
60	BD*A14	39.74	39.89	40.94	39.81	1.03	6.59	6/8/2014
61	BD*A15	39.83	40.08	40.18	39.95	1.01	2.02	6/8/2014
62	BD*A16	37.40	39.49	39.40	38.43	1.03	5.38	6/8/2014
63	BD*A17	40.02	38.06	36.67	39.03	0.94	2.48	6/8/2014
64	BD*A18	39.35	39.34	38.86	39.35	0.99	0.93	6/8/2014
65	BD*A19	39.88	38.79	38.54	39.33	0.98	8.93	6/8/2014
66	BD*A20	40.09	40.24	35.60	40.17	0.89	7.22	6/8/2014
67	6AR ②	53.59	51.05	63.25	52.32	1.21	3.82	5/12/2012
68	6AR ③	51.82	48.01	50.04	49.78	1.01	4.21	8/12/2012

Test Number	Sample ID	Size(mm)			Equivalent Width(mm)	Height to width ratio	UCS (Mpa)	Test Date
		Length	Width	Height				
69	6AR ④	52.07	50.29	43.94	51.05	0.86	1.80	5/12/2012
70	6AR ⑤	52.07	50.80	51.05	51.31	1.00	10.63	5/12/2012
71	6AR ⑥	53.85	53.09	60.45	53.34	1.13	2.13	8/12/2012
72	6AR ⑦	46.99	43.69	49.78	45.21	1.10	3.60	5/12/2012
73	6AR *1	55.88	54.36	51.56	55.12	0.94	7.00	5/12/2012
74	6AR *2	53.34	52.83	51.56	53.09	0.97	4.14	5/12/2012
75	1S ①	52.32	50.04	68.33	51.05	1.34	5.32	5/12/2012
76	1S ②	52.07	50.04	81.28	51.05	1.59	3.50	8/12/2012
77	1S ③	51.31	51.31	79.76	51.31	1.55	3.43	8/12/2012
78	1S ④	52.07	49.53	92.46	50.80	1.82	3.81	8/12/2012
79	1S ⑤	52.07	51.82	45.72	51.82	0.88	3.00	5/12/2012
80	1S ⑥	50.29	50.04	85.34	50.04	1.71	2.20	8/12/2012
81	1S⑦	50.55	50.29	45.97	50.29	0.91	3.25	5/12/2012
82	1S⑩	52.07	48.51	48.26	50.29	0.96	3.66	5/12/2012
83	W. J.	48.51	53.59	53.85	51.05	1.05	24.55	6/4/2011
84	2x 2x2	47.24	51.56	60.71	49.28	1.23	8.95	6/4/2011
85	W.J.2	50.80	45.72	70.10	48.26	1.45	21.99	5/12/2012
86	2x2x3	51.82	52.83	76.45	52.32	1.46	8.69	6/4/2011
87	12 AR 2	49.68	48.20	54.98	48.93	1.12	4.37	6/8/2014
88	Bd*-1	48.19	53.87	54.90	50.95	1.08	12.85	6/8/2014
89	3x3x3	76.71	76.45	86.87	76.45	1.14	17.67	5/12/2012
90	6AR ①	77.47	74.68	84.33	75.95	1.11	5.25	5/12/2012
91	W.J.-Big	91.19	90.17	93.73	90.68	1.03	1.53	5/12/2012
92	Un-1	74.51	71.76	105.98	73.12	1.45	2.83	6/8/2014
93	Un-2	76.42	80.63	82.74	78.49	1.05	1.84	6/8/2014
94	E1	110.21	110.88	113.30	110.54	1.02	0.95	6/8/2014
95	E2	116.92	109.04	124.34	112.91	1.10	4.36	6/8/2014

APPENDIX B : FRICTION ANGLE FOR DIFFERENT TYPES OF SAND (Holtz and Kovacs ,1981)

TABLE 11-2 Angle of Internal Friction of Cohesionless Soils*

No.	General Description	Grain Shape	D_{10} (mm)	C_u	Loose		Dense	
					e	ϕ(deg)	e	ϕ(deg)
1	Ottawa standard sand	Well rounded	0.56	1.2	0.70	28	0.53	35
2	Sand from St. Peter sandstone	Rounded	0.16	1.7	0.69	31	0.47	37†
3	Beach sand from Plymouth, MA	Rounded	0.18	1.5	0.89	29	—	—
4	Silty sand from Franklin Falls Dam site, NH	Subrounded	0.03	2.1	0.85	33	0.65	37
5	Silty sand from vicinity of John Martin Dam, CO	Subangular to subrounded	0.04	4.1	0.65	36	0.45	40
6	Slightly silty sand from the shoulders of Ft. Peck Dam, MT	Subangular to subrounded	0.13	1.8	0.84	34	0.54	42
7	Screened glacial sand, Manchester, NH	Subangular	0.22	1.4	0.85	33	0.60	43
8‡	Sand from beach of hydraulic fill dam, Quabbin Project, MA	Subangular	0.07	2.7	0.81	35	0.54	46
9	Artificial, well-graded mixture of gravel with sands No. 7 and No. 3	Subrounded to subangular	0.16	68	0.41	42	0.12	57
10	Sand for Great Salt Lake fill (dust gritty)	Angular	0.07	4.5	0.82	38	0.53	47
11	Well-graded, compacted crushed rock	Angular	—	—	—	—	0.18	60

*By A. Casagrande.

†The angle of internal friction of the undisturbed St. Peter sandstone is larger than 60° and its cohesion so small that slight finger pressure or rubbing, or even stiff blowing at a specimen by mouth, will destroy it.

‡Angle of internal friction measured by direct shear test for No. 8, by triaxial tests for all others.

APPENDIX C: MINERALOGY OF ST. PETER SANDSTONE BASED ON X-RAY DIFFRACTION

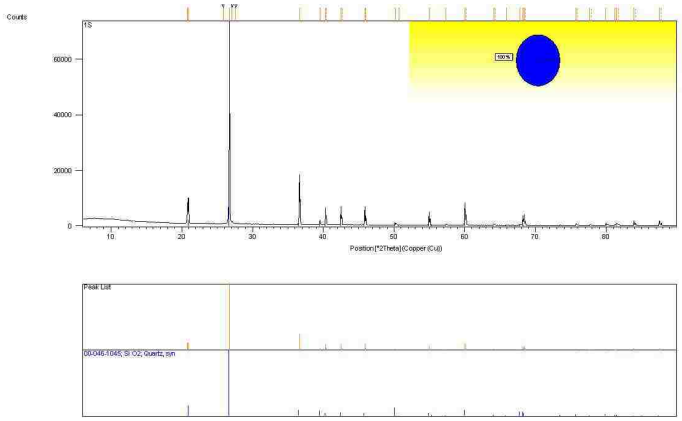

FigureC1. X-Ray diffraction result for St. Peter sandstone (sample ID: 1S)

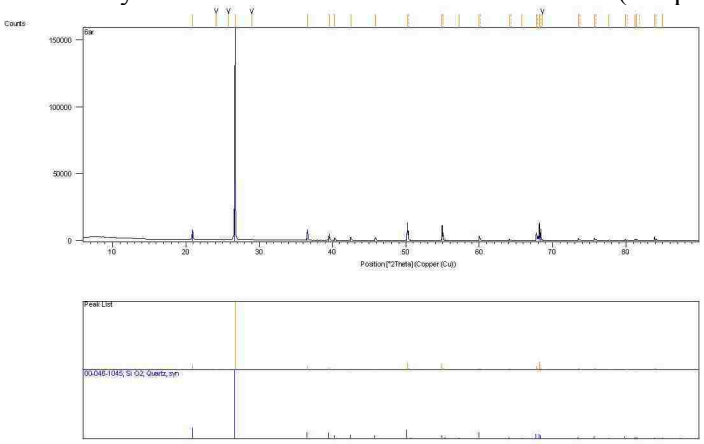

Figure C2. X-Ray diffraction result for St. Peter sandstone (sample ID: 6AR)

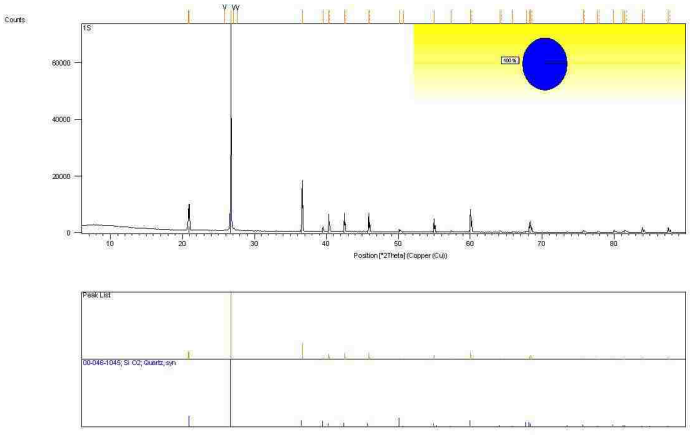

Figure C3. X-Ray diffraction result for St. Peter sandstone (sample ID: 3AS)

APPENDIX D: POROSITY STUDY BASED ON PETROGRAPHIC IMAGES

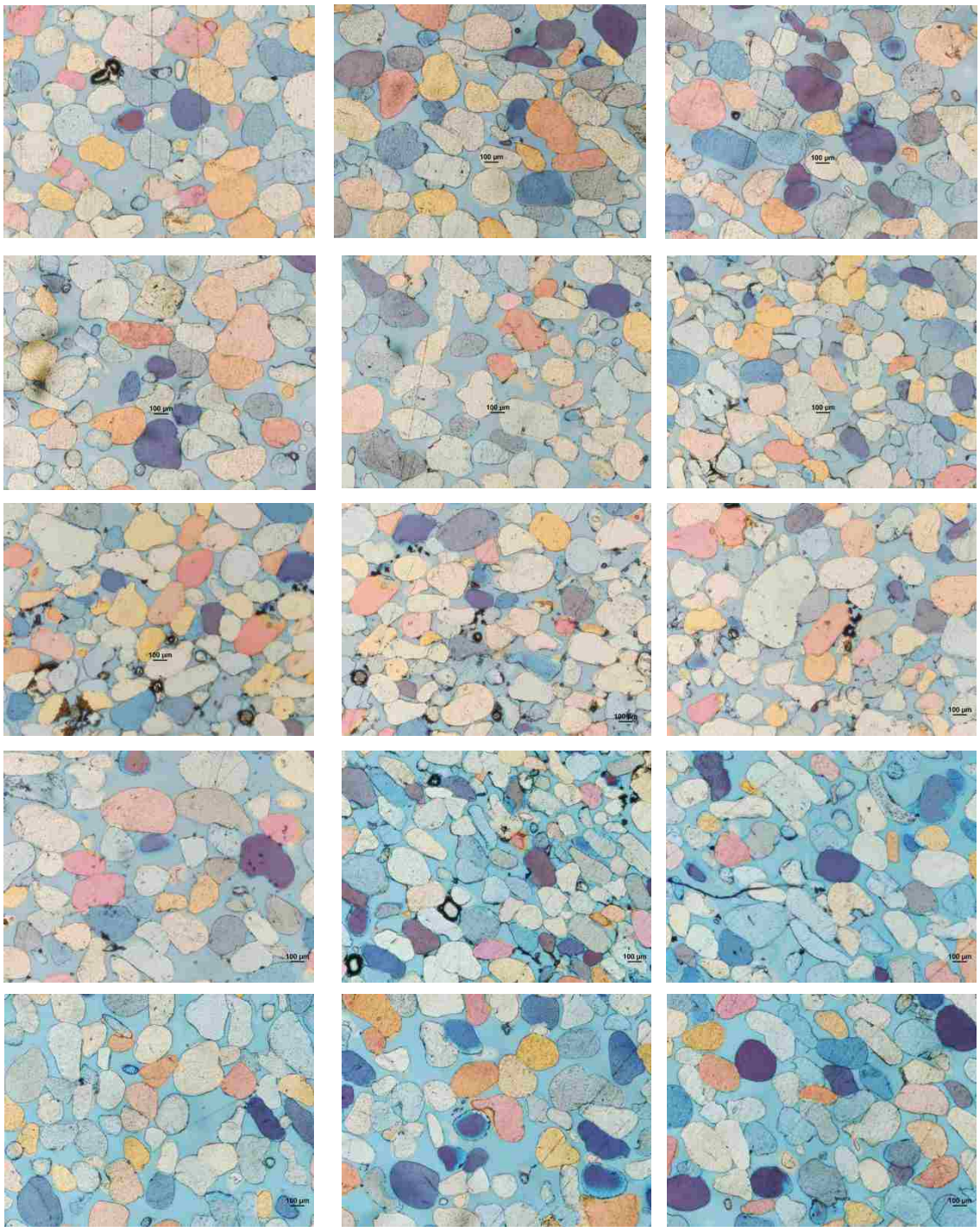

Figure D1 1S images from Texas

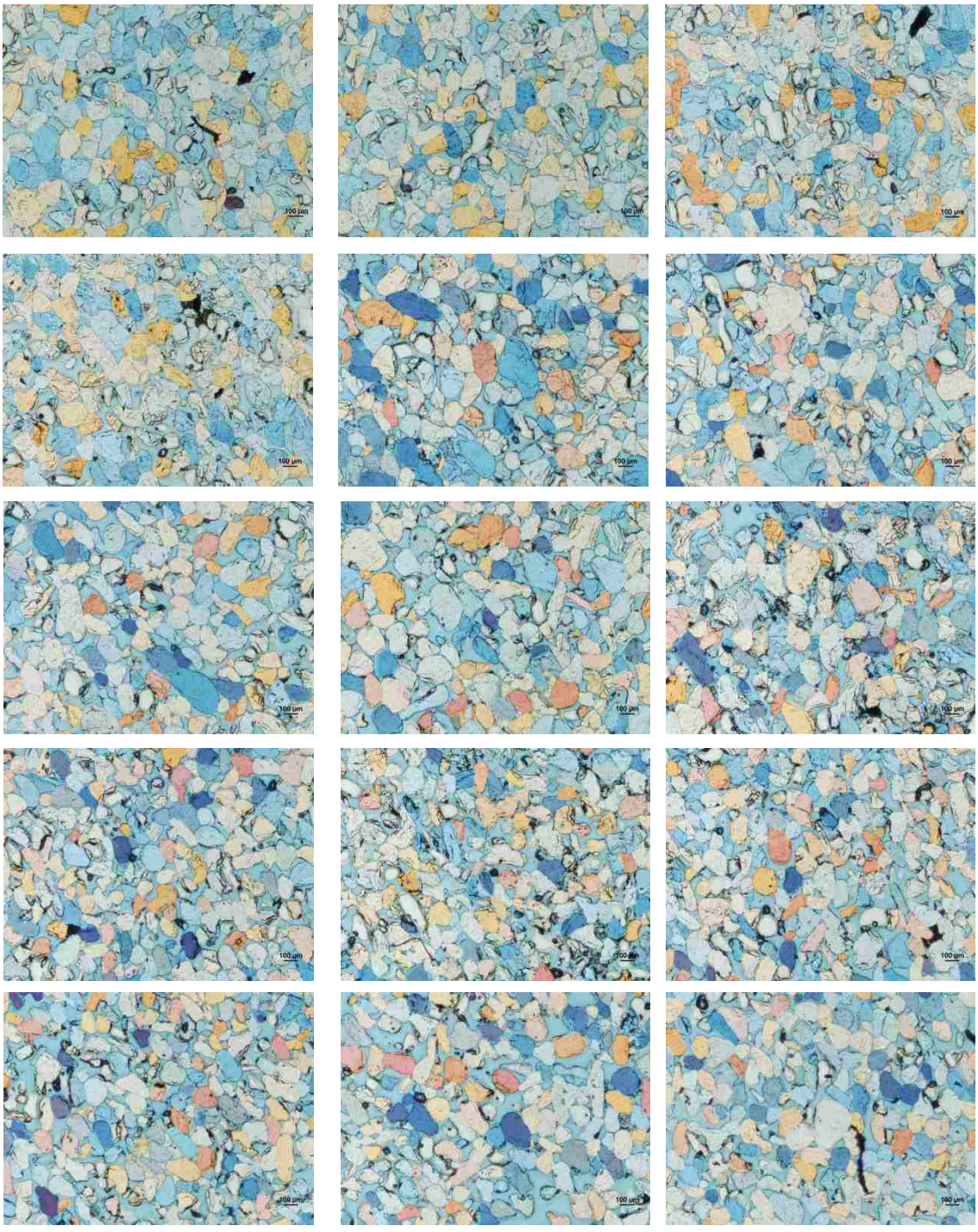

Figure D2 6AR images from Texas.

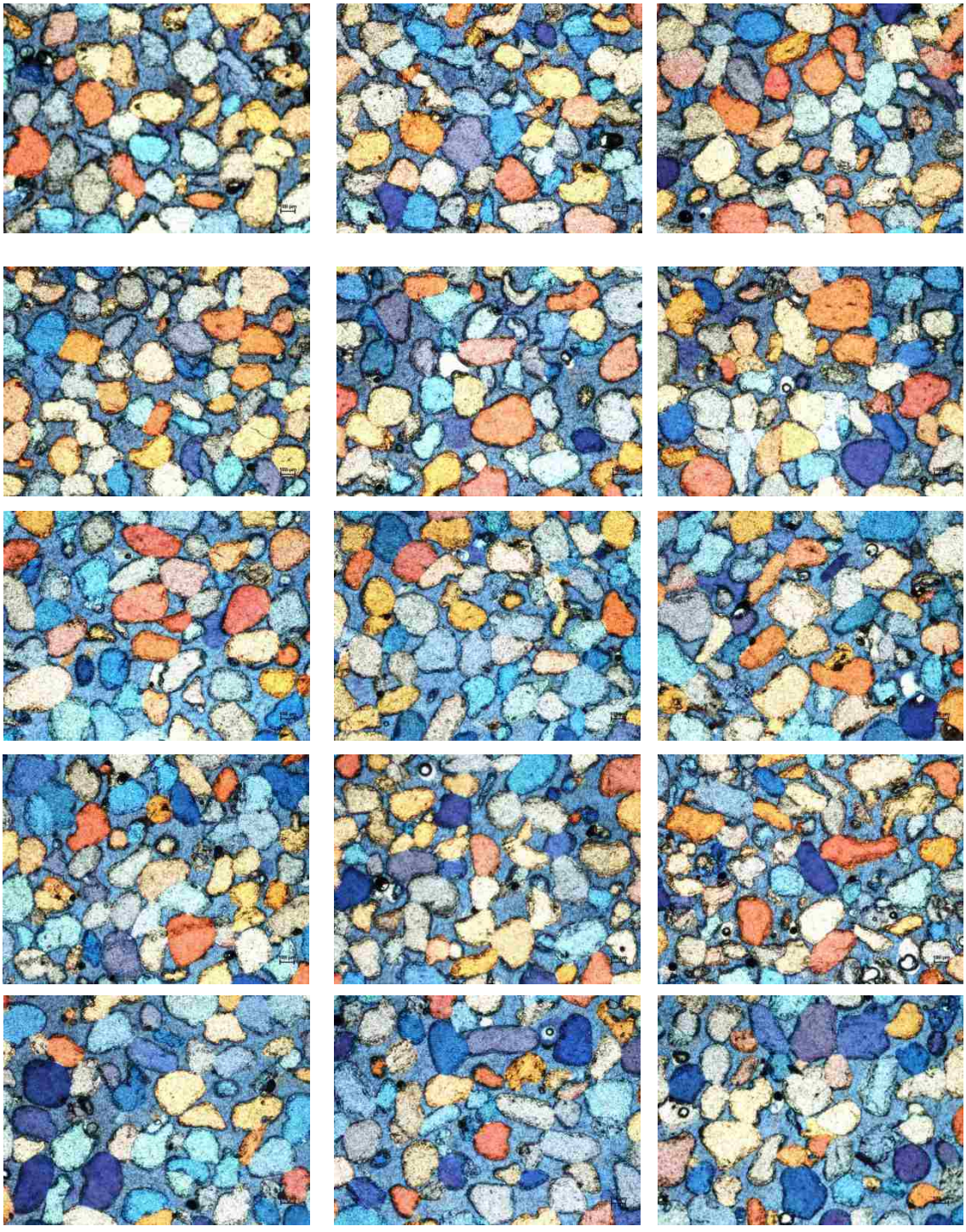

Figure D3 1S images from Washington.

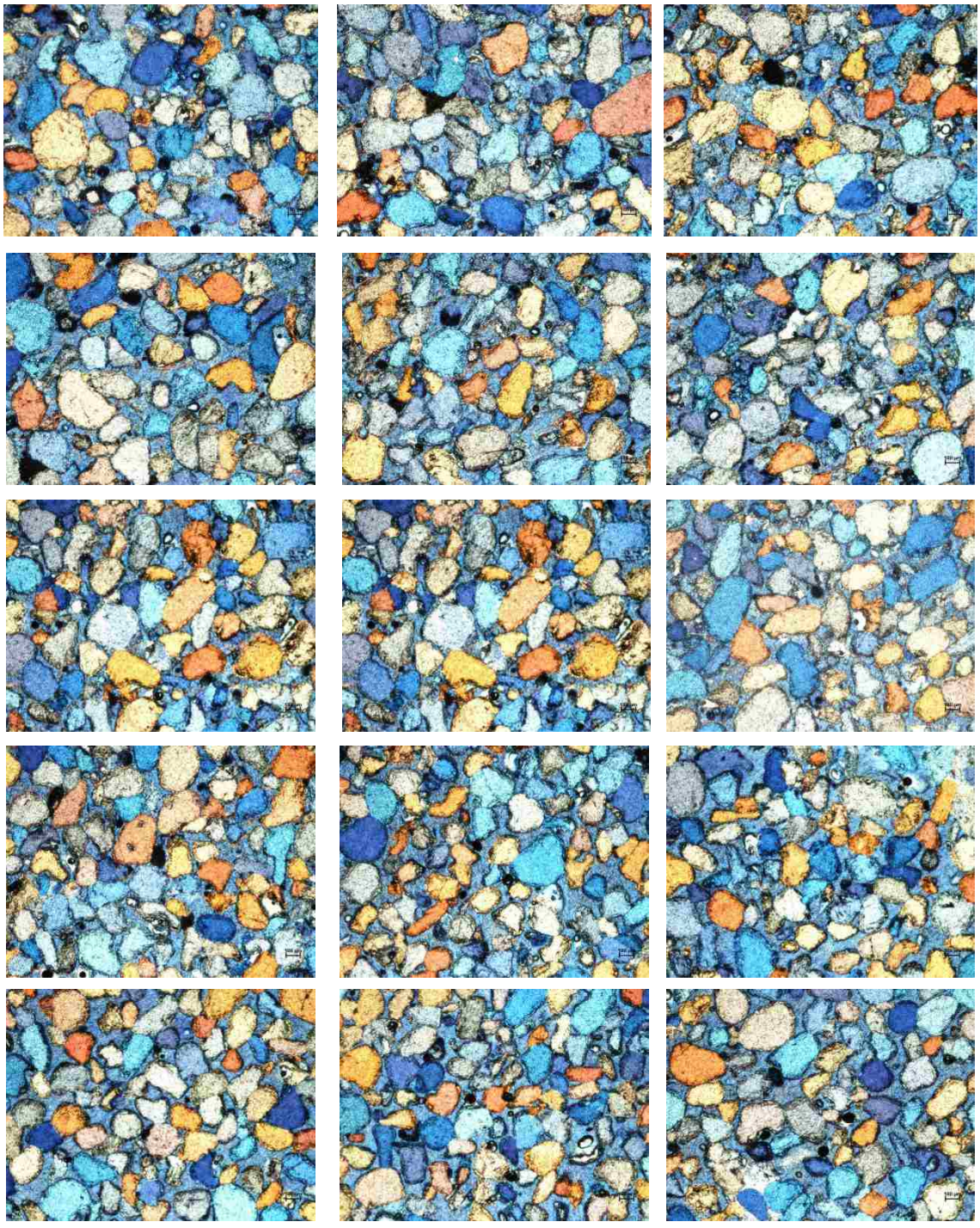

Figure D4 6AR images from Washington

BIBLIOGRAPHY

Amaral, E. J., and Pryor, W. A., 1976, *Depositional environment of the St. Peter Sandstone deduced by textural analysis*, Journal of sedimentary petrology, Vol., 47, 32-52.

ASTM D7012-14, *Standard test methods for compressive strength and elastic moduli of intact rock specimens under varying state of stress and temperatures*.

Barton, M. E. (1993. Cohesive sands: *The natural transition from sand to sandstones*. Proc., Geotechnical Eng. of Hard Soils—Soft Rocks, Int. Symp., A. Anagnastopoulos, F. Schlosser, N. Kalteziotis, and R.Frank, eds., Balkema, Rotterdam, The Netherlands, 367–374.

Boggs, S., Jr., 2006, *Principles of Sedimentology and Stratigraphy*, 4th edition, Prentice Hall, 662 p.

Bieniawski, Z. T., 1972. *Propagation of brittle fracture in rock*, Proceedings, 10th Symposium on Rco Mechanics (AIME), pp. 409-427.

Bieniawski, Z. T. and Van Heerden, W. L., 1975. *The significance of in-situ tests on large rock specimens*, Int. J. Rock Mech. Min. Sci. 12: 101-113.

Bieniawski, Z. T., 1984, *Rock mechanics design in mining and tunneling*, A.A. Balkema, 272. p.

Brady, B. H. G. and E. T. Brown, 1993. *Rock Mechanics for underground minin*g. Kuwer Academic Publishers, Dordrecht, The Netherlands.

Corps of Engineers, 1958, *St. Antony Fall upper Lock and Dam*, Report UL-3, Corps of Engineers, St. Paul, Minnesota.

Coulomb, C. A.1776, *Essai sur une application des règles de maximis et minimis a quelques problèmes de statique*, relatifs a l'architecture, Mémoires de Marhématique de l'Académie Royale des Sciences, Paris, 7, 343 – 82.

Cresswell, A, 1999, *Sampling and strength testing an unbonded locked sand*', Southampton University (United Kingdom), 1-190.

Dake, C.L., 1921, *the problem of the St. Peter sandston*e, Bulletin of Missouri University School of Mines and Metallurgy, Tech. Ser., Vol. 6, 228 p.

Dapples, E. C., 1955, *General lithofacies relationships of St. Peter Sandstone and Simpson Group*, American Association of Petroleum Geologists Bulletin, v. 39,444.-467.

de Freitas, M.H, 1993, *Weak arenaceous materials, Engineering Geolog*y Special Publication No. 8: The Engineering Geology of Weak Rock, Editors: Cripps, Coulthard, Culshaw, Forster, Hencher, Moon, Publisher: Geological Society of London, 115-123.

Dittes, M. and J.F. Labuz, 2002. *Field and Laboratory Testing of St. Peter Sandstone*. Journal of geotechnical geoenvironmental engineering, 128, 372-380.

Dusseault, M. B. 1977. *The geotechnical characteristics of the Athabasca Oil Sands*. Unpublished thesis submitted to the Faculty of Graduate Studies of the University of Alberta, 472pp.

Dusseault, M. B. and N. R. Morgenstern, 1979. *Locked sands*. Q. J. Eng. Geol., 12, 117 – 131.

Elliott, G. M., 1982. *An investigation of a yield criterion for rock*. PhD thesis, University of London.

Energy Information Administration (EIA). *2010 Annual Energy Outlook Report*,

http://www.eia.gov/oiaf/aeo/pdf/0383(2010).pdf.pdf, retrieved 3/20/2014.

Energy Information Administration (EIA). *2013 Annual Energy Outlook Report*,

http://www.eia.gov/forecasts/aeo/pdf/0383(2013).pdf , retrieved 3/20/2014.

Frank, F.C. and B.R. Lawn, 1967. *On the theory of Hertzian fracture*. Proceedings of the Royal Society, A, 299, 291-306.

Ge, M, Ding, Z., Bagherieh, A, 2014a, *Characteristics of interstitial spaces of rhomobohedral packing: A porosity model for St. Peter sandstone*, to be submitted to Journal of Geology.

Ge, M, Bagherieh, A, Ding, Z., 2014b, *Rhomobohedral modeling f high friction angle of St. Peter Sandstone*, to be submitted to International Journal of Rock Mechanics.

Giles, A. W., 1930, *St. Peter and older Ordovician sandstone of northern Arkansas*, Arkansas geological survey Bulletin, 187 p.

Goodman, R. F., 1988. *Introduction to rock mechanics*. John Willey and Sons, Inc., New York.

Graton, L.C. and H.J. Fraser, 1935. *Systematic packing of spheres: with particular relation to porosity and permeability*. The Journal of Geology, 43, 785-909.

Hoek, E. and J. W. Bray. 1977. *Rock slope engineering*. The Institution of Mining and Metallurgy, London.

Holtz, R. D. and W. D. Kovacs, 1981. *An introduction to geotechnical engineering*. Preentice-Hall, In., Englewood Cliffs, New Jersey, 07632.

ISRM, 1981, *Rock Characterization, Testing and Mentoring*, ISRM suggested methods, E. T. Brown (ed.), Pergamum Press, 211p.

Jaeger, J. C. and N. G. W. Cook, 1979. *Fundamentals of rock mechanics*. Chapman and Hall, London.

Johnson, C.B., Marshall, J.R., Mazzullo, J.M., 1989, *St. Peter Sandstone: a closetr look, discussion*, Journal OF Sedimentary Petrology, Vol 59, NO. 3, May, 1989, v. 494---497

Kamb, H.R., 1932, *Report of Layne-Northwest Company to the City Council, Minneapolis*, Minnesota.

Krauland, N. and Soder, P.E. , 1987, *Determining Pillar Strength From Pillar Failure Observations*. Eng. Min. Journal, 8:34-40.

Karman, TH. Von, and Duwez, P., 1950. *The propagation of plastic deformation in solids*. J. Appl. Phys., 21, 987-94.

Labuz, J. F., Zietlow, W. K., and Chen L-H. 1998. *Laboratory testing for the Minnesota Library Access Center*. Tech Rep.

Lamar, J. E., 1928, *Geology and economic resources of the St. Peter Sandstone of Illinois*, Urbana (Springfield: Jeffersons Printing Co.), 175 p

Lawn, B. and R. Wilshaw, 1975. *Review Indentation fracture: principles and applications*. Journal of materials science, 10, 1049-1081.

Mazzullo, J. M., and Ehrlich, R., 1983, *Grain-shape variation in the St. Peter sandstone: Arecord of eolian and fluvial sedimentation of an early Paleozoic cratonic sheet sand*, Journal of sedimentary petrology, Vol. 53, NO. 1, 105–119.

Milligan, M. F., 1976, *Model Studies for a friable sandstone*. Master degree thesis.

Department of Civil Engineering, University of Alberta, Edmonton, Alberta.

Mohr, O, 1900, *Welche Umstände Bedingen die Elastizitätsgrenze und den Bruch eines Materials?* Zeit des Ver Deut Ing 44: 1524–153

Mostly Maps, Sands of time, http://mostlymaps.wordpress.com/2009/12/20/sands-oftime/,retrieved 3/20/2014.

Obert, L., Windes, S. L., and Duvall, W. I. (1946): *Standardized tests for determining the physical properties of mine rock*. U.S. Bur. Mines Rept. Invest., No. 3891.

Payne, C. M., 1967. *Engineering aspects of the St. Peter sandstone in the Minneapolis-St. Paul area of Minneso*ta. Master thesis, University of Arizonan, AZ.

Pettijohn, F. J., Potter, P. E., Siever, R., 1987, *Sand and Sandstone*, Springer-Verlag, 553 p.

Petersen, D. L., 1978, *estimating the strength of St. Peter sandstone pillars*, Master's thesis, University of Minnesota, Minneapolis.

Russell, W. L, 1926, *a method for determining porosity,* American association Petroleum Geology, Bulletin, Vol. 10, 931-938.

Sardeson, F. W., 1896, *the Saint Peter Sandstone, Minnesota Academy of Natural Sciences*, 4, Paper D, 64–88.

Schwartz, G. M., 1939, *Foundation conditions at the sites of the proposed St. Anthony Falls locks Minneapolis,* Minnesota.'' Report to the U.S. Army Corps of Engineers, St. Paul District.

Sterling, R.L., 1977, *Roof design for near surface Bedded Rock Foundation*, Ph.D.

Dissertation, University of Minnesota, Minneapolis.

Sterling, R.L., 1977, *unpublished, quoted by Lee D. Petersen (1978)* , Estimating the strength of St. Peter sandstone pillars, Master's thesis, University of Minnesota, Minneapolis, 49-50.

Sjöberg, J., 1992*, Failure Modes and Pillar Behaviour in the Zinkgruvan Mine*, in Rock Mechanics (Proceedings, 33rd U.S. Symposium, Santa Fe, June 1992),. 491-500. J. R. Tillerson and W. R. Wawersik, Eds. Rotterdam: Balkema,.

Thiel, G.A., 1935. *Sedimentary and petrographic analysis of the Saint Peter sand*stone. Geological Society of America Bulletin, 46, 559-614.

Torsæter, O, Abtahi, M, *experimental reservoir engineering laboratory work book, Department of Petroleum engineering and Applied Geophysics*, Norwegian University of Science and Technology, august 2000, 25-30.

Twenhofel, W. H, Thwaites, F. T., 1919, *the Paleozoic section of the Tomah and Sparta quadrangles*, Wisconsin, Jour. Geol., Vol. 27, 614-633.

USGS Minerals Information: Minerals Yearbooks (2006-2011), *silica statics and information*, http://minerals.usgs.gov/minerals/pubs/commodity/silica/index.html#myb, retrieved 3/20/2014

Watson, J. D., 1938. *Triaxial compression tests on St. Peter sandstone*. Report to the U.S. Army Corps of Engineers, St. Paul District.

Wawersik, W. R. and Fairhurst, C., 1970. *A study of brittle rock facture in laboratory compression experiments*. Int. J. Rock Mech. Min. Sci & Geomech. Abstr., 7, 561-75.

Wilshaw, T.R., 1971. *The Hertzian fracture test*. J. Phys.D: Appl. Phys., 4, 1567-1583.

Winfree, K. E., 1983, *Depositional environments of the St. Peter Sandstone of the upper Midwest, Master's thesis*, University of Wisconsin, 114 p.

Yardley, D., 1978, unpublished, quoted by Lee D. Petersen (1978) , *Estimating the strength of St. Peter sandstone pillars*, Master's thesis, University of Minnesota, Minneapolis, pp:48-49

Zeng K., Breder K., Rowcliffe D.J. ,1992, *The Hertzian stress field and formation of cone cracks – I theoretical approach*, Acta Metallurgica et Materialia, Vol. 40, issue 10,.2595–2600

VITA

Amir Hossein Bagherieh was born in Hamedan, Iran, on September 11, 1980. He received his B.S. of Mining Engineering degree in 2004 and his M.S.degree in Mining Engineering in 2007 from the Imam Khomeini International University and Science and Research Campus of I. Azad University respectively. After graduation with master degree, he worked as a mining engineer for different companies. He was involved in a wide range of mining engineering problems such as the design and construction of an underground mine, blast design, and mineral processing plant. He also taught several courses for research and training institute of Iranian ministry of mines and metals.

He began his PhD at Missouri University of Science and Technology (MS&T) in August 2009. During his stay on MS&T, he worked as graduate research and teaching assistant under supervision of Dr. Maochen Ge. In May 2015, he received his Ph.D in Mining Engineering from at Missouri University of Science and Technology, Rolla, Missouri, USA.

He published seven journal papers. He also presented in SME annual conferences. Amir Bagherieh has been a member of the Society of Mining and Metallurgical Engineers (SME) since 2009.